Document generated on 01/14/2025 6:24 a.m.

**Geoscience Canada**
Journal of the Geological Association of Canada
Journal de l'Association Géologique du Canada

# The End-Cryogenian Glaciation of South Australia

Catherine V. Rose, Adam C. Maloof, Blair Schoene, Ryan C. Ewing, Ulf Linnemann, Mandy Hofmann and John M. Cottle

Volume 40, Number 4, 2013

URI: https://id.erudit.org/iderudit/1021066ar

See table of contents

Publisher(s)

The Geological Association of Canada

ISSN

0315-0941 (print)
1911-4850 (digital)

Explore this journal

Cite this article

Rose, C. V., Maloof, A. C., Schoene, B., Ewing, R. C., Linnemann, U., Hofmann, M. & Cottle, J. M. (2013). The End-Cryogenian Glaciation of South Australia. *Geoscience Canada*, *40*(4), 256–293.

All Rights Reserved © The Geological Association of Canada, 2013

This document is protected by copyright law. Use of the services of Érudit (including reproduction) is subject to its terms and conditions, which can be viewed online.

https://apropos.erudit.org/en/users/policy-on-use/

érudit

This article is disseminated and preserved by Érudit.

Érudit is a non-profit inter-university consortium of the Université de Montréal, Université Laval, and the Université du Québec à Montréal. Its mission is to promote and disseminate research.

https://www.erudit.org/en/

# Paul F. Hoffman Series

## The End-Cryogenian Glaciation of South Australia

**Catherine V. Rose [a,b], Adam C. Maloof[a], Blair Schoene[a], Ryan C. Ewing[c], Ulf Linnemann[d], Mandy Hofmann[d], and John M. Cottle[e]**

[a]*Department of Geosciences*
*Princeton University*
*Guyot Hall, Washington Road*
*Princeton, NJ, USA 08544*

[b]*Department of Earth and Planetary Sciences*
*Washington University in St. Louis*
*1 Brookings Drive, St. Louis, MO, USA 63130*
*E-mail: crose@eps.wustl.edu*

[c]*Department of Geology and Geophysics*
*Texas A&M University, MS 3115,*
*College Station, Texas, TX, USA 77843*

[d]*Senckenberg Naturhistorische Sammlungen Dresden*
*Museum für Mineralogie und Geologie*
*Königsbrücker Landstrasse 159, D-01109*
*Dresden, Germany*

[e]*Department of Earth Science*
*University of California*
*Santa Barbara, CA, USA 93106*

### SUMMARY

The Elatina Fm. records the younger Cryogenian ice age in the Adelaide Rift Complex (ARC) of South Australia, which has long-held the position as the type region for this low-latitude glaciation. Building upon a legacy of work, we document the pre- and syn-glacial sedimentary rocks to characterize the dynamics of the glaciation across the ARC. The Elatina Fm. records an array of well-preserved glacial facies at many different water depths across the basin, including ice contact tillites, fluvioglacial sandstones, dropstone intervals, tidal rhythmites with combined-flow ripples, and turbidites. The underlying Yaltipena Fm. records the pro-glacial influx of sediment from encroaching land-based ice sheets. The onset of the glaciation is heralded by the major element ratios (Chemical Index of Alteration) of the pre-glacial facies across the platform that show a reduction in chemical weathering and a deterioration in climate towards the base of the Elatina Fm. The advancing ice sheets caused soft-sediment deformation of the beds below the glacial diamictite, including sub-glacial push structures, as well as sub-glacial erosion of the carbonate unit beneath. Measured stratigraphic sections across the basin show glacial erosion up to 130 m into the carbonate platform. However, $\delta^{13}C$ measurements of carbonate clasts within the glacial diamictite units were used to assess provenance and relative timing of $\delta^{13}C$ acquisition, and suggest that at least 500 m of erosion occurred somewhere in the basin. Detrital zircon provenance data from the Elatina Fm. suggest that glacial sediment may have been partially sourced from the cratons of Western Australia and that the Whyalla Sandstone, even if stratigraphically correlative, was not a sediment source. The remainder of the Elatina Fm. stratigraphy mostly records the deglaciation and can be divided into three facies: a slumped sandstone, dropstone diamictite, and current-reworked diamictite. The relative sea level fall within the upper Elatina Fm. requires that regional deglaciation occurred on the timescale of ice sheet – ocean gravitational interactions (instant) and/or isostatic rebound (~$10^4$ years). Structures previously interpreted as soft-sediment folds within the rhythmite facies that were used to constrain the low-latitude position of South Australia at the time of the Elatina glaciation are re-interpreted as stoss-depositional transverse ripples with superimposed oscillatory wave ripples. These combined-flow ripples across the ARC attest to open seas with significant fetch during the initial retreat of local glaciers. In addition, this interpretation no longer requires that the magnetization be syn-depositional, although we have no reason to believe that the low-latitude direction is a result of remagnetization, and positive reversal tests and tectonic fold tests are at least consistent with syn-depositional magnetization. Together, these paired sedimentological and chemostratigraphic observations reveal the onset of the glaciation and advance of the ice sheet from land to create a heavily glaciated terrain that was incised down to at least the base of the pre-glacial Trezona Fm.

 © 2013 GAC/AGC®

## SOMMAIRE

La Formation d'Elatina représente la phase précoce de l'âge glaciaire du Cryogénien de l'Adelaide Rift Complex (ARC) dans le sud de l'Australie, région qui a longtemps été la région type de cette glaciation de basse latitude. À partir d'un legs de travaux, nous nous sommes appuyés sur l'étude des roches sédimentaires préglaciaires et synglaciaires pour caractériser la dynamique de la glaciation à travers l'ARC. La Formation d'Elatina renferme une gamme de faciès glaciaires bien préservés correspondant à différentes profondeurs d'eau à travers le bassin, dont des tillites de contact glaciaire, des grès fluvioglaciaires, des intervalles à galets de délestage, des rythmites tidales avec des combinaisons de rides d'écoulement, et des turbidites. La Formation sous-jacente de Yaltipena est constituée de sédiments proglaciaires provenant de lentilles de glace en progression. Le début de la glaciation est reflété dans les ratios des éléments majeurs (indice d'altération chimique) des faciès préglaciaires de la plateforme qui montre une réduction de l'altération chimique et une détérioration du climat à l'approche de la base de la Formation d'Elatina. La progression des nappes de glace a entraîné une déformation des lits de sédiments meubles sous la diamictite glaciaire, montrant entre autres des structures de poussée sous-glaciaires ainsi que de l'érosion sous-glaciaire de l'unité de carbonate sous-jacente. Les mesures de coupes stratigraphiques à travers le bassin montrent que l'érosion glaciaire a enlevé jusqu'à 130 m du carbonate de la plateforme. Toutefois, les signatures isotopiques $\delta^{13}C$ de fragments de carbonate dans les unités de diamictites glaciaires utilisées pour établir la provenance et la chronologie d'acquisition relative de la signature $\delta^{13}C$ des fragments, permet de penser qu'il y a eu au moins 500 m d'érosion quelque part dans le bassin. Les données de provenance sur zircons détritiques de la Formation d'Elatina permettent de penser que les sédiments glaciaires provenaient partiellement des cratons de l'Australie occidentale et que le grès de la Formation de Whyalla, bien que stratigraphiquement corrélé, n'a pas été une source de sédiments. Ce qui reste de la stratigraphie de la Formation d'Elatina représente principalement la déglaciation, laquelle peut être divisée en trois faciès : un grès plissé, une diamictite à galets de délestage, et une diamictite remaniée par des courants. La baisse du niveau relatif de la mer dans la partie supérieure de la Formation d'Elatina suppose une déglaciation régionale sur une échelle de temps de l'ordre de celle de la nappe de glace – interactions gravitationnelles de l'océan (instantanées) et/ou rebond isostatique (~ $10^4$ ans). Des structures décrites précédemment comme des plis de sédiments mous dans des faciès de rhythmites qui impliquait une position de basse latitude pour l'Australie du Sud à l'époque de la glaciation Elatina, sont réinterprétées comme des rides sédimentaires transverses asymétriques avec des rides de vagues oscillatoires superposées. Ces combinaisons de rides d'écoulement à travers l'ARC confirment l'existence d'un milieu marin ouvert d'une ampleur certaine au moment de la retraite initiale des glaciers locaux. En outre, cette interprétation ne nécessite plus que la magnétisation soit synsédimentaire, bien que nous n'ayons aucune raison de penser que l'orientation magnétique de basse latitude soit le résultat d'une ré-aimantation, et que les tests de réversibilité positifs et les tests de plissement tectonique sont au minimum conformes à une magnétisation synsédimentaire. Ensemble, ces observations sédimentologiques et chimiostratigraphiques mettent en lumière le début de la glaciation et l'avancée du couvert de glace continental menant à une région fortement englacée qui a été incisée jusqu'à à la base de la Formation préglaciaire de Trezona.


## INTRODUCTION

At least two Neoproterozoic glacigenic, poorly sorted conglomeratic units are present on all continents except Antarctica, commonly interrupting carbonate platform sequences, and in some cases found near the paleomagnetic equator. Therefore, at least twice during this era, continental glaciers reached sea level in the low-latitudes (Embleton and Williams 1986; Schmidt and Williams 1995; Sohl et al. 1999; Evans 2000; Macdonald et al. 2010). These two Cryogenian glaciations are colloquially referred to as the older 'Sturtian' and younger 'Marinoan' low-latitude glaciations (Hoffman and Schrag 2002; Hoffman 2005, 2011). Banded iron formation within the thick Sturtian diamictite units, and sedimentologically and geochemically distinctive 'cap' carbonate sequences that consistently drape both glacial deposits (Williams 1979; Kennedy 1996; Kennedy et al. 1998; Hoffman et al. 2007; Rose and Maloof 2010), may indicate long-term isolation of the ocean from the atmosphere. Together, these observations led to the controversial 'snowball Earth' hypothesis, wherein an ice-albedo runaway feedback caused ice to advance rapidly to the equator and seal the entire ocean in ice for millions of years (Kirschvink 1992; Hoffman et al. 1998, 2002).

Early work on these enigmatic low-latitude glaciations focused on identifying and describing the glacial deposits around the world (Spencer 1971; Deynoux and Trompette 1976; Hambrey and Harland 1981; Deynoux 1985; Lemon and Gostin 1990). However, this focus on the glacial deposits led to different interpretations and some workers proposed a debris flow origin for the conglomeratic beds (Schermerhorn 1974; Eyles 1993; Arnaud and Eyles 2006). Eyles and Januszczak (2004) argued that both the glacigenic deposits and associated carbonate rocks could be explained by continental rifting, with carbonate deposited in restricted basins starved of clastic input. Although not widespread, high-latitude carbonate and evaporite rocks coexist with glacigenic sediments today (Walter and Bauld 1983). A close examination of the pre- and post-glacial Neoproterozoic rocks in the North Atlantic region, however, determined that these carbonate units were probably deposited in warm water and thus climatic fluctuations between 'balmy' and 'icy' conditions occurred quite rapidly (Fairchild 1993).

The snowball Earth hypothesis (Kirschvink 1992; Hoffman et al. 1998; Hoffman and Schrag 2002) was proposed by Kirschvink (1992) in an attempt to explain the presence of banded iron formation within the thick older Cryogenian diamictite units, which were deposited near the equator. Further work also identified the dis-

tinctive 'cap' carbonate sequences that consistently drape both glacial deposits (Williams 1979; Kennedy 1996; Kennedy et al. 1998; Hoffman et al. 1998, 2007), which were not explained by previous models. Both of these observations imply perturbations to seawater chemistry that are consistent with long term isolation of the ocean from the atmosphere. Hence, since its most recent formulation in 1998, tests of the snowball Earth hypothesis turned their attention to the geochemistry of the cap carbonates (Williams 1979; Fairchild 1993; Hoffman et al. 1998; Grotzinger et al. 2000; James et al. 2001; Kennedy et al. 2001; Shields 2005; Hoffman and Schrag 2002; Higgins and Schrag 2003; Hoffman et al. 2007; Rose and Maloof 2010; Hoffman 2011). Despite advances toward understanding this non-uniformitarian climate state, relatively little recent work has been done on the glacial sediments themselves. This inattention arises in part because these deposits are spatially heterogeneous and difficult to interpret. Recently, some limited observations of thick glacial deposits intercalated with wave-rippled and hummocky cross-stratified interglacial sandstones (Allen and Etienne 2008; Le Heron et al. 2011a,b) indicated ice-front mobility or advance–retreat cycles (Christie-Blick et al. 1999; Condon et al. 2002; Leather et al. 2002; Rieu et al. 2007b; Allen and Etienne 2008). These studies present their observations as a challenge to a 'hard' snowball scenario, which completely encompasses the world with ice, questioning the ideas that sea ice would be globally present and that moisture from sea-ice sublimation alone would have been sufficient to drive the dynamics of polythermal ice with active subglacial hydrology. However, glacial diamictite successions may be deposited entirely during deglaciation, and such arguments for advance–retreat cycles may not be relevant to peak snowball conditions. Yet, importantly, these few studies highlight the need for a re-evaluation of low-latitude glacial deposits themselves. Our work re-focusses attention back to the glacial deposits, investigating the Marinoan-age Elatina Fm. in the Adelaide Rift Complex (ARC), South Australia. However, rather than studying the diamictites in isolation, we also build a comprehensive multidisciplinary dataset from the adjacent strata to evaluate both the transition into and out of the ice-house event. This study demonstrates that an approach that integrates basin-scale analysis with detailed sedimentology and chemostratigraphy, when set in the context of the pre- and post-glacial sediments, can provide new insights into the dynamics of extensive glaciations of the Cryogenian.

The Elatina Fm. is of global importance because: 1) its sedimentology is diverse and well preserved, recording transitions in glacial facies at different water depths across the basin; 2) it represents the type region for the Marinoan glaciation (Williams et al. 2008); 3) it has yielded the most robust paleomagnetic data for any late Cryogenian glacigenic succession (Evans and Raub 2011), and 4) the recently established Ediacaran System and Period (Knoll et al. 2006) has its Global Stratotype Section and Point (GSSP) at the base of the Nuccaleena Fm. overlying the Elatina Fm. in the central Flinders Ranges. The glacial origin of the Elatina Fm. was first recognized by Mawson (1949) following his discovery of diamictite containing faceted and striated clasts in Elatina Creek in the central Flinders Ranges, and he proposed the term 'Elatina glaciation' (Williams et al. 2008; Fig. 1 [17]). Since these initial observations, several studies have been published on the Elatina Fm. Additional mapping extended observations of the Elatina Fm. laterally across the ARC (Dalgarno and Johnson 1964; Leeson 1970). This careful work led to Elatina Creek being nominated as the type section (Dalgarno and Johnson 1964) and to correlations to other Elatina Fm. sections in the southern (Binks 1968; Miller 1975; Jablonski 1975) and northern (Coats et al. 1973; Preiss and Forbes 1981) Flinders Ranges. Lemon and Gostin (1990) presented a detailed sedimentological study of the Elatina Fm. within the central Flinders Ranges, which established three correlative facies for the Elatina Fm. that were interpreted as recording the advance of the ice and subsequent deglaciation. Most workers document the advance of grounded ice or scouring by icebergs, which attest to the glacial nature of the Elatina Fm. (Lemon and Gostin 1990; Lemon and Reid 1998; Williams et al. 2008). However, it has been suggested that the upper Elatina Fm. consists of glacially influenced debris flows resulting from local slope collapse (Le Heron et al. 2011a; Le Heron 2012), and some workers have even proposed that the entire succession records tectonically triggered mass flow deposits (Schermerhorn 1974; Eyles et al. 2007).

Williams (1989, 1991, 1998, 2000) and Williams et al. (2008) described rhythmic laminations within siltstone of the upper Elatina Fm. at Warren Gorge, Pichi Richi Pass in the southern Flinders Ranges, and Marino Rocks south of Adelaide (Fig. 1 [2, 4]). The rhythmites consist of 1–2 cm-thick bundles of mm-scale couplets that were originally interpreted as varves deposited in a periglacial lake (Williams 1981), where each clastic lamina represents annual deposition of sediment by glacial meltwater (Williams 1981, 1985; Williams and Sonett 1985). Williams (1985) argued that the periodic deposition of cyclic laminae correlated with sunspot cycles, though the mechanism by which Marinoan climate was controlled by sunspots was not clearly articulated. Furthermore, astronomical models suggest that the sunspot cycle during the Neoproterozoic was 3-10% shorter than today (Noyes et al. 1984), whereas the Elatina Fm. data suggest that the mean cycle was ~8% longer at that time (Williams 1988). By comparing the Elatina rhythmites to two other putatively correlative rhythmite deposits in Southern Australia, the Reynella Siltstone Member and Chambers Bluff Tillite, Williams determined that the packages of laminae represent fortnightly cycles of spring-neap lunar tide deposits as a distal part of an ebb-flood tidal delta (Zahnle and Walker 1987; Williams 1988). The literature since has focused on correlating rhythmite periodicities with tidal periodicities and elucidating the implications for the history of the Earth-Moon orbit (Williams 1997, 1998, 2000). Under this model, one couplet represents a semi-diurnal or diurnal depositional cycle, strictly constraining the rate of bedform migration and aggradation of the rhythmite sequences.

The rhythmites also are the

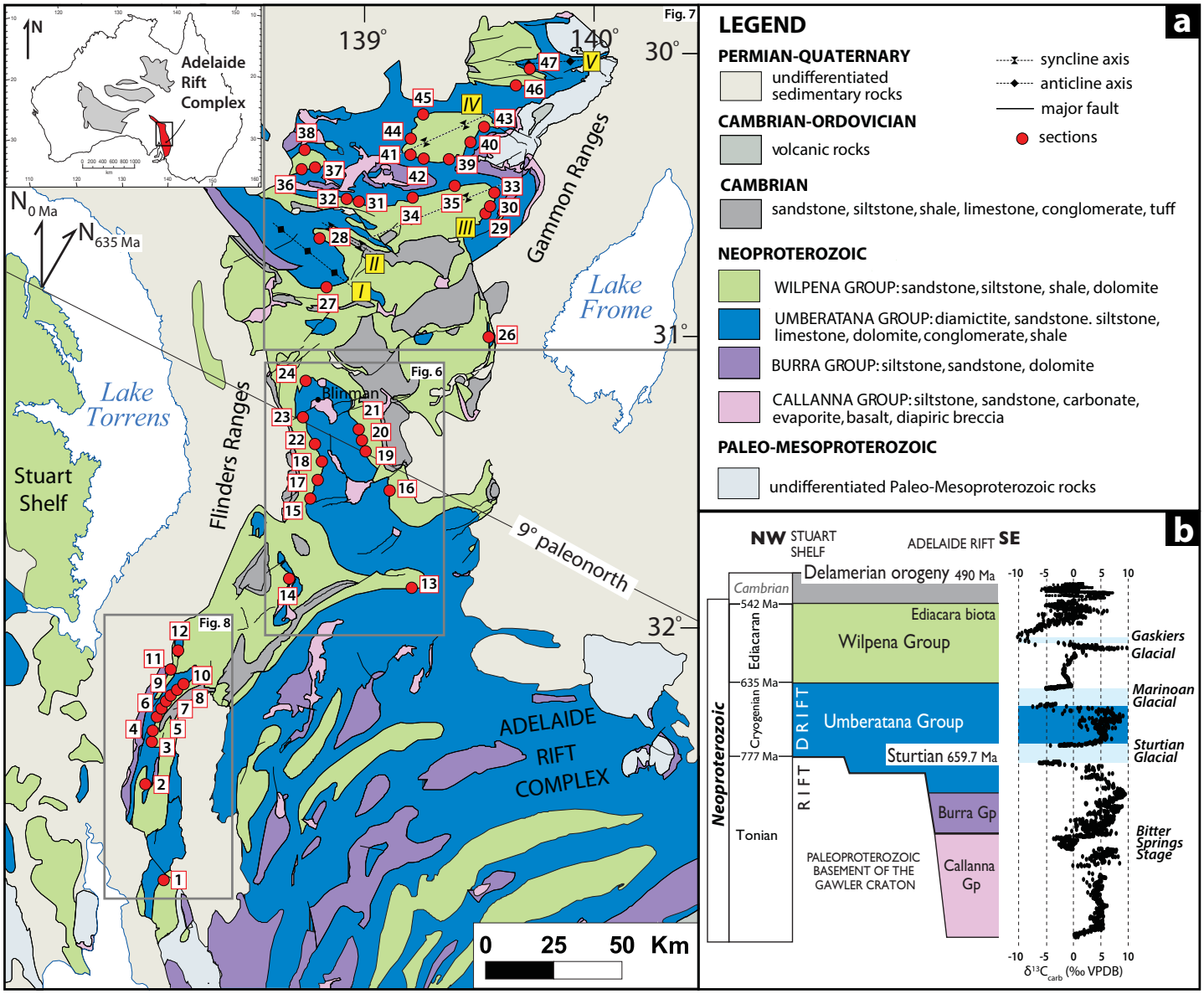


**Figure 1.** (a) Simplified geological map of the study area within the Adelaide Rift Complex (ARC) adapted from Preiss and Robertson (2002). Locations of measured stratigraphic sections are denoted by red circles and labeled with numbered squares. Fold axes within the Adelaide Rift Complex are denoted by dashed lines and labeled with Roman numerals: (I) Mount Morris anticline; (II) Mount Jeffery syncline; (III) Arkaroola syncline; (IV) Umberatana syncline; and (V) Mount Fitton anticline. The large grey boxes represent the areas of the detailed maps presented in Figures 6, 7 and 8. (b) Schematic NW-SE stratigraphic cross-section of the Adelaide Rift Complex, highlighting the rift-to-drift transition and major sequence boundaries (adapted from Lemon and Gostin 1990). $\delta^{13}C$ profile adapted from Halverson et al. (2005) time-aligned with the right-hand edge of the stratigraphic cross-section. A SHRIMP U–Pb zircon age of 659.7 ± 5.3 Ma from a tuffaceous horizon in the Wilyerpa Fm., just above the Appila (Sturtian) diamictite, provides a maximum age for the base of the interglacial sedimentary units (Fanning 2006). The overlying Nuccaleena Fm. is dated by correlation to the uppermost Marinoan glacial deposits and the associated cap dolostone in Oman (Bowring et al. 2007; Rieu et al. 2007a), Namibia (Hoffmann et al. 2004) and South China (Condon et al. 2005), which contain ID–TIMS U–Pb zircon ages of ~635 Ma.

centre-piece of a key paleomagnetic constraint for Cryogenian low-latitude glaciation and the snowball Earth hypothesis. Results of a fold test on putative soft-sediment folds within these rhythmites indicated that the characteristic remnant magnetism (ChRM) was syn-depositional in age and constrained the Elatina glaciation to an equatorial paleolatitude (<10°) (Sumner et al. 1987). A stratigraphically consistent polarity reversal test confirmed the primary component of ChRM in the Elatina Fm. and suggested a paleolatitude of 2.7 ± 3.7° (Schmidt et al. 2009). Raub and Evans (2008) and Schmidt et al. (2009) found a steeper mean inclination for the Nuccaleena Fm. of 27°, possibly due to the less-compacted carbonate lithology, which results in a paleolatitude of 14 ±

2º (Evans and Raub 2011). The syn-sedimentary fold test represents the most reliable paleomagnetically derived low-latitude constraint for a late Cryogenian glacial deposit. The 'fold' structures used are spaced ~50 cm apart within the rhythmite facies, have been documented in Warren Gorge and Pichi Richi Pass, and have been interpreted as gravity slides that were triggered by storm waves (Williams 1996).

The existence of multiple reversals suggests that the Elatina glacial epoch lasted for several $10^5$ to a few $10^6$ years (Schmidt and Williams 1995; Sohl et al. 1999). Similarly, multiple magnetic reversals recorded in the Nuccaleena Fm. cap dolostone suggest that it took $>10^5$ yrs for its deposition (Trindade et al. 2003; Kilner et al. 2005; Raub and Evans 2006; Schmidt et al. 2009). However, the giant wave ripples present in cap dolostone units around the world indicate extremely fast aggradation (Hoffman et al. 2007; Raub and Evans 2008; Lamb et al. 2012). This sedimentological constraint implies that the multiple polarity chrons in the Nuccaleena Fm. are perhaps not true reversals but are a rare recording of geomagnetic excursions that can occur in less than ~2 ky (Gubbins 1999; Hoffman et al. 2007). Thus the timescale for the duration of the Elatina glacial epoch remains controversial.

Although carbonate carbon and bulk organic carbon records have played key roles in understanding the pre-glacial (Rothman et al. 2003; Fike et al. 2006; Swanson-Hysell et al. 2010; Rose et al. 2012) and post-glacial carbonate succession (Hoffman et al. 1998; Grotzinger et al. 2000; Kennedy et al. 2001; Hoffman and Schrag 2002; Higgins and Schrag 2003; Hoffman et al. 2007; Rose and Maloof 2010), few studies have looked beyond the sedimentology with regard to the glacial diamictite units. The Chemical Index of Alteration (CIA) is a weathering proxy that uses ratios of major elements in siliciclastic rocks (Nesbitt and Young 1982, 1989; Fedo et al. 1995; McLennan et al. 1993; Nesbitt and Young 1996; Colin et al. 1998; Corcoran and Mueller 2002; Sheldon et al. 2002; Scheffler et al. 2003). High CIA values reflect the removal of mobile cations ($Ca^{2+}$, $Na^{+}$, $K^{+}$) relative to stable residual constituents ($Al^{3+}$, $Ti^{4+}$) during chemical weathering, which is enhanced during humid and warm climate conditions. In contrast, low CIA values indicate the near absence of chemical weathering, and consequently might reflect cool and/or arid conditions. Such compositional variation of siliciclastic rocks has been used to evaluate Paleoproterozoic, Cambro-Ordovician, Neogene and Quaternary glaciations (Krissek and Kyle 1998; Young 2002; Dobrzinski et al. 2004; Bahlburg and Dobrzinski 2011). Several Cryogenian glacial successions record low CIA values within the glacial diamictites and relatively high CIA values in intercalated siltstone, including the Port Askaig Fm., Scotland (Panahi and Young 1997), the Nantuo Fm., South China (Dobrzinski et al. 2004), the Huqf Fm., Oman (Rieu et al. 2007c) the Smalfjord and Mortensnes Fms., northern Norway, and Ghaub Fm., Namibia (Bahlburg and Dobrzinski 2011). However, this geochemical proxy has not been performed on the siliciclastic-dominated glacial Elatina Fm., or assessed in multiple sections across a basin to determine the variable role of provenance, diagenesis, and grain size on CIA values.

The ARC provides a unique opportunity to examine the three-dimensional paleo-landscape and the evolution of the glaciation that may allow us to test specific predictions of the snowball Earth hypothesis. We aim to establish the extent of sub-glacial erosion and advance–retreat cycles to test the predictions of a cold-based ice sheet, an attenuated hydrological cycle, and rapid onset and deglaciation assumed to be required by a snowball Earth. We aim to determine the provenance of the glacially transported sediments to test the snowball Earth prediction that the onset of the glaciation in the tropics is represented by the advance of sea-ice onto the continents (Hoffman et al. 2002). Furthermore, we aim to establish if open water existed on shallow platforms during the Marinoan glaciation, which has been cited in opposition to the 'hard' snowball Earth model. Such an open water scenario would be compatible with a Jormungand climate state where a thin strip of the tropical ocean remains exposed (Abbot et al. 2011).

In this paper, we present detailed sedimentological observations paired with high resolution $\delta^{13}C$ and major element data from the pre-glacial carbonate platform and syn-glacial sediments of the Marinoan glaciation across the ARC, South Australia. We quantify the degree of erosion, characterize the provenance, and establish the style of the glaciation across the basin. A total of 47 stratigraphic sections document the syn-glacial facies that corroborate the seminal work of Lemon and Gostin (1990), and extend analysis to the entirety of the basin. We document a regression within the upper Elatina Fm. that suggests that the regional deglaciation occurred on the timescale of gravitational withdrawal (instant) and/or isostatic rebound (~$10^4$ years). We propose that the 'soft-sediment folds' in the rhythmite facies across the ARC are combined-flow ripples, which attest to open seas with significant fetch during the initial retreat of local glaciers. The current and wave ripples also cast doubt on the veracity of the syn-depositional paleomagnetic constraint, requiring that the low-latitude direction only need be pre-Late Cambrian folding in age. We quantify the amount of glacial truncation across the platform from 29 $\delta^{13}C$ chemostratigraphic sections through the pre-glacial carbonate platform. This work allows correlation of formations across facies transitions to unify and simplify the pre-existing stratigraphic classifications across the basin. We show that $\delta^{13}C$–$\delta^{18}O$ values for 269 carbonate clasts within the diamictite were acquired before glacial erosion, and that deep glacial incision into the carbonate platform likely was responsible for exhumation of clasts that record the full stratigraphic range in $\delta^{13}C$ values. We present detrital zircon data from the ARC and Stuart Shelf to establish possible temporal and spatial changes in the provenance of the glacial sediments. Finally, we present new bulk compositional data (major elements) from 13 sections to test whether CIA records are coherent basin-wide, and may record paleo-weathering intensity, or whether the CIA proxy is controlled by the secondary processes of sorting and/or diagenesis.

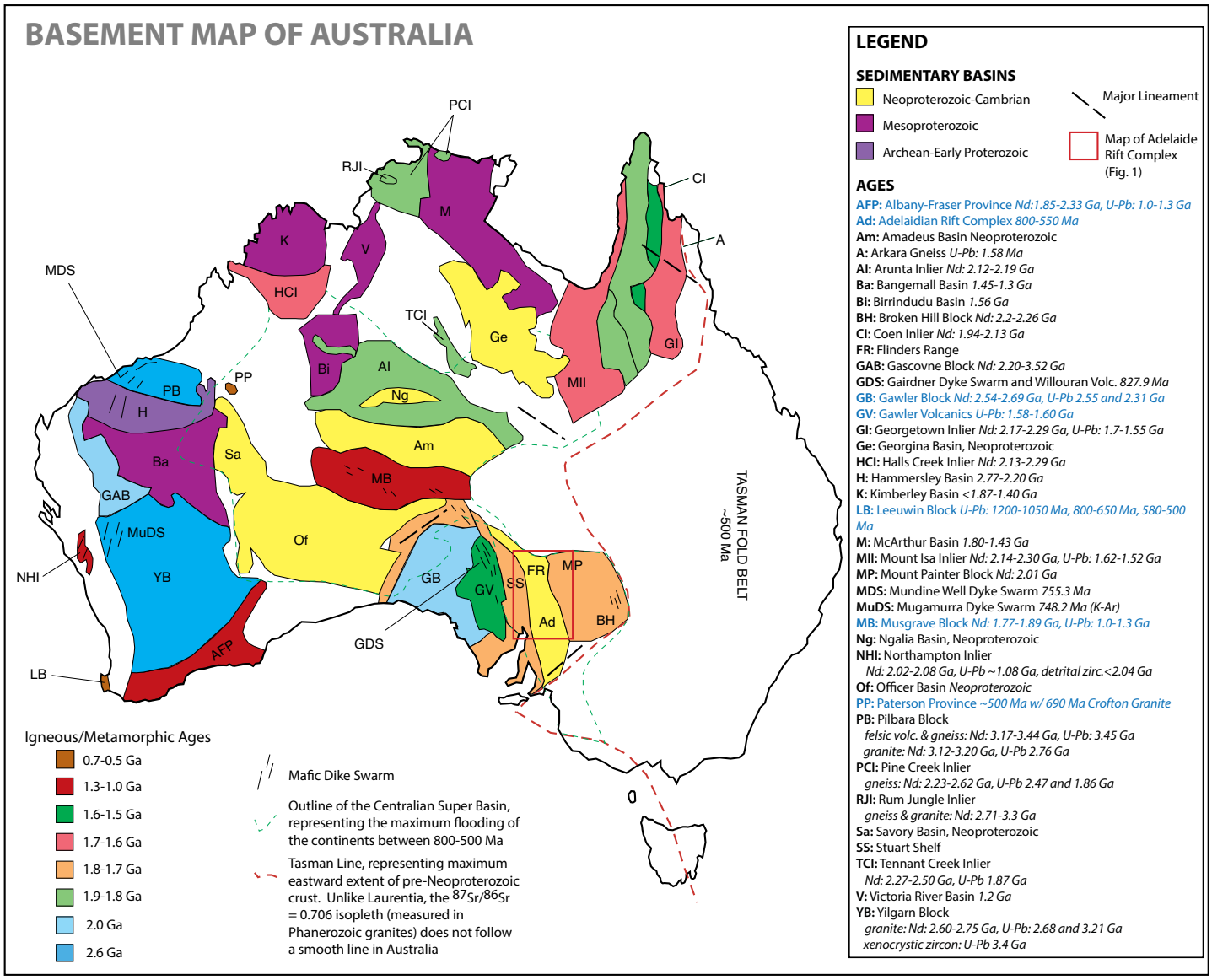


**Figure 2.** Map of Australia denoting the ages of basement complexes and outlining the Precambrian sedimentary basins. The U–Pb ages of the Gawler Craton and Adelaide Rift Complex (ARC), as well as the Musgrave Block, Albany-Fraser Province, Paterson Province, and Leeuwin Block, are highlighted in blue in the key (adapted from Pell et al. 1997).

## GEOLOGICAL BACKGROUND

The Adelaide Rift Complex (ARC) is part of a continental margin formed to the present-day east of the Stuart Shelf (Preiss 2000; Fig. 1a). The basement beneath the Gawler Craton to the west of the ARC is composed of late Archean–early Mesoproterozoic magmatic lithologies and metasedimentary rocks (Fig. 2). Similarly, the Curnamona Province to the east, and the Mt. Painter Inlier to the south of the ARC consist of Paleoproterozoic–Mesoproterozoic granite, gneiss and metasedimentary rocks (Willis et al. 1983; Preiss 2000; Compston et al. 1966; Coats and Blisset 1971; Teale 1993; Elburg et al. 2001). The basement beneath the ARC has only limited exposure but may be a distinctly younger geological province than most of the Gawler Craton (Preiss 2000). It is likely that there was a late Paleoproterozoic precursor basin occupying much the same area as the Neoproterozoic ARC, with sedimentation and volcanism between ~1.75–1.65 Ga, and orogeny at ~1.6 Ga (Preiss 2000).

Paleoproterozoic to Mesoproterozoic cratonic basement of the ARC is overlain by a 7-12 km thick Neoproterozoic to Cambrian sedimentary package that is subdivided into four units: the Callana, Burra, Umberatana and Wilpena Groups (Preiss 1987, 2000). The ARC was a zone of deep subsidence, punctuated by episodes of syn-sedimentary faulting and diapiric mobilization of Callanna Group evaporites (Preiss 1987; Fig. 1b). Neoproterozoic sediment accumulation is attributed to a succession of rift and thermal subsidence phases, with the main rifting commencing at ~827–802 Ma (Fanning et al. 1986; Jenkins 1990; Wingate et al. 1998). It is not known exactly when rifting terminated, but large-scale crustal normal faulting is thought to have diminished by the Cryogenian Period (Preiss 2000). Deposition ceased and the sedi-

mentary rocks were folded during the Cambro-Ordovician Delamerian orogeny (ca. 514–490 Ma; Drexel and Preiss 1995; Foden et al. 2006) to create a region of elevated topography forming the Flinders and Gammon Ranges (Thomson et al. 1964).

## Stratigraphy of the Adelaide Rift Complex

The Burra Group consists of basal carbonate rocks with evaporite and clastic units (Preiss 1987), and the Umberatana Group is characterized by a ~4.5 km thick interglacial succession bounded by the older Sturtian-equivalent and younger Marinoan-equivalent glacimarine deposits (Fig. 1b). These glacial deposits within Australia are referred to as the 'Sturt' and 'Elatina' glaciations respectively, because these terms are consistent with local stratigraphy (Williams et al. 2008). The Wilpena Group records the end-Cryogenian post-glacial sequence, which then shallows upwards in two parasequences from deep marine siltstone to shallow marine sandstone. These sequences are followed by transgressive Early Cambrian shallow-marine sandstone and deeper water carbonate and shale (Preiss 1987).

The interglacial succession between the Sturtian and Marinoan glacials of the Umberatana Group consists of the Tapley Hill Fm., Etina Fm., Enorama Fm., and Trezona Fm. (Fig. 3). The Tapley Hill Fm. consists of dark grey, laminated siltstone deposited during the post-Sturt glacial sea level rise. This unit shoals up into the Etina Fm., which consists of shallow marine sandstone, grey cross-bedded oolitic grainstone and sandy limestone, and microbial reefs interbedded with green dolomitic siltstone and shale (Fig. 4a). The base of the Enorama Fm. marks a major flooding surface and consists of finely laminated grey-green and minor red shale with minor fine sandstone beds. To the north, the nomenclature for the Tapley Hill–Enorama Fm. stratigraphy consists of the Balcanoona, Yankaninna, and Amberoona Fms. (Preiss et al. 1998; Fromhold and Wallace 2011; Fig. 3). The extent to which these formations are laterally correlative to one another and to the stratigraphy within the central Flinders Ranges is debated.

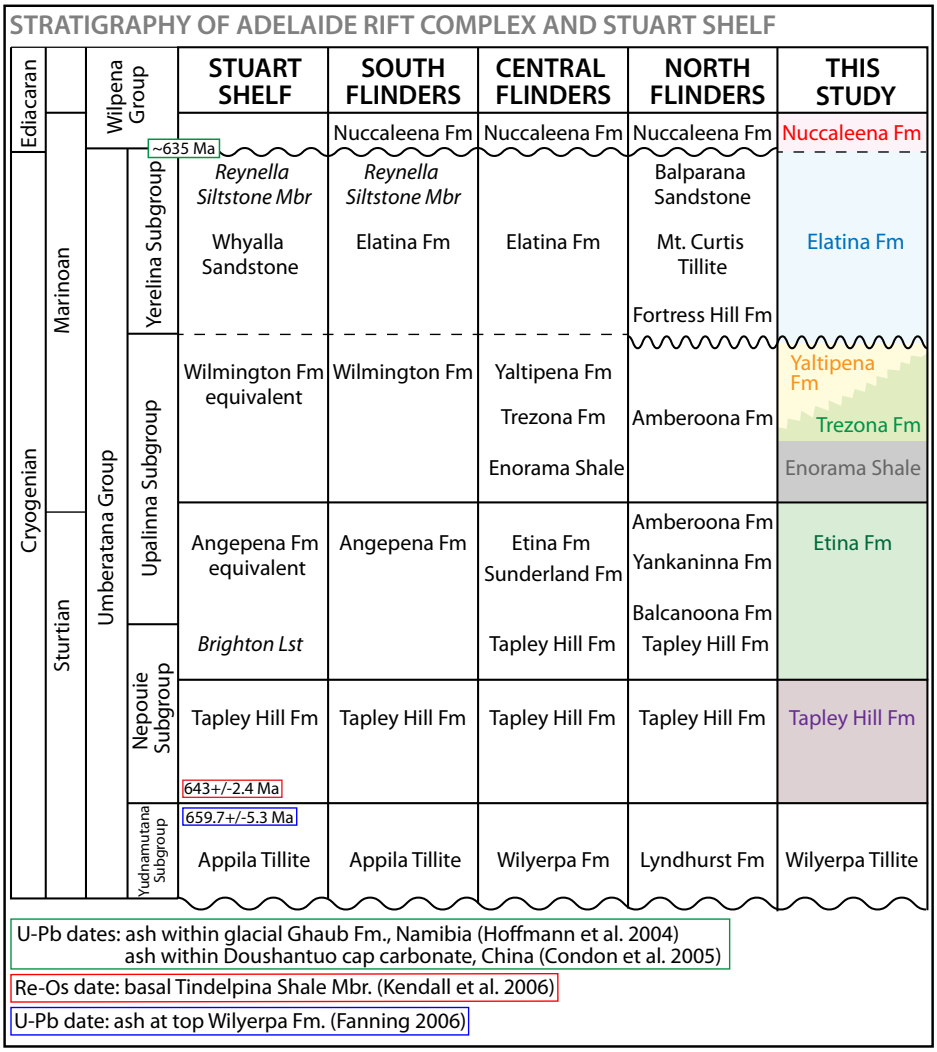


**Figure 3.** Cryogenian stratigraphy of the Adelaide Rift Complex (ARC) and neighbouring Stuart Shelf (modified from Preiss et al. 1998). The two Cryogenian glacially related series represent lower and upper deposits of the Umberatana Group and are assigned to Sturtian and Marinoan time divisions (Preiss et al. 1998). Note the name changes between each area in South Australia, which historically has made detailed correlations of the interglacial stratigraphy difficult. The final column outlines the formation names that are used in this study for the end-Cryogenian interglacial–glacial stratigraphy across the entire ARC in an attempt to simplify and unify current nomenclature.

The Enorama Fm. is followed by a gradual coarsening and shoaling-upward sequence that culminates in intraclastic limestone breccia, stromatolite bioherms, oolitic grainstone and siltstone of the Trezona Fm. The Trezona Fm. contains putative fossil debris in packstones that onlap and drape the stromatolite bioherms and that have been interpreted as sponge-grade metazoan body fossils (Maloof et al. 2010). Detailed mapping and 26 measured stratigraphic sections show that the Trezona carbonate facies record a progressive deepening towards the north of the ARC (Rose et al. 2012; Fig. 1). In the south, the temporal equivalent of the pre-glacial Trezona Fm. is a thick, dark red, mud-cracked sandstone and siltstone deposit with medium-coarse grit lenses (Yaltipena Fm.; Fig. 4b–d). These sedimentary units inter-finger with the nearshore channelized limestone grainstones, stromatolites and associated facies of the Trezona Fm. in the central region (Fig. 4e, f), and transition to stormy outer shelf carbonate ribbonite and grey-green calcareous shale in the north (Fig. 4g). The overlying syn-gla-

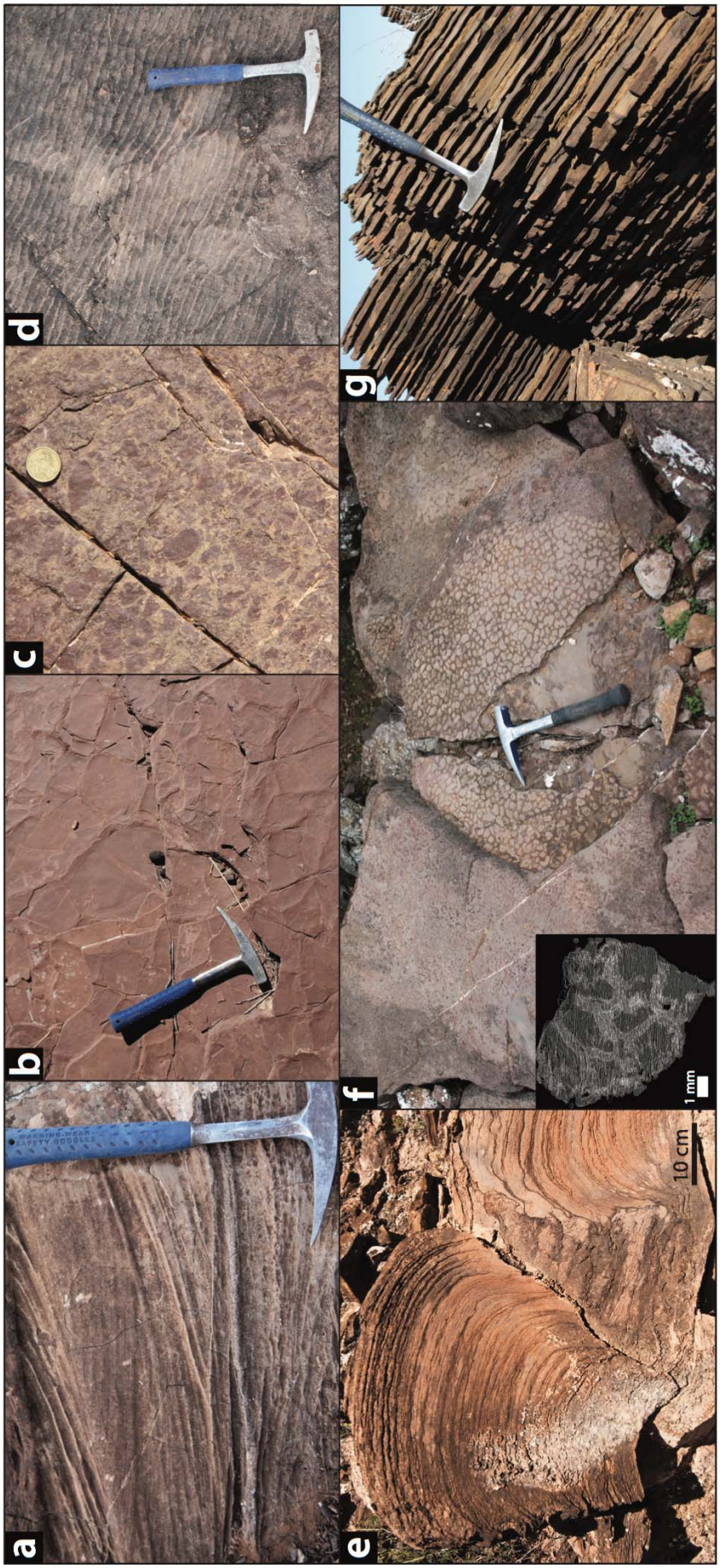


**Figure 4.** Sedimentology of the pre-glacial Trezona and Yaltipena Fms. (a) Cross-bedded coarse grainstone with quartz grains within the interglacial sedimentary rocks of the Etina Fm., Moolooloo (Fig. 1 [24]). (b-d) Mud-cracked siltstone, mud-chip breccia and symmetric micro-wave ripples within the Yaltipena Fm. at Trezona Bore, indicating intermittent subaerial exposure and very shallow water, respectively. (e) Stromatolites within the pre-glacial Trezona Fm., Trezona Ranges (Fig. 1 [18]). (f) Outcrop of the Trezona Fm. showing putative skeletal morphologies in fossil debris onlapping and draping a stromatolite bioherm (under the 30 cm long hammer) (Maloof et al. 2010; Fig. 1 [18]). A 3D reconstruction of one such fossil is shown in the inset image. (g) Interbedded carbonate ribbonite and grey-green calcareous shale of the Trezona Fm. in the northern Flinders Ranges, Umberatana (Fig. 1 [40]).

cial Elatina Fm. exhibits impressive facies variability, from marine sandstones in the south, to ice-contact tillites, fluvioglacial and shallow marine sandstones in the central region, and debris flows and turbidites in the north (Coats 1981; Preiss 1987; Eyles et al. 2007; Fig. 5). To the west, the Elatina Fm. transitions to the periglacial-eolian Whyalla Sandstone on the Stuart Shelf (Williams and Tonkin 1985; Williams 1986, 1994). The Elatina–Nuccaleena Fm. contact marks the onset of the post-glacial transgression, the base of the Wilpena Group (Williams 1977; Plummer 1979; Dyson 1992; Kennedy 1996) and the beginning of the Ediacaran Period (Knoll et al. 2006). The Nuccaleena Fm. consists of buff-colored dolomite grainstone that is overlain by red laminated siltstone and fine-grained sandstone of the Brachina Fm.

Many irregular breccia bodies mapped throughout the ARC have been interpreted as syn-sedimentary diapirs (Webb 1960; Coats 1965; Dalgarno and Johnson 1968). These bodies formed by the intrusion of evaporite from the Callana Beds with subsequent dissolution near the surface, leaving a cap of insoluble interbeds and other rocks dragged to the surface by halite. Active salt diapirism is thought to have occurred at least throughout the deposition of the Etina Fm. and lower two thirds of the Enorama Fm. (Lemon 2000). Thickening of these formations towards the diapir in the central Flinders Ranges, which is particularly evident at the northern fold axis of the central anticline, shows that this interval was a time of active salt withdrawal and diapir growth (Lemon 2000; Fig. 1a).

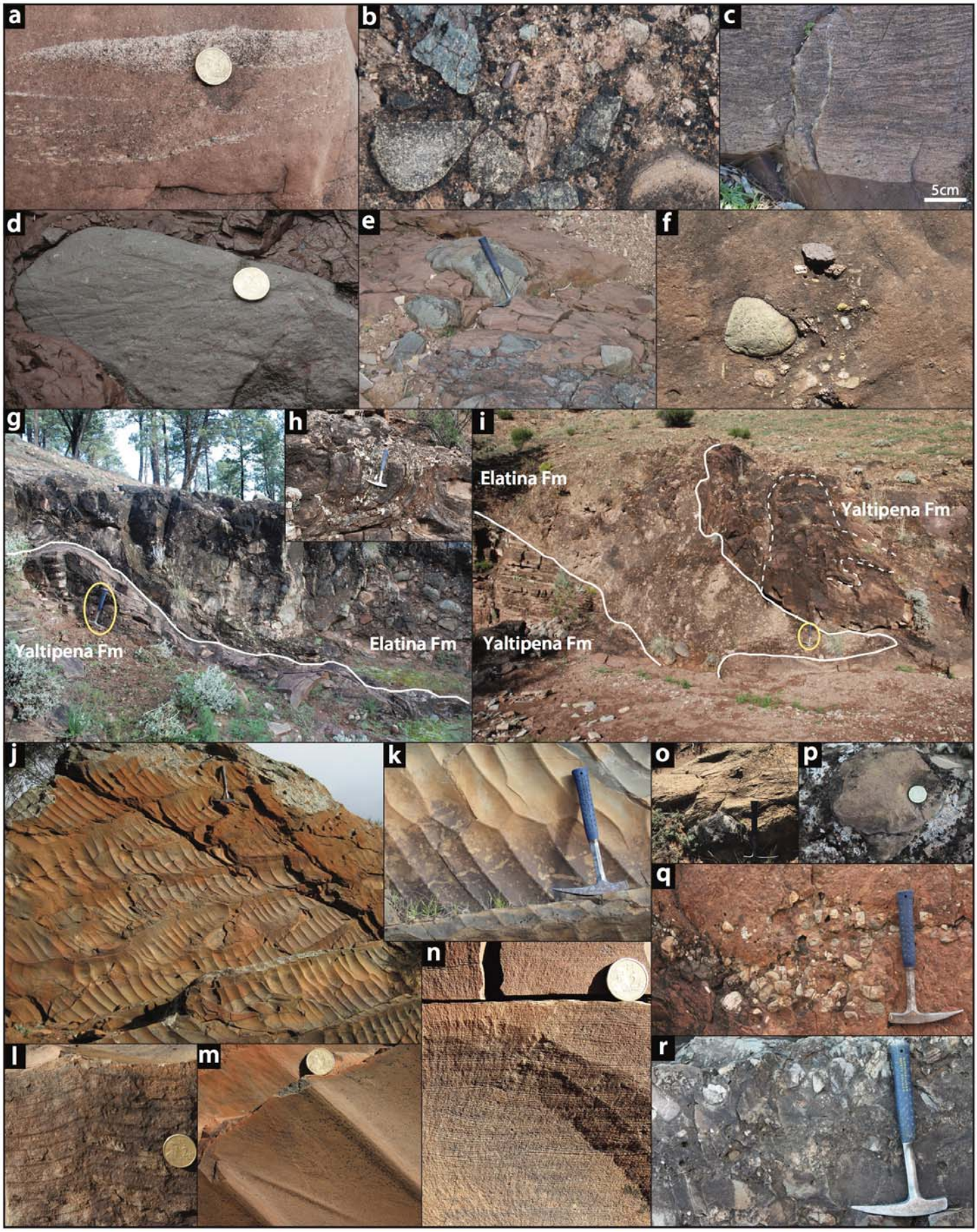
a
b
c
5cm
d
e
f
g
h
i
Elatina Fm
Yaltipena Fm
Yaltipena Fm
Elatina Fm
Yaltipena Fm
j
k
o
p
q
n
l
m
r

**Figure 5.** *(previous page)* Sedimentology of the syn-glacial Elatina Fm. (a) Coarse grit lenses and trains within a pink slumped sandstone of the Elatina Fm., Elatina Creek (Fig. 1 [17]). (b) Poorly sorted diamictite with angular and facetted clasts of a range of basement lithologies within a red silt matrix, Trezona Bore (Fig. 1 [18]). (c) Ripple cross-laminated sandstone derived from the reworking of underlying diamictite, Bunyeroo Gorge (Fig. 1 [15]). (d) Glacially striated green microgabbro clast within red silt matrix of diamictite, Trezona Bore (Fig. 1 [18]). (e) Plan view of green basalt clasts forming lag deposits within red silt matrix of diamictite, Bulls Gap (Fig. 1 [22]). (f) Plan view of lag within coarse, poorly sorted, pink slumped sandstone, Trezona Bore (Fig. 1 [18]). (g) Elatina Fm. diamictite resting unconformably on tidal flat sandstone of the Yaltipena Fm. as a result of ice-contact deposition, Trezona Bore (Fig. 1 [18]). (h) Soft-sediment deformation in the upper sandstone of the Elatina Fm., Trezona Bore. (i) Sub-glacial push structure lying unconformably on the Yaltipena Fm. (right of image) at Trezona Bore. Note hammer for scale (circled). The scoured basal contact and contorted diamictite beds indicate local ice-contact deposition. (j) Wave ripples within the upper Elatina Fm., Warren Gorge (Fig. 1 [4]). (k) Plan view of geometric bifurcations of secondary ripples, Warren Gorge (Fig. 1 [4]). (l) Cross-section through large-scale ripple showing lamination bundles and couplets in the southern Flinders Ranges, Warren Gorge (Fig. 1 [4]). (m) Plan view of grainflow originating from crest of a ladder ripple, Warren Gorge (Fig. 1 [4]). (n) Cross-section of lamination couplets in the northern Flinders Ranges, Oodnaminta Hut (Fig. 1 [33]). (o) Granitoid clast within microbialite bioherm of the Trezona Fm. at Punches Rest (Fig. 1 [36]). (p) Trezona Fm. fossiliferous packstone clast within the glacial diamictite of the Elatina Fm., near Oodnapanicken Bore (Fig. 1 [32]). (q) Diamictite of the Curtis Tillite with quartzite, granite, basalt, and rare dolomite clasts, near Mt. Curtis (Fig. 1 [44]). (r) Diamictite reworked by graded debris flows within the Elatina Fm., Billy Springs (Fig. 1 [47]).

### Radiometric Age Constraints

There are no direct age constraints for the onset or duration of the Elatina Fm. A SHRIMP U–Pb zircon age of 659.7 ± 5.3 Ma from a tuffaceous horizon in the Wilyerpa Fm., just above the Appila (Sturtian) diamictite, provides a maximum age for the base of the interglacial sedimentary rocks (Fanning 2006). A black shale in the Tindelpina Shale Member of the lowermost Tapley Hill Fm. has given a Re-Os age of 643.0 ± 2.4 Ma (Kendall et al. 2006). The post-glacial Nuccaleena Fm. 'cap dolostone' may be ~635 Ma. This age is determined by correlating the formation, based upon sedimentology and chemostratigraphy, to the late Cryogenian glacial deposit and base-Ediacaran cap dolostone in Namibia (635.5 ± 0.6 Ma; Hoffmann et al. 2004) and South China (635.2 ± 0.6 Ma; Condon et al. 2005), respectively, where zircons collected from ash deposits intercalated within the formations have been dated using the U–Pb system.

## METHODS

### Chemical Index of Alteration Methods

The chemical index of alteration (CIA) is a proxy for evaluating paleoclimatic conditions using ratios of major elements in siliciclastic rocks (Nesbitt and Young 1982, 1989; Fedo et al. 1995; McLennan et al. 1993; Nesbitt and Young 1996; Colin et al. 1998; Corcoran and Mueller 2002; Scheffler et al. 2003), and is expressed as:

$$CIA = \frac{Al_2O_3}{Al_2O_3 + K_2O + Na_2O + CaO^*} \times 100 \quad \text{(Eq.1 )},$$

using molar proportions. CaO* represents CaO present in silicate minerals, as opposed to carbonate or phosphate minerals (Nesbitt and Young 1982). CIA is expressed as a dimensionless number between 0 and 100.

X-ray fluorescence (XRF) determination of the major element compositions of 63 samples ($Li_2B_4O_7$-fused glass pellets) was carried out at Michigan State University using a Bruker AXS S4 Pioneer instrument. Inorganic carbon content of each sample was determined at Northwestern University using a UIC CM5012 Coulometer. The results were used to calculate the carbonate-derived calcium content (wt %). XRF analyses for the remaining 70 samples were made at Actlabs using a Panalytical Axios Advanced wavelength dispersive XRF spectrometer. Inorganic carbon content of each sample was determined at Actlabs using an Eltra CW-800 analyzer and the coulometric technique. The results were used to calculate the carbonate-derived calcium content (wt %). For all samples, the dolomite and calcite molar ratio was determined using X-Ray Diffraction (XRD) analysis by a Rigaku MiniFlex XRD at Princeton University.

### $\delta^{13}C$ Methods

Carbonate rocks were sampled at ~1.0 m resolution from 23 measured stratigraphic sections from across the ARC. Clean dolostone and limestone without siliciclastic components, secondary veining or cleavage were targeted. A total of 2439 samples were slabbed and polished perpendicular to bedding and 5 mg of powder were microdrilled from individual laminations for isotopic analysis. Note that data from 1042 of these samples have been previously published in Rose et al. (2012). At the University of Michigan Stable Isotope Laboratory, all powders were heated to 200ºC to remove volatile contaminants and water. Samples were then placed in individual borosilicate reaction vessels and reacted at 76ºC with 3 drops of $H_3PO_4$ in a Finnigan MAT Kiel I preparation device coupled directly to the inlet of a Finnigan MAT 251 triple collector isotope ratio mass spectrometer. $\delta^{13}C$ and $\delta^{18}O$ data were acquired simultaneously and are reported in the standard delta notation as the ‰ difference from the VPDB standard. Measured precision was maintained at better than 0.10‰ (1σ) for both $\delta^{13}C$ and $\delta^{18}O$. At Princeton University, all carbonate powders were heated to 110ºC to remove water. Samples were then placed in individual borosilicate reaction vials and reacted at 72ºC with 5 drops of $H_3PO_4$ in a GasBench II preparation device coupled directly to the inlet of a Thermo DeltaPlus continuous flow isotope ratio mass spectrometer. $\delta^{13}C$ and $\delta^{18}O$ data were acquired simultaneously and are reported in the standard delta notation as the ‰ difference from the

VPDB standard. Precision and accuracy of data are monitored through analysis of 21 standards that are run for every 59 samples. Measured precision is maintained at better than 0.10‰ (1σ) for both $\delta^{13}C$ and $\delta^{18}O$.

### Geochronology Methods

Twelve zircon concentrates were separated from 2 to 4 kg of sample material at the Senckenberg Naturhistorische Sammlungen Dresden using standard methods. Zircon grains of all grain sizes and morphological types were hand-picked, mounted and analyzed for U, Th, and Pb isotopes by LA–ICP–MS techniques at the Museum für Mineralogie und Geologie (GeoPlasma Lab, Senckenberg Naturhistorische Sammlungen Dresden), using a Thermo-Scientific Element 2 XR sector field ICP–MS coupled to a New Wave UP–193 Excimer Laser System. U–Th–Pb analyses were conducted for 15 s background acquisition followed by 30 s data acquisition, using a laser spot-size of 25 and 35 μm, respectively. A common-Pb correction based on the interference- and background-corrected $^{204}Pb$ signal and a model Pb composition (Stacey and Kramers 1975) was carried out if necessary. The necessity of the correction was judged on whether the corrected $^{207}Pb/^{206}Pb$ lay outside of the internal errors of the raw, measured ratios. Raw data were corrected for background signal, common Pb, laser-induced elemental fractionation, instrumental mass discrimination, and time-dependent elemental fractionation of Pb/Th and Pb/U using an Excel spreadsheet program developed by Axel Gerdes (Institute of Geosciences, Johann Wolfgang Goethe-University Frankfurt, Frankfurt am Main, Germany). Reported uncertainties were propagated by quadratic addition of the external reproducibility obtained from the reference zircon 'GJ-1' (~0.6% and 0.5-1% for the $^{207}Pb/^{206}Pb$ and $^{206}Pb/^{238}U$, respectively) during individual analytical sessions and the within-run precision of each analysis. All uncertainties are quoted at the 95% confidence or 2σ level. For further details on analytical protocol and data processing, see Gerdes and Zeh (2006).

Eleven zircon concentrates were separated from 2 to 4 kg of sample material at Princeton University using standard methods. These concentrates were annealed in an oven at 900ºC for 3 days before being mounted in resin blocks and polished to half their thickness. The zircon grains were analyzed for U, Th and Pb isotopes using a Laser Ablation Multi-Collector Inductively Coupled Plasma Mass Spectrometer (LA–MC–ICP–MS) system housed at the University of California, Santa Barbara. Instrumentation consists of a Nu Plasma MC–ICP–MS (Nu Instruments, Wrexham, UK) and a 193 nm ArF laser ablation system (Photon Machines, San Diego, USA). Analytical protocol is similar to that described by Cottle et al. (2009a,b,c). U-Th-Pb analyses were conducted for 15 s each using a spot diameter of 24 μm, a frequency of 4 Hz and 1.2 J/cm$^2$ fluence (equating to crater depths of approximately 4 μm). U–Th–Pb data from 4 samples were collected over 4 days of continuous instrument operation. A primary reference material, '91500' zircon (1065.4 ± 0.3 Ma $^{207}Pb/^{206}Pb$ ID–TIMS age and 1062.4 ± 0.4 Ma $^{206}Pb/^{238}U$ ID–TIMS age (Wiedenbeck et al. 1995)) was employed to monitor and correct for mass bias as well as Pb/U and fractionation. To monitor data accuracy, a secondary reference zircon 'GJ-1' (608.5 ± 0.4 Ma $^{207}Pb/^{206}Pb$ ID–TIMS age (Jackson et al. 2004) and 601.7 ± 1.3 Ma $^{206}Pb/^{238}U$ ID–TIMS age) was analyzed concurrently (once for every 5–7 unknown samples) and corrected for mass bias and fractionation based on measured isotopic ratios of the primary reference material. Analyses of the GJ-1 secondary reference zircon during the analytical period yielded a weighted mean $^{206}Pb/^{238}U$ age of 603.9 ± 0.6, MSWD = 0.9. Data reduction was carried out using Iolite version 2.1.2 (Paton et al. 2010). All uncertainties are quoted at the 95% confidence or 2σ level and include contributions from the external reproducibility of the primary reference material for the $^{207}Pb/^{206}Pb$ and $^{206}Pb/^{238}U$ ratios.

## RESULTS

### Sedimentology

#### *Pre-glacial Trezona and Yaltipena Formations*

In the central Flinders Ranges, the Elatina Fm. unconformably overlies the Trezona Fm. and the Yaltipena Fm. of the Upalinna Subgroup (Lemon and Gostin 1990; Lemon and Reid 1998). The Trezona Fm., as defined by Dalgarno and Johnson (1964), is mainly restricted to, and attains its maximum thickness, around the central anticline of the Flinders Ranges (Fig. 6). Pale red and grey thin interbedded silt, microbialite, and intraclastic breccia characterize the lower part of the Trezona Fm. These decimetre-thick parasequences typically contain gutter casts and rip-up clasts, indicating a storm-dominated shelf environment (Myrow 1992). Up-section, microbialite transitions into stromatolitic facies with stromatolite flake breccia and bioclast packstone filling the space between stromatolite heads with up to one metre of synoptic relief (Rose et al. 2012). The upper Trezona is dominated by large stromatolitic mounds and oolitic and intraclastic breccia limestone. Stromatolites within the Trezona Fm. commonly are large, round mounds up to several metres in height, but can be elongate lobate mounds with cuspate valleys between them (Fig. 4e). To the north, the Trezona Fm. consists of cm-thick limestone laminite deposited below storm wave base that alternate with greenish-grey laminated calcareous shale and siltstone (Fig. 4g). The amount of siltstone between these 'ribbonite' packages increases to the north, until at Tower Gap the Trezona Fm. reaches ~600 m in thickness with barely any limestone beds (Fig. 7 [38]). To the south, the Trezona Fm. interfingers with and transitions into the partially correlative Yaltipena Fm (Fig. 8).

The Yaltipena Fm. was first recognized and distinguished from the overlying Elatina Fm. by Dalgarno and Johnson (1964), leading to Bulls Gap being nominated as its type section (Lemon and Reid 1998). Previously, Lemon and Reid (1998) determined that the Yaltipena Fm. commences with a transgressive, red intraclastic conglomerate, comprised of flat discoidal pebbles of lithified micrite in a matrix of sand-sized intraclasts that is in disconformable contact with underlying stromatolitic, oolitic and intraclastic limestones of the Trezona Fm. However, this nominated bed is indis-

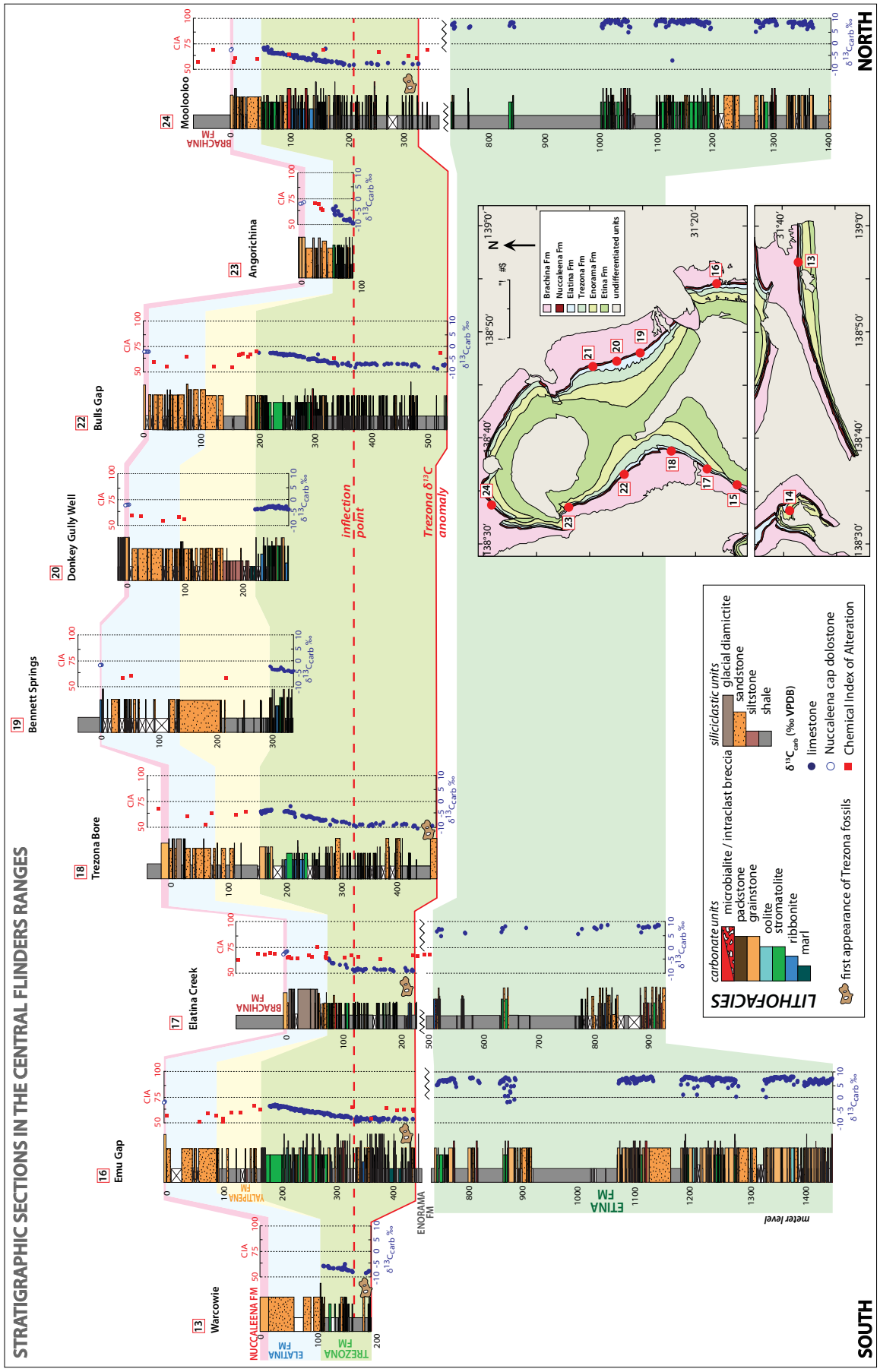


**Figure 6.** Selection of stratigraphic sections from the central anticline of the Adelaide Rift Complex (ARC) numbered to correspond with Figure 1. Pre-glacial $\delta^{13}C$ data within the Etina and Trezona Fms. are denoted by solid blue circles and $\delta^{13}C$ data within the post-glacial Nuccaleena Fm. cap dolostone are denoted by open blue circles (Rose and Maloof 2010). All sections are hung from a datum chosen at the inflection point at the base of the recovery from the Trezona negative $\delta^{13}C$ anomaly. The Yaltipena Fm. thins until it is missing entirely at the Warcowie [13], Elatina Creek [17], Angorichina [23], and Mooloolo sections [24]. Differential glacial erosion truncated the Yaltipena Fm. during the ice advance. Furthermore, the $\delta^{13}C$ data indicate truncation of the reproducible carbon isotopic trend in the Trezona Fm., thereby quantifying the degree and lateral variability of glacial erosion. Note that the Enorama Fm. consists of shale with no associated $\delta^{13}C$ data and therefore is not shown in the stratigraphic sections for clarity. The average thickness of the Enorama Fm. is ~300 m. The location of the mapped area within the ARC is outlined by a grey box in Figure 1.

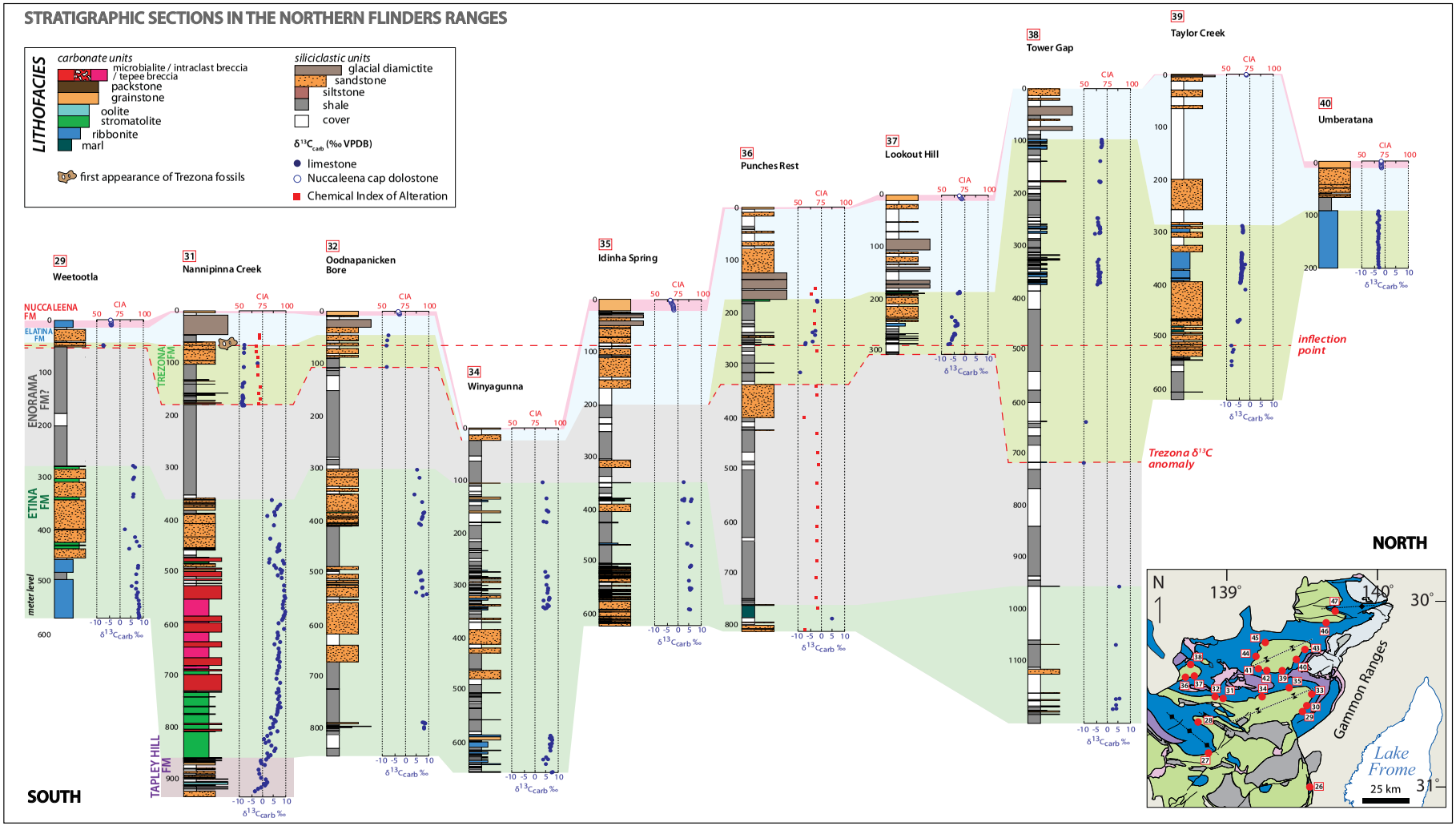


**Figure 7.** Stratigraphic sections of the northern Flinders Ranges numbered to correspond with Figure 1. Pre-glacial $\delta^{13}C$ data within the Etina and Trezona Fms. are denoted by solid blue circles and $\delta^{13}C$ data within the post-glacial Nuccaleena Fm. cap dolostone are denoted by open blue circles (Rose and Maloof 2010). All sections are hung from a datum chosen at the inflection point at the base of the recovery from the Trezona negative $\delta^{13}C$ anomaly. Fewer $\delta^{13}C$ data points in this region make correlations tentative when using this $\delta^{13}C$ inflection point. The Enorama Shale is of unknown thickness with contacts determined by the $\delta^{13}C$ values of the underlying Etina Fm. and overlying Trezona Fm. The location of the mapped area within the Adelaide Rift Complex is outlined by a grey box in Figure 1.

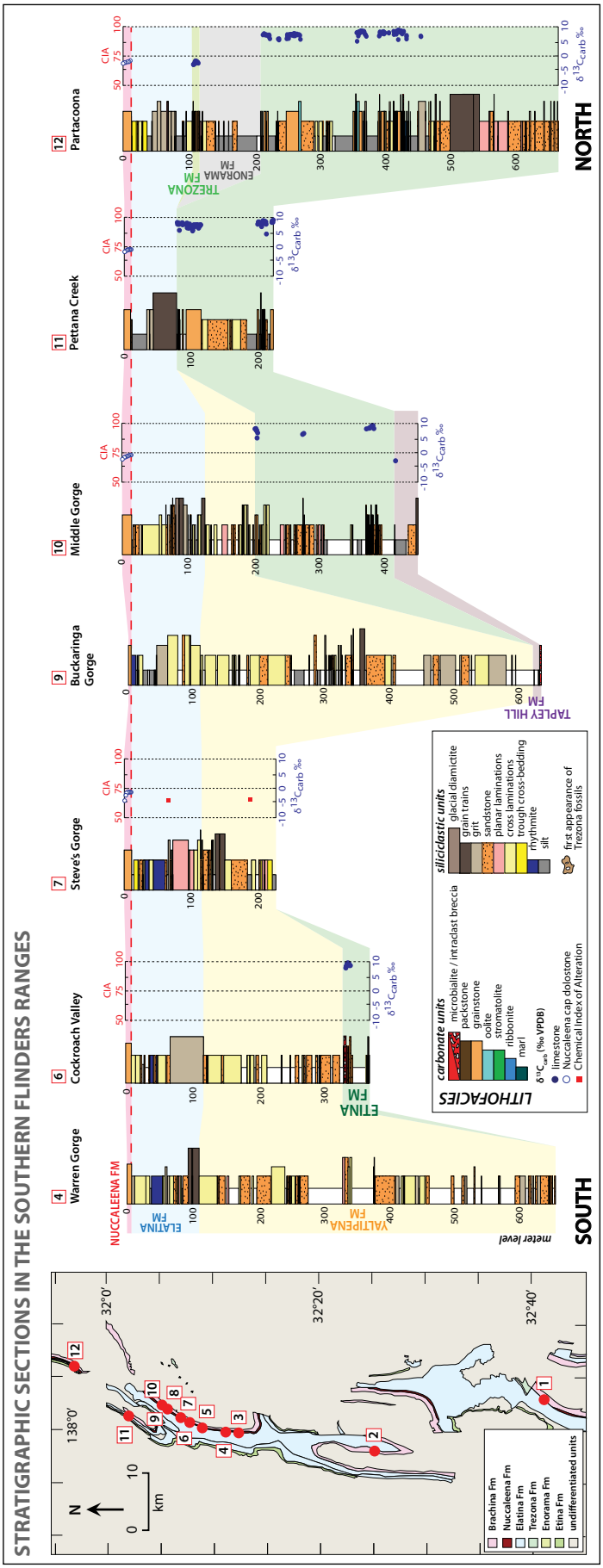


**Figure 8.** Selection of stratigraphic sections from the southern Flinders Ranges numbered to correspond with Figure 1. Pre-glacial $\delta^{13}C$ data within the Etina and Trezona Fms. are denoted by solid blue circles and $\delta^{13}C$ data within the post-glacial Nuccaleena Fm. cap dolostone are denoted by open blue circles (Rose and Maloof 2010). All sections are hung from a datum at the base of the Nuccaleena Fm. The location of the mapped area within the Adelaide Rift Complex is outlined by a grey box in Figure 1.

tinguishable from many of the intraclastic beds within the Trezona Fm. and the disconformity is not laterally continuous. We propose the base of the red siltstone to represent the beginning of the Yaltipena Fm.

The Yaltipena Fm. (<100 m) is a coarsening upwards sequence, with red siltstone grading upwards into very-fine sandstones that transition to medium-grained sandstones upsection (Lemon and Reid 1998). The base of the thick siltstone interval is characterized by low-amplitude starved ripples and lenticular bedding. Further up section, these beds become generally well-laminated and show many indications of shallow water, including small wavelength (~20 mm) symmetrical and linguoid ripples, planed-off ripples, ladder ripples, and interference ripples (Fig. 4d). Abundant desiccation cracks and possible raindrop impressions indicate intermittent subaerial exposure (Fig. 4b). Thin channels of clean, white quartz sandstone with mud rip-up clasts at the bases are the first indication of the coarser interval above the siltstone (Fig. 4c). These coarser sandstones are both planar and trough cross-bedded with foresets between 0.05-0.2 m thick. Glacial clasts up to 1 m across pierce the top of the Yaltipena Fm. and the upper contact typically is contorted and scoured (Fig. 5g, i).

In the southern Flinders Ranges, the Yaltipena Fm. (referred to locally as the Wilmington Fm.) consists of thinly bedded red siltstone, with mudchips, desiccation cracks, and short wavelength interference ripples, but the formation reaches a thickness of >500 m (Fig. 8). Near the base of the formation, rare discontinuous metre-scale stromatolite bioherms are present that likely are correlative to the Etina Fm. Towards the top of the formation, the siltstone layers coarsen up into grey-green and red-brown, fine to medium-grained well-sorted, planar cross-bedded quartzite, sandstone, sandy siltstone, and minor arkose. The Yaltipena Fm. progressively thins towards the central anticline and at Bulls Gap the basal contact is transitional as the red siltstone interfingers with the intraclast limestone of the upper few metres of the Trezona Fm. (Fig. 6 [22]). Therefore, the Yaltipena Fm. was being

deposited in the south during deposition of the Enorama and Trezona Fms. in the central anticline (Fig. 8).

## *Syn-glacial Elatina Formation*

### *Central Flinders Ranges*

A thin basal conglomerate and overlying massive boulder diamictite up to 5 m thick are present locally in the central Flinders Ranges. These discontinuous diamictite beds at the base of the Elatina Fm. are contorted, have a scoured basal contact, and contain large (~1 m) extrabasinal boulders of granitic gneiss that pierce the top of the underlying Yaltipena Fm. (Lemon and Gostin 1990; Fig. 5g-i; Fig. 9 [18, 19, 22]). Some of the clasts in the diamictite beds are faceted and striated, attesting to their glacially influenced deposition, with the striations typically oriented parallel to the long-axes of the clasts (Mawson 1949; Dalgarno and Johnson 1964; Preiss 1987; Lemon and Gostin 1990; Fig. 5b, d). This clast suite consists predominantly of basalt, well-rounded quartzite, and granitic gneiss.

The remainder of the glacial facies overlying these discontinuous diamictite beds can be traced across the central anticline of the Flinders Ranges (Fig. 1), and can be described by three distinct facies (Lemon and Gostin 1990): 1) a lower slumped sandstone; 2) a middle interval of dropstone diamictites; and 3) an upper interval of current reworked diamictite. The first facies consists of a suite of coarse, slumped sandstone beds that may directly overlie the basal unconformity at the base of the Elatina Fm. Approximately 5 m of channeled, cross-bedded, coarse-grained sandstone are present at the base of the unit (Lemon and Gostin 1990). This sandstone grades upwards into flaser-bedded, muddy sandstone, and is overlain by several 1 m beds with large ball-and-pillow structures (Lemon and Gostin 1990; Fig. 5h). Above this soft sediment deformation, lies a ~50 m thick interval of white, pink- to reddish-brown, poorly sorted feldspathic sandstone (Facies 1). These feldspathic sandstone beds contain sub-angular to sub-rounded quartz and feldspar grains, plus lithic fragments and heavy mineral grains (Preiss 1987), and gener-

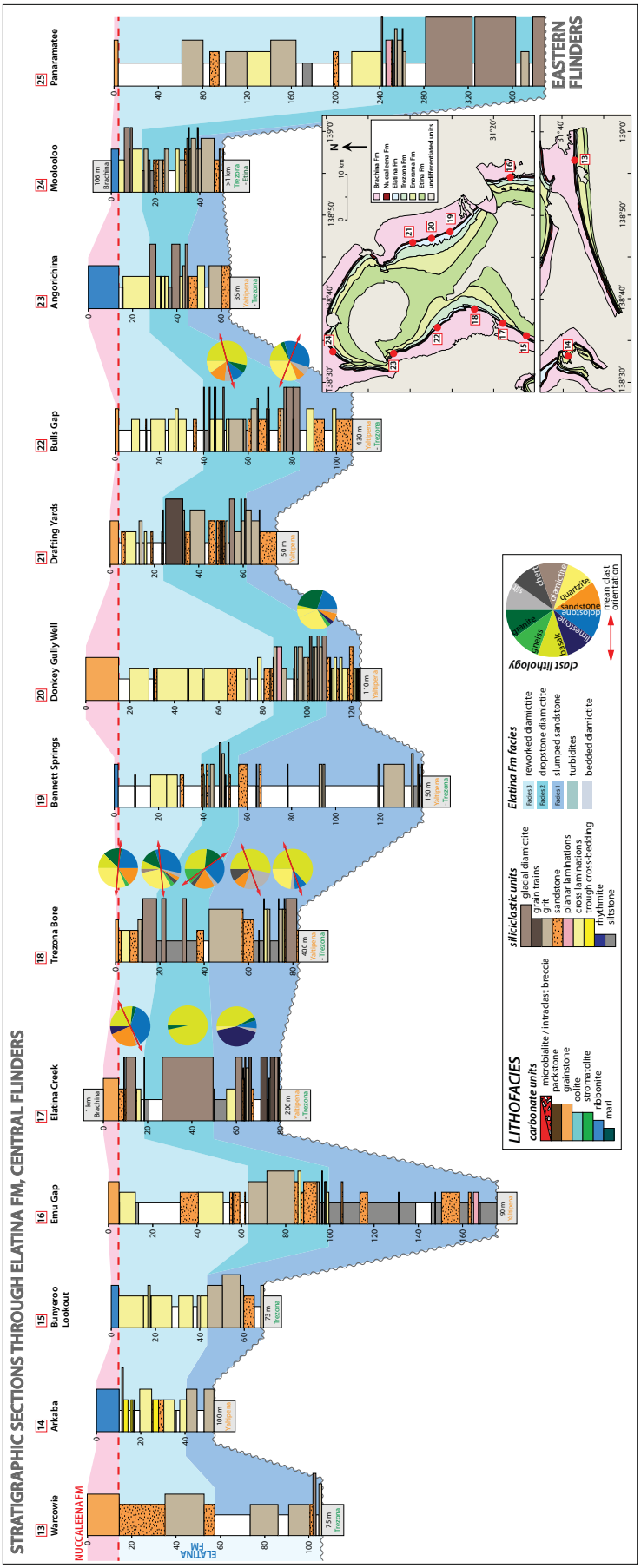


**Figure 9.** Detailed stratigraphic sections of the Elatina Fm. across the central Flinders Ranges numbered to correspond with Figure 1. The Elatina Fm. can be described by three distinct facies (Lemon and Gostin 1990): 1) a lower, coarse, slumped sandstone with contorted granule layers and trough cross-bedding; 2) a middle interval of well-laminated red siltstone dropstone diamictite; and 3) an upper interval of current-reworked diamictite with distinctive gravel lags and ripple cross-laminations. The overlying Nuccaleena Fm. cap dolostone varies from buff cross-stratified dolomite grainstone with m-scale giant wave ripples to red silty dolomite ribbonite with low-angle cross-stratified laminations (Rose and Maloof 2010). The 'ribbon' facies consists of swaley dolosiltite. All sections are hung from a datum at the base of the Nuccaleena Fm. The location of the mapped area within the Adelaide Rift Complex is outlined by a grey box in Figure 1.

ally are bimodal, marked by a dominance of coarse silt to fine sand and very coarse sand to granule fractions. The sandstones lack distinct bedding but have thin, discontinuous, and commonly contorted granule layers (Fig. 5a). The less deformed intervals contain slumped, trough cross-bedded sets up to 1 m thick with normal grading. Rare isolated pebbles to large oversized clasts also may be present in these sandstone layers, typically associated with dolomite, quartz and granite fragments.

The slumped sandstone beds grade upward into a massive to well-laminated red siltstone with a few dropstones (Facies 2). These diamictite beds are dominated by carbonate clasts that have been presumed to originate from the underlying Trezona Fm., and basalt clasts (Lemon and Gostin 1990). Finally, current-reworked diamictite beds dominate the top third of the Elatina Fm. (Facies 3). These diamictites have undergone significant reworking, creating prominent beds of distinctive gravel lags and lonestones capped by mm- to cm-scale ripple cross-laminated fine- to very fine-grained sandstone within an otherwise massive unit (Fig. 5c, f). Sections measured at the northern rim of the central anticline and between Elatina Creek and Trezona Bore record another diamictite at the top of the formation within the current-reworked interval (e.g. Moolooloo; Fig. 9 [24]). These beds contain basalt clasts and, in contrast to previous observations by Lemon and Gostin (1990) and Williams et al. (2008), we did not note clasts of ooid and algal limestone from the Trezona Fm. (Fig. 5e).

### North Flinders Ranges

Despite variations in thickness of each facies, the total thickness of the Elatina Fm. remains relatively uniform (~70–100 m) in the central anticline. However, to the east and north, the Elatina Fm. thickens to >300 m and eventually the diamictites transition into stratified debris flows and turbidites (Fig. 5q, r; Fig. 10). At Punches Rest, isolated rounded ~0.2–1.0 m diameter granite and gabbro clasts are incorporated within the upper two metres of a Trezona Fm. stromatolite bioherm that records the highest $\delta^{13}C$

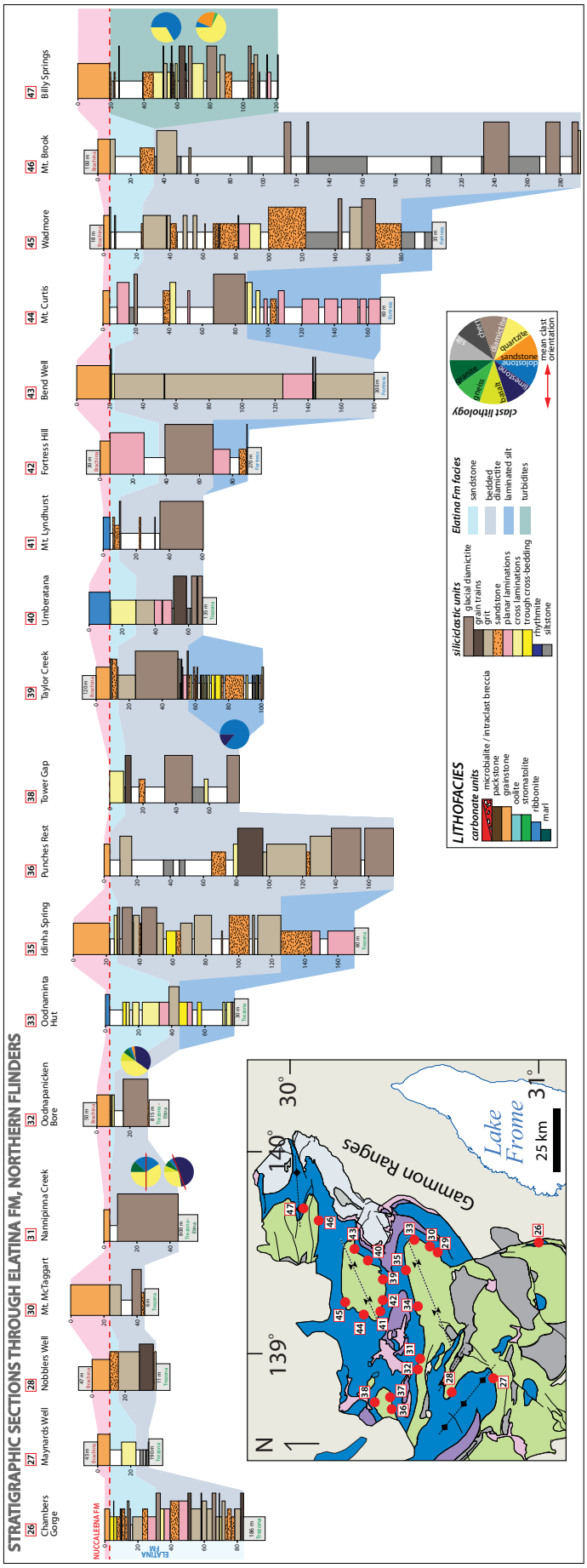


**Figure 10.** Detailed stratigraphic sections of the Elatina Fm. across the northern Flinders Ranges numbered to correspond with Figure 1. All sections are hung from a datum at the base of the Nuccaleena Fm. The location of the mapped area within the Adelaide Rift Complex is outlined by a grey box in Figure 1.

following the Trezona anomaly (Rose et al. 2012; Fig. 5o; Fig. 7 [36]). This layer is laterally discontinuous on the km-scale and has not been documented elsewhere.

Overall, there are three broad facies to the Elatina Fm. in the north Flinders Ranges: a laminated siltstone, a diamictite, and a coarse feldspathic sandstone. These three facies are laterally widespread but are not always all present at every locality. The first facies consists of grey-green (weathering reddish-brown), finely laminated siltstone with rare scattered pebbles, cobbles, and gritty lenses. Known as the Fortress Hill Fm., this siltstone is overlain sharply by sandstone and a diamictite layer. This diamictite is the second facies, referred to locally as the Mount Curtis Tillite, and consists of sparse lonstones of pebble- to boulder-size in a grey-green, massive and laminated, sandy siltstone matrix. Diamictite clast lithologies are mostly quartzite, limestone and dolostone, and less commonly granite and gneiss, and the long axes of clasts retain a general east-west orientation (Fig. 10 [31]). Some of the clasts are faceted and striated, and rare granite boulders may reach up to 3 m x 8 m (Williams et al. 2008). Sub-angular limestone packstone clasts of the Trezona Fm. (~20 cm), which contain distinctive skeletal fossil debris (Maloof et al. 2010), are present as clasts within the Elatina Fm. diamictite near Punches Rest and Oodnapanicken Bore (Fig. 5f). The third facies consists of pale grey and brownish grey, medium-grained, feldspathic sandstone with interbeds and lenses of calcareous siltstone and pebble conglomerate and overlies the Mt. Curtis Tillite (referred to locally as the Balparana Sandstone). The clasts are mostly of vein quartz, with some quartzite, siltstone and granite clasts. At Billy Springs, which is the most northern locality within the ARC, the Elatina Fm. consists of decimetre- to metre-thick reverse-graded turbidites that coarsen upwards from planar laminated fine sand to coarse sand with quartzite and sandstone clasts (Fig. 5q, r; Fig. 10 [47]).

### *South Flinders Ranges*

In the southern Flinders Ranges, the base of the Elatina Fm. is not always clear, but was taken to coincide with the first influx of lithic granules (Fig. 11). The formation can be split into a lower member of grey, fine sandstone with granule trains, a middle member of purple siltstone and fine sandstone with scattered coarse grains, and an upper member of pale grey, fine sandstone with trough cross-bedding (Jablonski 1975; Miller 1975). The middle purple siltstone member commonly grades into a planar laminated unit within the upper 50 m of the Elatina Fm. This facies outcrops almost continuously between Saltia Creek to Buckaringa Gorge, although the best exposure is at Warren Gorge where the unit is ~30 m thick. The following descriptions are based on observations made at Warren Gorge (Fig. 1 [4]).

The planar laminations consist of ~1–2 cm-thick bundles of thickening and thinning, normally graded very fine sandstone to siltstone couplets (Fig. 5l, n). The number of couplets within each bundle varies, however, fifteen is the maximum number per bundle. These rhythmites document a nested hierarchy of periodicities consistent with the number and relative thickness of couplets that are interpreted to be tidal in origin (Williams 1989, 1991, 1998, 2000). Superimposed on these laminae throughout the stratigraphy are three categories of bedforms, which are herein referred to as primary, secondary, and tertiary bedforms. The primary bedforms have the largest wavelength, typically between 20 and 40 cm, and a mean amplitude of 1.3 cm (n=44) (Fig. 12a). The bedforms are very slightly asymmetrical with a pale-

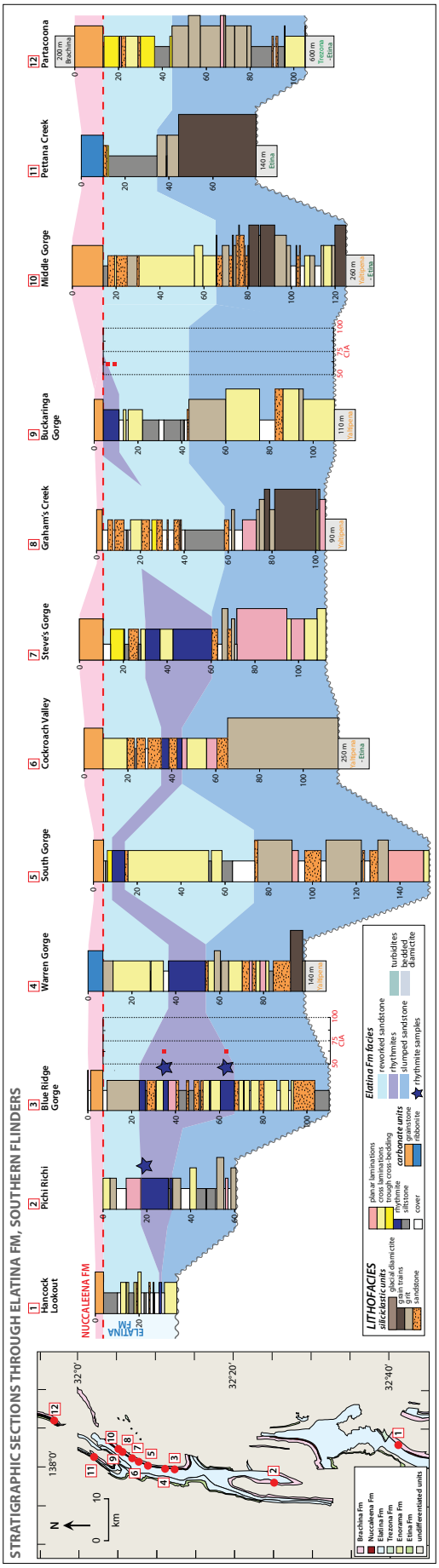


**Figure 11.** Detailed stratigraphic sections of the Elatina Fm. across the southern Flinders Ranges numbered to correspond with Figure 1. All sections are hung from a datum at the base of the Nuccaleena Fm. The location of the mapped area within the Adelaide Rift Complex is outlined by a grey box in Figure 1.

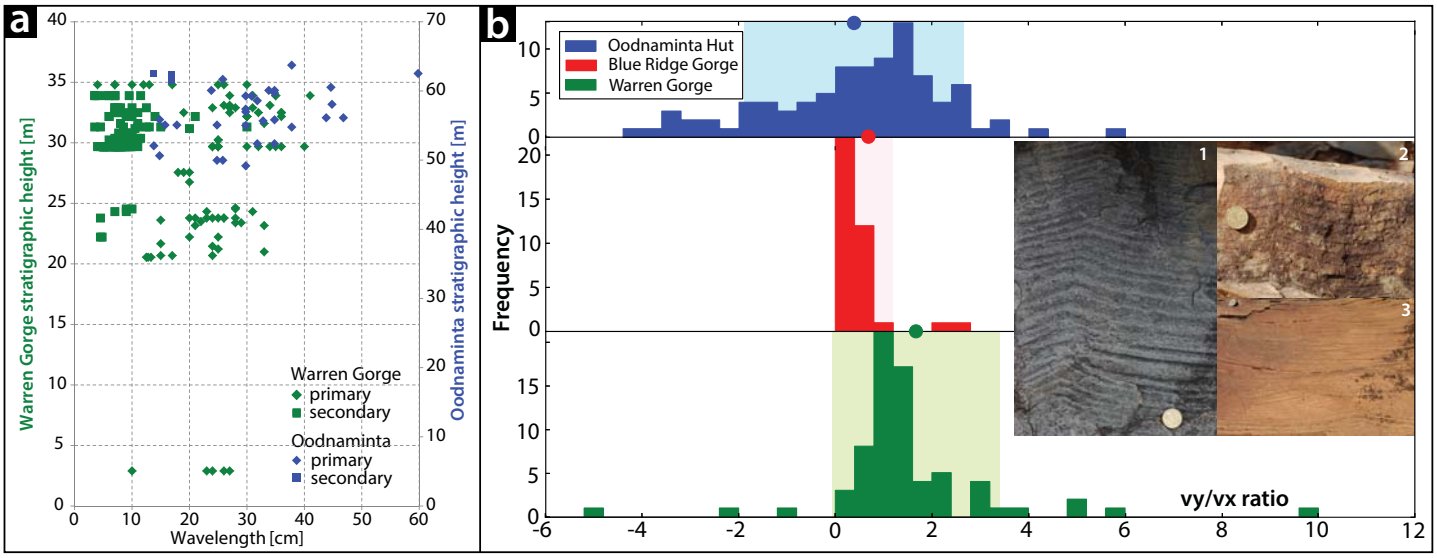


**Figure 12.** (a) Graph plotting the wavelengths for the primary and secondary ripples at Warren Gorge and Oodnaminta Hut versus stratigraphic height. (b) Histogram of bedform climbing vectors at Blue Ridge Gorge, Warren Gorge, and Oodnaminta Hut, where *vy* = rate of accumulation and *vx* = rate of migration determine the angle of climb of the bedforms (Rubin and Hunter 1982). Mean values are denoted with solid circles and 1σ errors are shown with a shaded box behind the histogram. Note that the ripples at Oodnaminta Hut show the greatest lateral migration in two directions. The inset shows cross-sections of the primary (1) and secondary (2) ripples at Warren Gorge, and the primary ripples at Oodnaminta Hut (3).

oflow towards 325º, and have gently sinuous, bifurcating crestlines (Fig. 5j; Fig. 12b). The secondary bedforms have a wavelength between 4 and 12 cm and a mean amplitude of 0.8 cm (Fig. 12a). These smaller symmetrical bedforms occur within the troughs of the larger ripples and have linear crestlines perpendicular to the crests of the primary bedforms (Fig. 5j), creating a ladder ripple morphology (Fig. 5j). In plan view, the crestlines terminate with distinct geometric bifurcations (Fig. 5k). In cross-section, the primary and secondary ripples show vertical aggradation of crestlines for many metres with only very slight sinuous laterally migrating crestlines (Fig. 5l; Fig. 12b). There is evidence of rare micro-faulting showing mm-scale normal offset on the limbs of the secondary bedforms. The tertiary bedforms have parallel to slightly oblique crestlines to those of the secondary bedforms and have a wavelength of 4–8 cm. These crestlines are typically discontinuous and decrease in amplitude towards the centre of the secondary troughs (Fig. 5k, m). Grainflows from the crests of the secondary bedforms are common and can extend up to 27 cm and typically trend to 030º (Fig. 5m). Further up-section, the distinction between primary and secondary ripples is blurred as the bedding surface becomes covered with interference ripples of equal wavelength that creates a polygonal distribution of crests. The number of couplets recorded on either side of the crest of an individual bedform does not vary systematically, suggesting that the bedforms do not influence the rhythmic laminations. Above the rhythmite unit is a reappearance of a fine sandstone with some granule layers and scattered coarse grit throughout (Jablonski 1975; Miller 1975).

An isolated outcrop of similar cyclically laminated facies also can be found in the northern Flinders at Oodnaminta Hut (Fig. 1 [33]; Fig. 5n). At this locality, the rhythmic laminations are most pronounced at the base of the section and typically display silt drapes. At the base of the rhythmites, there are isolated rounded granules <1 cm, suggesting overlying ice was present at least at the onset of deposition. Further up-section, the primary bedforms are well developed with few examples of secondary ripples. The average wavelength and amplitude of the primary bedforms are ~30 cm and 0.9 cm, respectively. In contrast to the bedforms in the south, these have strongly sinuous laterally migrating crestlines, leading to truncation of the planar laminae (Fig. 12b) and record a strong asymmetry to the NW and weak asymmetry to the SE. The rhythmites in the Flinders Ranges have been correlated to the Reynella Siltstone Member of the Marino Arkose, near Adelaide, suggesting a wide area of deposition across the basin (Preiss 1987).

Two observations of the upper Elatina Fm. contact with the overlying Nuccaleena Fm. suggest that there is not a low-angle unconformity on outcrop scale (Forbes and Preiss 1987; Lemon and Gostin 1990; Preiss 2000; Williams et al. 2008). Firstly, the basal Nuccaleena Fm. contact does not display an angular cross-cutting relationship in any of our 47 measured sections (Rose and Maloof 2010). Secondly, the contact may be winnowed, knife sharp, or transitional with silt and ice-rafted debris. This variably sharp contact may suggest the presence of a local disconformity between the two formations. However, although it is uncertain as to how much time is missing in each section, it is known that the basal cap carbonate was deposited when glaciers were present (Rose and Maloof 2010).

## Geochemistry

### *Chemical Index of Alteration*

A total of 133 samples from 13 strati-

graphic sections across the ARC record a decline in CIA values through the Yaltipena Fm. from the underlying interglacial stratigraphy to the lowest values in the glacial diamictite, before recovering to pre-glacial values in the overlying Brachina Fm. (Fig. 13; Fig. 14; S1 in supplementary online material). The transition in the Yaltipena Fm. declines from ~67 to ~58 at the basal Elatina Fm. contact. There is significant scatter in CIA values within the Elatina Fm. However, this scatter has a broad geographic distribution with sections in the central Flinders Ranges typically recording values below 60, whilst sections to the northern regions record values greater than 60.

To the north, the Punches Rest section records CIA values between 56 and 72 (Fig. 7 [36]). The Enorama records a mean of 70 that gradually declines through the Trezona Fm. to values between 64 and 68 within the glacial facies. Similarly, the CIA values at Nannipinna Creek show a gradual decline in the CIA values towards the glacial unit but recover to a relatively high index (72) within the diamictites (Fig. 7 [31]). The CIA dataset in the southern Flinders Ranges is limited, which in part is due to the limited outcrop and arenaceous facies that reduces the sampling selection. The Yaltipena and Elatina Fms. record similar CIA values of 65–66. Four rhythmite samples from Blue Ridge Gorge and Buckaringa Gorge have consistently low CIA values between 59 and 61.

### *Carbon isotopes*

The Etina Fm. is characterized by sustained high $\delta^{13}C$ values with a mean of ~+8‰. An increase in scatter and a decrease in mean $\delta^{13}C$ values occur along parasequence boundary surfaces between limestone and siltstone, likely representing local secondary fluid alteration. The Enorama Fm. consists of ~300 m of shale with no associated $\delta^{13}C$ data. There is no evidence to suggest unconformities at either the top of the Etina Fm. or the base of the Trezona Fm. Thus, all stratigraphic sections within the central anticline of the ARC show an inferred dramatic shift in $\delta^{13}C$ from ~+9‰ to ~–9‰ within the Enorama Fm. The overlying pre-glacial Trezona Fm. remains at –9‰

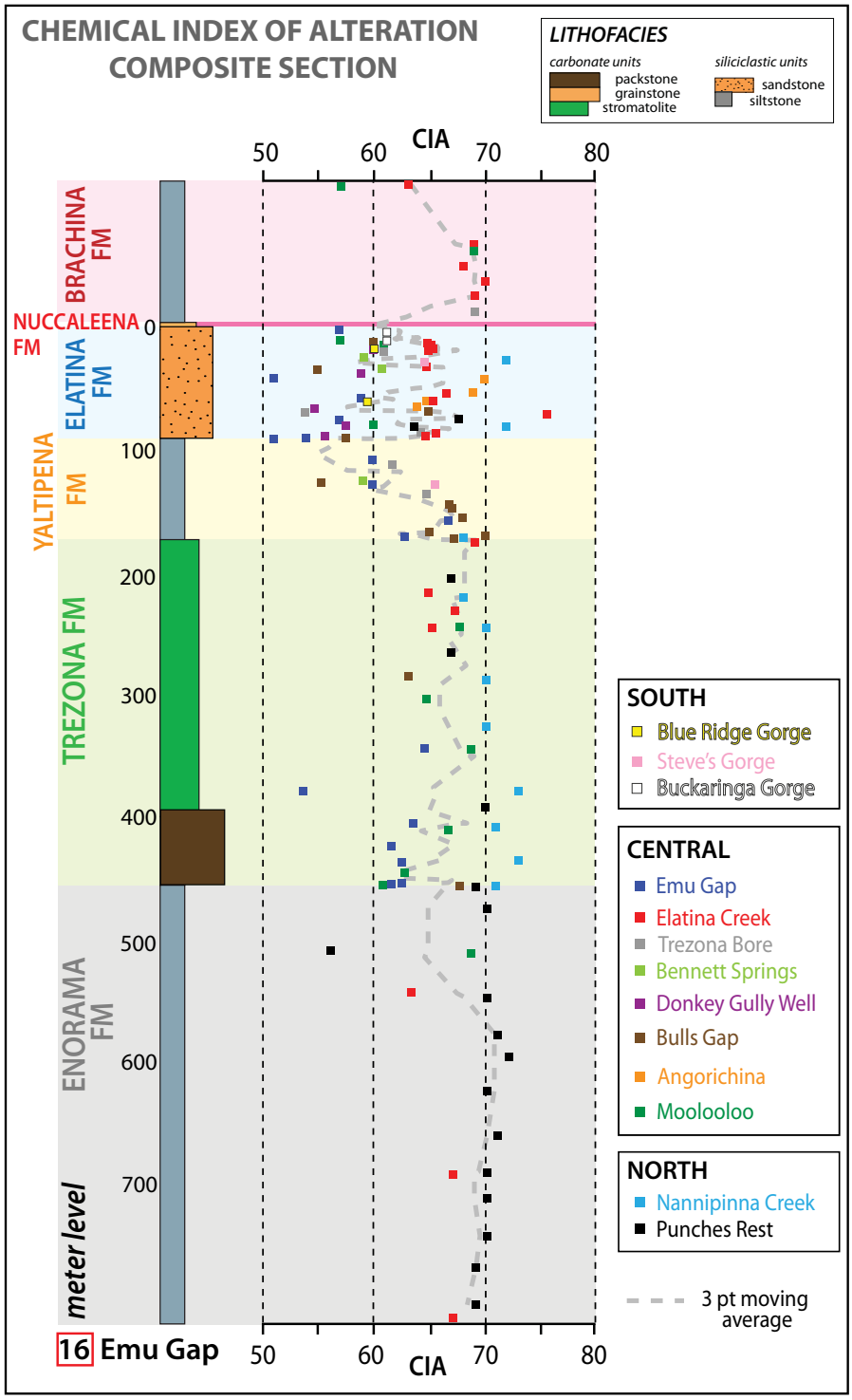


**Figure 13.** Stratigraphic variations in the Chemical Index of Alteration (CIA) weathering proxy through the Umberatana Group. Each formation with CIA data from stratigraphic sections across the Adelaide Rift Complex was adjusted to fit the thickness of the correlative formations within the nominated Emu Gap reference section (Fig. 6 [16]). Low CIA values are associated with glacial conditions inferred from sedimentological facies, and relatively high CIA values are associated with pre- and post-glacial deposits. The upper Yaltipena Fm. and Elatina Fm. record lower minimum CIA values compared to those of the other pre-glacial and post-glacial formations. Note that the stratigraphic section is simplified and all the samples analyzed for major elements were siltstones or the siltstone matrix of the diamictites.

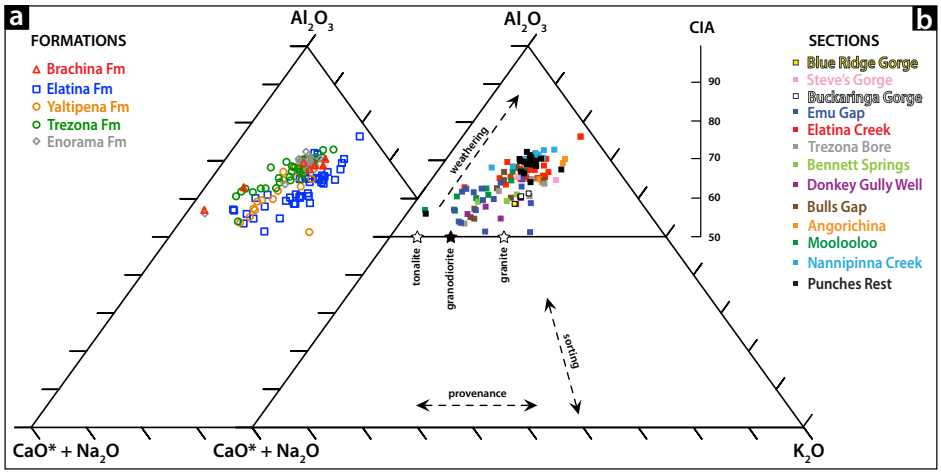


**Figure 14.** Compositional variations of siltstone samples of the pre-, syn-, and post-glacial stratigraphy illustrated in A–CN–K ($Al_2O_3$–CaO+$Na_2O$–$K_2O$) compositional space, which are colour-coded by formation (a) and stratigraphic section (b). The trend defined by the data with low Chemical Index of Alteration (CIA) values roughly follows that expected from variable extents of chemical weathering of a granodioritic source (solid black star). However, this trajectory diverges with higher CIA values, indicating a change in source and/or diagenesis. Based on the weathering trajectory being parallel to the A-CN boundary and minimal field evidence for a diagenetic origin, we calculate that 45% of the trend can be explained by weathering and 55% is a result of a change in provenance.

for up to 150 m before gradually recovering towards 0‰. The upper ~15 m of the Trezona Fm. typically record a ~1‰ decline in $\delta^{13}C$, with an increase in scatter and a decrease in mean $\delta^{18}O$ values (Rose et al. 2012). However, these characteristics are truncated in the Warcowie, Elatina Creek, Angorichina and Moolooloo sections, where the Yaltipena Fm. also is entirely missing (Fig. 6 [13, 17, 23-24]).

Despite the increase in siltstone towards the north of the ARC, sections record a similarly dramatic ~18‰ shift in $\delta^{13}C$ across pre-glacial Etina- and Trezona-equivalent formations. The Nannipinna Creek section (Fig. 7 [31]) records the most complete record of the Etina-equivalent anywhere within the ARC. The $\delta^{13}C$ values gradually increase from 0‰ towards ~+10‰. All other northern sections record a portion of this Etina-equivalent enriched $\delta^{13}C$ signature. The Trezona-equivalent Fm. records a similar $\delta^{13}C$ trajectory as the central sections. The complete Trezona $\delta^{13}C$ trends are present in the most northerly sections within the ARC basin, for example, Taylor Creek shows a gradual rise from –9‰ to –2‰ (Fig. 7 [39]). In contrast, the Weetootla, Nannipinna Creek and Oodnapanicken Bore $\delta^{13}C$ trajectories to the south are severely truncated, with the upper value of the Trezona Fm. reaching only ~–8‰ (Fig. 7 [29, 31-32]). The entire Trezona $\delta^{13}C$ trend is missing from both the Winyagunna and Idinha Spring sections (Fig. 7 [34-35]).

To the south of the Flinders Ranges, the Etina Fm. laterally pinches out to intermittent, thin stromatolitic bioherms that record ~+9‰ values (e.g., Cockroach Valley; Fig. 8 [6]). Similarly, the Trezona Fm. thins and at Partacoona the formation spans less than 15 m, recording $\delta^{13}C$ values of ~–2‰, before laterally transitioning into the siliciclastic Yaltipena Fm. further south.

In paleomagnetic studies, a conglomerate test is used to determine whether clasts in a conglomerate were magnetized prior to transport and deposition (preserving random magnetic directions) or after deposition (preserving uniform magnetic directions, despite random clast orientations). Analogously, we performed an isotope conglomerate test (DeCelles et al. 2007; Husson et al. 2012) on the Elatina Fm. diamictites at 8 localities across the ARC to assess the provenance and relative timing of acquisition of $\delta^{13}C$ and $\delta^{18}O$ by measuring the isotopic values of 269 carbonate clasts of the Elatina Fm. (Fig. 15). Collectively, the diamictites record $\delta^{13}C$ variability between –9‰ and +10‰. However, the distribution of $\delta^{13}C$ values for individual diamictite localities can vary dramatically, even on a short spatial scale. For example, the Trezona Bore and Enorama Creek localities are less than 1 km apart but the clast $\delta^{13}C$ data vary from –5‰ to +10‰ and 0‰ to +2.5‰, respectively. At Oodnapanicken Bore, clasts of the distinct Trezona fossiliferous packstone facies were analyzed and record a mean $\delta^{13}C$ value of –7.3‰ compared to a mean of –5.4‰ for $\delta^{13}C$ of generic carbonate clasts from the same locality. Note that there are numerous clasts with $\delta^{13}C$ values between 0‰ to +4‰, which fall in 'no man's land' because these carbon isotope values are rarely recorded within either the pre-glacial stratigraphy of the Etina or Trezona Fms. (Fig. 15).

### *Detrital zircons*

U–Pb LA–ICP–MS ages have been determined for detrital zircons from 22 samples across the ARC within the pre-glacial Trezona and Yaltipena Fms., and the syn-glacial Elatina and Whyalla Fms. (Fig. 16; S2 in supplementary online material). The zircon-age spectra for the Trezona Fm. show a single ~1.2 Ga peak. Two samples were analyzed for detrital zircon from the Yaltipena Fm. at Trezona Bore (Fig. 1 [18]). The spectra show peaks at ~690 Ma, ~1.1 Ga and ~1.7 Ga producing a more varied signal than the underlying Trezona Fm. to the north.

Eleven detrital zircon spectra from the syn-glacial Elatina Fm. all record dominant peaks at ~1.1 Ga and ~1.2 Ga. In addition, localities to the north and south show young peaks at Halletts Cove (~665 Ma), Lame Horse Gully (~760 Ma), and Chambers Gorge and Walters Well (~730 Ma). The Stuart Shelf records a prominent ~1.7 Ga peak throughout the stratigraphy from the Mesoproterozoic Pandurra Fm. to the directly overlying Elatina-equivalent Whyalla Fm. In addition, the Whyalla Fm. shows ~1.6 Ga, ~1.1 Ga and ~1.2 Ga peaks from five samples across the shelf.

## DISCUSSION

The eastern edge of the Gawler Cra-

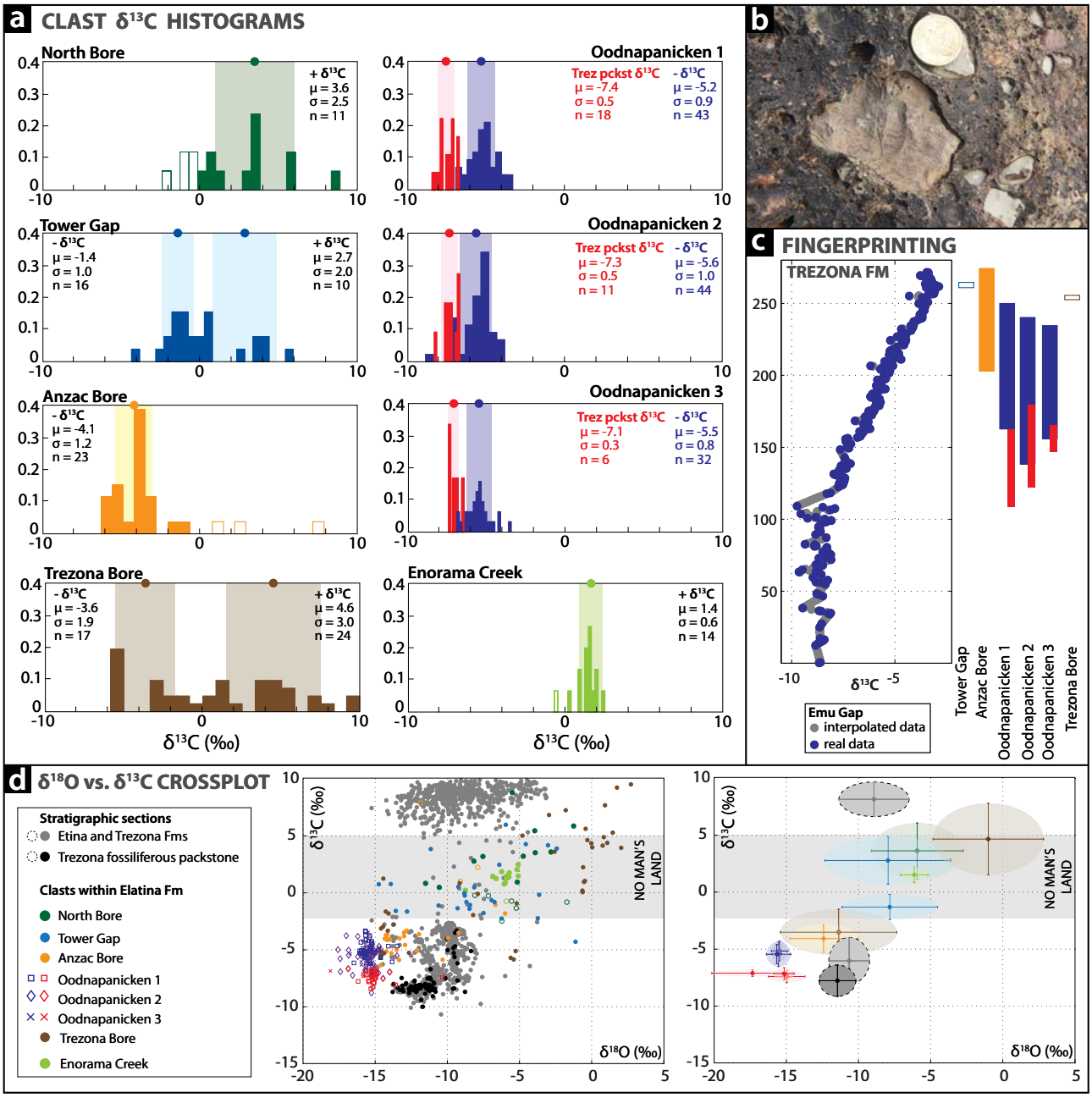


**Figure 15.** (a) Histograms of $\delta^{13}C$ for carbonate clasts within the Elatina Fm. The clast count locations are labeled on Figure 1. Note that the purple and red histogram bars at Oodnapanicken correspond to data from carbonate clasts and Trezona fossiliferous packstone (pckst) clasts, respectively. Hollow histogram bars indicate where the sample size for clasts with positive or negative $\delta^{13}C$ values was too small to be included in statistical 'fingerprinting' analysis. The positive and negative $\delta^{13}C$ values are treated as different clast populations that are putatively sourced from the Etina Fm. and Trezona Fm., respectively. Dots denote the mean $\delta^{13}C$ for positive and negative $\delta^{13}C$ values and/or Trezona fossiliferous packstone clasts at each location, and the pale shaded areas mark the range of $\delta^{13}C$ covered by one standard deviation from either side of the mean for each clast group. (b) Fossiliferous packstone clast from the Trezona Fm. and generic grey limestone clasts within the glacial diamictite of the Elatina Fm., near Oodnapanicken Bore. (c) Trezona Fm. 'fingerprinting' solutions for carbonate clasts within the Elatina Fm. Both the interpolated and real $\delta^{13}C$ data sets for the Trezona Fm. are depicted. Coloured bars mark the stratigraphic range of possible sourcing for the clasts. Hollow bars indicate unreliable 'fingerprinting' solutions due to a non-normal distribution and/or small sample size (n<20) (Chen 2012). (d) Crossplots showing $\delta^{18}O$ *vs* $\delta^{13}C$ data from the Etina and Trezona Fms. from the Emu Gap, Elatina Creek, Trezona Bore, Bulls Gap and Moolooloo stratigraphic sections (Fig. 1; Fig. 6 [16-18, 22, 24]), and data from carbonate clasts within the Elatina Fm. The crossplot on the right shows the mean and standard deviation (1σ) of $\delta^{13}C$ and $\delta^{18}O$ for each dataset. The stratigraphic Etina and Trezona Fms. ellipses are opaque and highlighted with a dashed border. Note that many of the $\delta^{13}C$ values of the carbonate clasts predominantly fall in 'no man's land' between –2.5‰ to +5‰, where the stratigraphic sections of the Trezona and Etina Fms. rarely have $\delta^{13}C$ values within this zone.

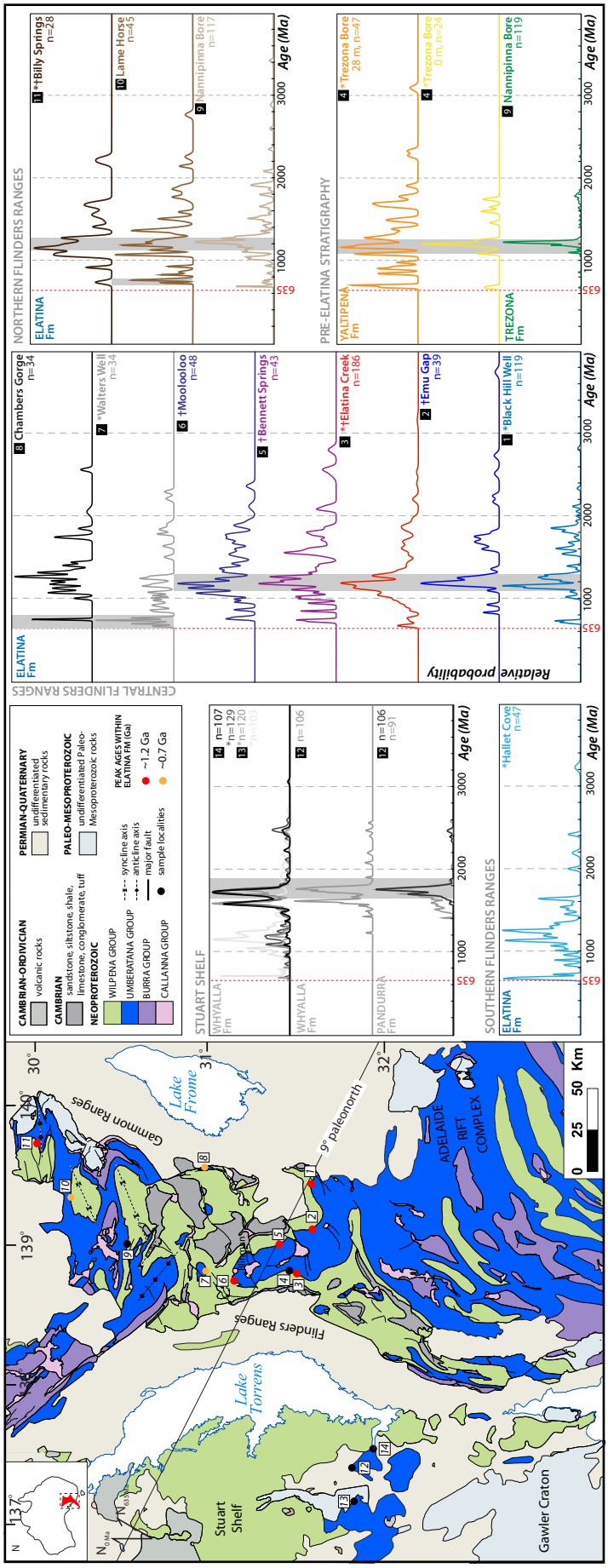


**Figure 16.** Map of sample localities and individual probability distribution functions for U–Pb detrital zircon ages collected from the Pandurra and Whyalla Fms. on the Stuart Shelf, and from the Trezona, Yaltipena and Elatina Fms. from across the Adelaide Rift Complex (ARC). Note that the probability distribution function for Elatina Creek includes zircon grains collected from two samples. The samples yielding the youngest zircon grains are denoted by an asterisk (*). Sections with samples taken from more than 50 m above the base of the formation are denoted with a cross (†). The ~1.7 Ga zircon grains within the Whyalla Fm on the Stuart Shelf are sourced from the underlying Pandurra Fm. Samples from locality 15 are from the eolianite facies of the Whyalla Fm. Note that ~1.7 Ga zircon grains are not found within the pre-glacial or Elatina Fm. stratigraphy within the ARC, indicating that the Whyalla eolian sand sheet did not act as the main source of sediment during the glaciation. Likely sources for the ~1.2 Ga zircons within the ARC are the Musgrave Block and Albany-Frazier Province within Australia, and/or the Wilkes Province of East Antarctica. To the north of the ARC, the Elatina Fm. records an ~0.7 Ga peak for which the zircon could be sourced from the Mt. Crofton Granite in Paterson Province and/or the Leeuwin Complex of Western Australia. Note that 8 potentially young zircon grains (<690 Ma) from the Elatina and Whyalla Fms. have been dated using ID–TIMS (Table S3 in supplementary online material).

ton runs approximately north-south and it is this paleo-coastline and the deepening of the ARC basin to the north that controls the variability in depositional environments and facies of the Etina–Elatina succession. The cross-bedded oolitic and sandy facies of the Etina Fm. was deposited under predominantly high-energy conditions, possibly as migrating shoals that were intercalated with small stromatolite bioherms and calcareous siltstone. Preiss (1987) proposed that the presence of quartz throughout the Etina facies is evidence for an influx of sand from the Gawler Craton. Towards the south, the Etina Fm. is restricted to a few small stromatolite bioherms (<5 m) surrounded by siliciclastic sand. These stromatolites may have been colonizing the edges of tidal channels that were prograding out towards the shelf along the Gawler Craton coastline (Preiss 1987). The basin deepens towards the north, resulting in the stromatolitic and oolitic facies of the central region transitioning to siltier facies. There is a prograding reef complex to the northeast at Oodnaminta Hut that is eroded, creating a submarine escarpment with large olistoliths that mark the shelf–slope transition (Giddings et al. 2009). Farther north, the facies deepen to silt and carbonate ribbonite interbeds that record $\delta^{13}C$ values of up to +10‰. Thus, we provide geochemical evidence that the Balcanoona, Yankaninna and Amberoona Fms. are the northern equivalents of the Etina Fm. Farther to the northwest, the Etina Fm. consists of carbonate tepee breccia, which indicates subaerial exposure. This tepee breccia is restricted in lateral extent and surrounded by silt. Such a juxtaposition of facies suggests that a paleo-high or promontory existed in the north of the basin. Such paleotopography, which occurs over a short spatial scale, may have been generated by salt diapirs that caused a fringing reef to become periodically exposed. The closest diapir to this paleohigh crosscuts the lower 50 m of the Trezona Fm. in map view to the northwest of Nannipinna Creek, suggesting that diapirism was active throughout the deposition of the Etina Fm. (Fig. 1 [31]).

In addition to abrupt lateral facies changes over short spatial scales, there is a distinct relationship between lateral facies variability in the pre- and syn-glacial sedimentary rocks and the axes of three 50-km scale south verging-open folds (Rose and Maloof 2010; Fig. 1I–V). Generally, across each fold the pre-glacial Etina Fm. records grainstone and stromatolite facies south of the fold axis and siltstone, shale and olistostromes to the north (Coats et al. 1973; Preiss 1987; Giddings and Wallace 2009). Similarly, the Trezona Fm. transitions from siltstone and limestone ribbons on the southern fold limb to turbidites on the northern limb (Coats et al. 1973). The Elatina Fm. facies change from laminated siltstone and rarer boulder tillite on the southern fold limbs to conglomeratic debris flows, diamictite, and massive gritty siltstone on the northern limbs (Rose and Maloof 2010). We propose that the sedimentary facies and the presence of basin-bounding normal faults influenced the subsequent Delamerian tectonic deformation to create the distinct relationship between lateral facies variability in the pre- and syn-glacial stratigraphy and the axes of the folds (Rose and Maloof 2010). We agree with the interpretation of Giddings and Wallace (2009) that the pre-glacial Etina Fm. facies variation marks a reef margin to slope setting across the Arkaroola syncline (Fig. 1 III), and further suggest that the abrupt lateral facies changes across the folds to the north represent the transition from the outer ramp or upper slope to the lower slope (Rose and Maloof 2010). Above the Etina Fm., the Enorama Fm. is present both north and south of the fold axes and represents a marine transgression that caused inundation of the central Flinders Ranges carbonate platform and silt deposition. This formation of finely laminated green siltstone and claystone lacks current or wave ripples, cross-bedding or coarser clastic interbeds, until near the contact with the Trezona Fm., indicating that deposition occurred in a quiet, marine setting.

## The Advance of Land Ice

The onset of the glaciation is not recorded at the top of the Trezona Fm. by a basin-wide disconformity and/or karsted surface (Lemon and Gostin 1990). The Yaltipena Fm. records the encroaching glaciation. A drop in sea level and/or an increase in siliciclastic sediment supply caused the tidal flat and beach facies to prograde towards the east and north, until mud-cracked siltstone interfingered with the carbonate reef of the Trezona Fm. (Fig. 17). The progradation of the tidal flat is linked to the advancing ice sheets as glacial clasts up to 1 m across pierce the top of the Yaltipena Fm. and the upper contact typically is contorted and scoured. Associated soft-sediment deformation of the Yaltipena silt layers below the diamictite suggests the silt was unlithified and was rucked up during glaciation by overriding ice (Rose et al. 2012). Furthermore, in the northern ARC, isolated rounded granite and gabbro clasts within the upper two metres of a Trezona Fm. stromatolite bioherm, which records the highest $\delta^{13}C$ following the Trezona anomaly, represent the onset of glaciation (Rose et al. 2012). This ice-rafted debris requires floating, debris-laden icebergs in water possibly no deeper than the photic zone during terminal carbonate deposition on the outer shelf (Fig. 17). In addition to the sedimentology, the geochemistry of the pre- and syn-glacial sedimentary rocks can provide information about the encroaching ice sheet and the Cryogenian climate state.

The major-element geochemistry of siliciclastic rocks depends on the intensity of chemical weathering and, thus, should preserve a record of severe climatic changes (Nesbitt and Young 1982, 1996; Johnsson 1993; Fedo et al. 1997b; Corcoran and Mueller 2002; Rieu et al. 2007c). The CIA values for the Elatina Fm. have a mean value of 63 ± 5 (1σ error). If the CIA values accurately reflect the intensity of chemical paleoweathering, then this low value corroborates the glacigenic interpretation of the Elatina Fm. based on independent sedimentological evidence (Fig. 13). This CIA value is typical of other Marinoan glacial successions around the world (averages: Ghaub Fm., 63 ± 5; Mortensnes and Smalfjord Fms., 66 ± 1; Port Askaig Fm., 70 ± 5; all 1σ errors; Bahlburg and Dobrzinski 2011). Although the Enorama and Trezona Fms. record values of 68 ± 4 and 67 ± 4 (1σ error), respectively, which are

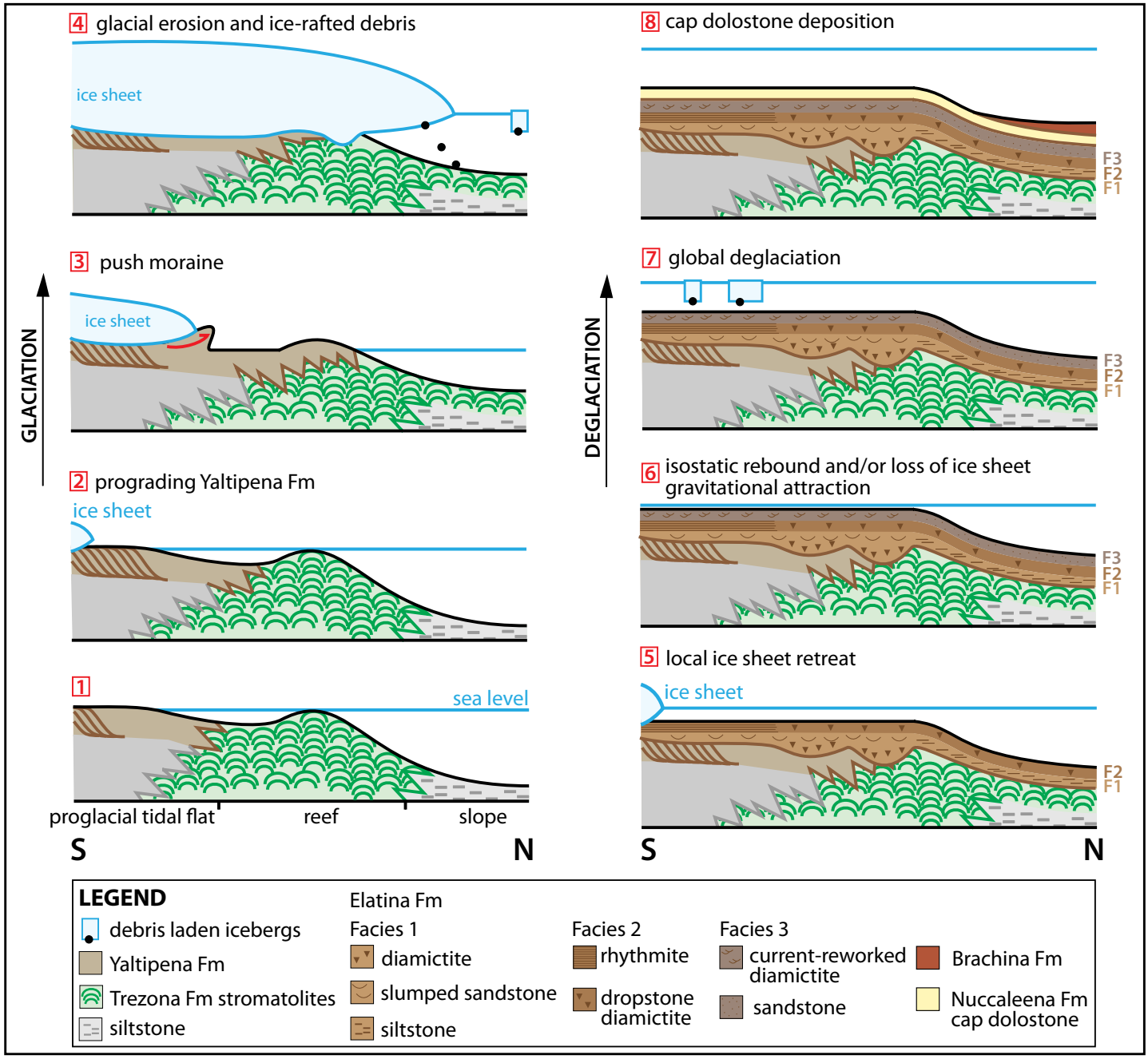


**Figure 17.** Schematic depositional model for the Elatina glaciation and deglaciation across the southern, central, and northern regions of the Adelaide Rift Complex. During the onset of the glaciation, ice-contact deformation of the Yaltipena Fm. and glacial truncation of the Trezona Fm. occured in the central fold [3]. To the north, synchronous deposition of dropstones within stromatolites is recorded in the uppermost Trezona Fm. [4]. During the deglaciation, slumped sandstone (F1) and dropstone diamictite (F2) were deposited in the central anticline [5]. As the local ice sheet continued to retreat, loss of ice sheet gravitational attraction and/or isostatic rebound led to a regression and current reworking of the underlying diamictite (F3) [6]. The global deglaciation is recorded by a final diamictite within the upper Elatina Fm. and the precipitation of the Nuccaleena Fm. cap dolostone and overlying Brachina Fm. [7-8].

lower than expected for a pre-glacial warm, tropical carbonate platform, these CIA values still show a relative decline across the Yaltipena Fm. The tight downturn in CIA from 68 to ~55 recorded in three sections across the Yaltipena Fm. (average 62 ± 5 (1σ error)) attests to the onset of the glaciation with an overall lowering of sea level and progradation of the tidal flat facies across the basin. In addition, the upper Yaltipena Fm. and Elatina Fm. record lower minimum CIA values compared to those of the other pre-glacial and post-glacial formations. The mean CIA value for the overlying Brachina Fm. is 67 ± 5 (1σ error), indicating a recovery to pre-glacial values. However, important factors other than climate need to be considered when evaluating the major element composi-

tion of siliciclastic sediments and sedimentary rocks, including the influence of source rock composition (McLennan et al. 1993; Fralick and Kronberg 1997), sediment recycling (McLennan et al. 1993; Cox et al. 1995), tectonic setting (McLennan et al. 1993; Corcoran and Mueller 2002), relief (Grantham and Velbel 1988; Johnsson 1993), sediment transport (Malmon et al. 2003), and diagenesis (Nesbitt and Young 1989; Fedo et al. 1995, 1997a).

The geochemical composition of sediments is strongly controlled by the composition of the rocks and regolith from which the sediment is derived (Nesbitt and Young 1989; McLennan et al. 1993; Fedo et al. 1996; Fralick and Kronberg 1997). An A–CN–K ($Al_2O_3$–$CaO+Na_2O$–$K_2O$) ternary plot shows that the major element composition of samples from the Trezona, Yaltipena and Elatina Fms. that have been little affected by chemical weathering were derived from rocks with an average granodioritic composition (Nesbitt and Young 1984, 1989; Fig. 14a). However, data from the Elatina Fm. are shifted towards the $K_2O$ apex, suggesting that the glaciation introduced rocks derived from a more granitic sediment source. In addition, the trend of the complete data set in the A–CN–K plot does not perfectly parallel the A–CN boundary (Fig. 14b). This drift mostly is represented by samples from northern sections, suggesting that there may be some variation in the composition of the sediment source rocks specific to this region. This observation is corroborated by the detrital zircon suites from the Elatina Fm. that record <760 Ma young zircon peaks in the northern Flinders Ranges (Fig. 16 [7-8]), and interestingly, both the Leeuwin Complex and Paterson Province of the Yilgarn Craton, which are proposed sources for these young zircon grains, are granitic.

The observed weathering trend also reflects the degree to which recycled sedimentary rocks have been mixed and incorporated into the glacigenic deposits (Bahlburg and Dobrzinski 2011). Glacial deposits recycle large quantities of sediment that may retain CIA values reflective of progressive weathering in previous climates, causing scatter in the CIA values (Cox et al. 1995). We interpret the variability in the CIA values for the Elatina Fm. to reflect in part sediment derived from the underlying Yaltipena Fm., which may record progressive weathering of sedimentary material under an equatorial climate over a series of recycling events. The Yaltipena Fm. sediment may have originated from different basins that experienced a different number and/or intensity of weathering regimes. Based on the weathering trajectory being parallel to the A-CN boundary and minimal field evidence for a diagenetic origin, we calculate that ~45% of the trend can be explained by weathering and ~55% is a result of a change in provenance.

An alternative hypothesis for why the Elatina Fm. samples plot towards the K-apex in A–CN–K compositional space is that the formation experienced burial diagenesis, with potassium metasomatism changing the bulk composition, and consequently the CIA, of sedimentary rocks (Fedo et al. 1995). Potassium metasomatism is suspected when the compositional variations in a sedimentary succession deviate from the ideal weathering trend, showing enrichment in potassium and thus diagenetically lowered CIA values. However, the underlying Yaltipena Fm. records a tight declining CIA trend that reaches a nadir of 55, and neither formation shows any physical evidence for pervasive diagenesis, such as significant liesegang commonly associated with migrating alteration fronts. Thus, the drop in mean CIA values from pre-glacial to glacial facies is more likely a result of climate deterioration and/or different weathering sources.

CIA values strongly depend on the abundance and composition of clay minerals, and therefore may be influenced by the effects of hydrodynamic sorting during deposition. Although this study is limited to siltstone rocks in order to reduce the effect of differential sorting on composition, subtle differences in grain size may exist between the samples. However, the magnitude of variability in CIA within the Elatina Fm. is not likely to be a consequence of such minor facies differences between samples.

Overall, the CIA results indicate that compositional variations in major element geochemistry within the ARC provide limited information when evaluating the paleoclimatic significance of the Marinoan siliciclastic succession because it is hard to accurately determine the degree to which a variable source rock and climate controlled the CIA values. Despite the lack of an unambiguous interpretation for the syn-glacial CIA values, we interpret the large scale CIA record to represent real climatic shifts during the pre- and post-glacial transitions to and from the Elatina glaciation. Therefore, the evidence for the Yaltipena representing encroaching land-based ice is a) the architecture of the Yaltipena Fm. as a prograding tidal flat complex, b) the presence of glacial dropstones in the stromatolites beyond the tidal flat edge, c) the sub-glacial deformation of the unlithified Yaltipena sediments, and d) the tight declining CIA trend that reaches a nadir of 55 towards the basal contact of the Elatina Fm.

## Subglacial Erosion

Local glacial erosion variably truncates the Yaltipena Fm., such that this formation is entirely missing in parts of the central Flinders anticline (Fig. 6 [17, 23]). The minimum amount of glacial incision into the underlying carbonate platform may be quantified by correlating the stratigraphic sections, using the inflection point at the base of the recovery from the Trezona negative $\delta^{13}C$ anomaly, and assuming that the maximum thickness of the Trezona Fm. in the central Flinders Ranges is recorded in the Emu Gap section, to which all sections within the central anticline are referenced (Halverson et al. 2002; Fig. 1 [16]). Thus, the *minimum* amount of glacial incision is calculated from the stratigraphic thickness of the Trezona $\delta^{13}C$ signature recorded above the inflection point. A total of 9 measured sections through the Trezona-Elatina Fms. across central Flinders Ranges show that up to ~130 m have been truncated by glacial erosion. To the north, although the stratigraphic correlations are more tentative and the Trezona Fm. could consist entirely of siltstone, it appears that the complete Trezona Fm. and overlying stratigraphy, up to 500 m thick, have been

removed and the Elatina Fm. is in contact with the Enorama Shale (Brenchley-Gaal 1985; Fig. 7 [34]). Progressive truncations of beds within the Trezona Fm. indicate that the unconformity is more pronounced to the north, west and south of Trezona Bore. The sections north of Punches Rest do not record glacial truncation, and we interpret these sections that record hundreds of metres of stratigraphy with $\delta^{13}C$ values remaining at ~–2‰ in the upper Trezona Fm. (Fig. 7 [38-40]) to record a deeper environment and an increase in accommodation space.

Further information on the extent of glacial incision comes from the carbonate clasts within the diamictites. Previous work determined that all carbonate clasts in the central anticline in the Elatina Fm. are thought to derive from the underlying Trezona Fm., due to distinctive ooid clasts identified near Bulls Gap (Lemon and Gostin 1990; Fig. 15). Although we find clasts of fossiliferous packstone near Oodnapanicken Bore (Fig. 15b), the remaining carbonate clasts are generic cream to grey limestone without unique sedimentary features to determine their origin. If the clasts acquired their $\delta^{13}C$ values *in situ* on the carbonate platform, then they should exhibit a random collection of values representing the full isotopic range present in the eroded carbonate platform $\delta^{13}C$ profile at the time of diamictite deposition (DeCelles et al. 2007; Husson et al. 2012). In contrast, if the extremely negative $\delta^{13}C$ values (down to –9‰) in the carbonate platform are a result of post-depositional diagenesis, then clasts from individual diamictite beds should either (a) reflect the original pre-diagenetic isotopic values in the platform (i.e., not extremely depleted in $\delta^{13}C$), or (b) have consistent diagenetic values that are roughly homogeneous within diamictite units. The wide variability of the clasts shows that they record the full isotopic range from –9‰ to +10‰ present in the carbonate platform $\delta^{13}C$ profile, and thus, rules out late-stage burial diagenesis (Fig. 15a). This *isotope conglomerate test* (DeCelles et al. 2007; Husson et al. 2012) does not preclude that the clasts reflect early meteoric diagenetic alteration of the carbonate platform $\delta^{13}C$ profile prior to local glacier advance. However, while a meteoric diagenesis hypothesis for the Trezona Fm. can be made consistent with the timing of exposure of the platform, it is inconsistent with top-down modification of the platform by meteoric fluids (Swart and Kennedy 2012) and with the lack of permeability-dependent $\delta^{13}C$ spatial variability between different lithofacies across the platform (Rose et al. 2012).

The negative $\delta^{13}C$ clasts with values < –2‰ can be attributed to the upper ~180 m of the Trezona Fm. (Fig. 15c). The fossiliferous packstone clasts have consistently lower $\delta^{13}C$ values in comparison to generic limestone clasts at Oodnapanicken Bore. This $\delta^{13}C$ value is characteristic of these packstone units, as they are most commonly associated with the initial proliferation of stromatolites within the lower half of the Trezona Fm. stratigraphy in the central anticline of the ARC. Only the Weetootla, Nannipinna, and Winyagunna sections in the northern Flinders Ranges document truncation of the Trezona $\delta^{13}C$ anomaly to the inflection point of –9‰ (Fig. 7 [29, 31, 34]). This observation suggests that either the clasts were not transported a long distance from Nannipinna Creek or the site of erosion is not exposed within the ARC. At Oodnapanicken Bore, the $\delta^{13}C$ values of the clasts ranges from –3‰ to –9‰, and almost record the full isotopic range of the Trezona Fm.; the $\delta^{18}O$ values, however, are ~5‰ more negative than those of the Trezona Fm. stratigraphy (Fig. 15d). This observation suggests that diagenesis has locally altered the $\delta^{18}O$ values. The timing of this diagenesis is unknown, but because only the clasts at Oodnapanicken Bore show modified $\delta^{18}O$ compared to the other northern clasts (Fig. 15a), it likely reflects late stage diagenesis local to Oodnapanicken Bore, rather than pan-basin early alteration during transportation of broken clasts in $\delta^{18}O$-depleted glacial meltwater.

The clasts with isotopically-enriched $\delta^{13}C$ values between +5‰ and +10‰ can be attributed to the Etina Fm. and northern equivalents (Fig. 15a). However, nowhere within the ARC does glacial erosion remove all of the Trezona and Enorama Fms., juxtaposing Elatina Fm. on top of the Etina Fm. Active salt diapirism throughout the deposition of the Etina Fm. and much of the Enorama Fm. are thought to be responsible for entraining brecciated blocks of the underlying stratigraphy and bringing them to the surface (Lemon 1985; Lemon and Gostin 1990; Lemon 2000). In map view, many of the diapirs cross-cut the Etina Fm. and the lower two-thirds of the Enorama Fm. in the central region (Lemon 2000), whilst in the north they impinge on the lowermost ~50 metres of the Trezona Fm. Despite the small Oratunga diapir in the central region that cross-cuts the Umberatana Group stratigraphy, for the most part diapirs were emergent and most active before deposition of the Trezona Fm. and Elatina Fm. (Webb 1960; Coats 1965; Lemon 2000).

One possibility is that the isotopically-heavy clasts originated from a distal diapir that sampled the Etina Fm., and was then eroded and transported by the ice sheet. Many of the clasts fall between –2‰ and +5‰, which are not values recorded in either the Etina or Trezona Fm. stratigraphy. These values may represent diagenesis of the Etina clasts but this seems unlikely given that the values are highly variable within a 5 m x 5 m cross-sectional area of diamictite. The only place in the interglacial stratigraphy that records these values is the transition from the Tapley Hills Fm. found below the Etina Fm., suggesting that either erosion of a diapir or a nearly 1 km deep glacial incision at an unobserved locality sourced these deeply buried formations. Alternatively, the shale of the Enorama Fm. might transition to carbonate facies, presently unobserved, and record the full isotopic down-turn of the Trezona $\delta^{13}C$ anomaly from +5‰ at the top of the Etina Fm. to the –9‰ nadir at the base of the Trezona Fm. Thus, the carbonate clasts might reflect at least ~500 m of glacial incision, possibly outside of the ARC. The Jakobshavn Isbræ ice stream in Greenland creates a fjord ~700 m deep (Holland et al. 2008) and paleofjords during the Cenozoic are thought to have incised up to 1 km below sea level in Antarctica (Young et al. 2011). Thus, although erosion of a diapir could source the

clasts, given a sufficiently large ice cap in Australia it seems likely an ice stream would be capable of eroding the entire Etina Fm.

## The Retreat of the Ice Sheet

The basal diamictite of the Elatina Fm. has a scoured contact and contorted diamictite beds at the base of the Elatina Fm. at the Trezona Bore section, indicating local ice-contact and sub-glacial push structures formed during an ice advance (Lemon and Gostin 1990; Fig. 5g-i; Fig. 17). Although numerous ice sheet advances could have occurred, these preserved facies record a singular major advance within the Elatina Fm. The overlying Elatina facies consist of cross-bedded channelized fluvioglacial sands that grade into shallow-marine sands with pervasive slumping (Facies 1) and dropstone diamictite deposits (Facies 2). These facies record the transgression associated with the subsequent deglaciation. Despite observations of some ripple cross-laminated and cross-stratified sandstone intercalated with diamictite throughout the succession (Le Heron et al. 2011a; Le Heron 2012), we document that the top third of the Elatina Fm. is dominated by current-reworked diamictite beds with distinctive gravel lags and lonestones capped by mm- to cm-scale ripple cross-laminated fine- to very fine-grained sandstone (Facies 3). This final facies which occurs throughout the central and southern Flinders Ranges records upward shallowing and reworking of the underlying diamictite beds. These observations and interpretations corroborate those of the seminal work of Lemon and Gostin (1990). The upper part of Facies 3 is correlative to the terminal shallowing sequence that transitions into gritty sandstone in the southern Flinders Ranges. In the central region, a thin diamictite is present in the upper part of Facies 3, just below the Nuccaleena cap carbonate, which we correlate to the gritty sandstone just below the cap dolostone at Warren Gorge and the surrounding region (Fig. 9 [24]; Fig. 11 [4]). Despite the northern Flinders Ranges predominantly consisting of deep marine diamictite, there are three broad facies to the Elatina Fm.: a laminated siltstone, a diamictite, and a coarse feldspathic sandstone. The upper sandstone facies consists of pale grey and brown feldspathic sandstone with lenses of calcareous siltstone and pebble conglomerate. We interpret this Balparana Sandstone to reflect the basin-wide shallowing within the northern ARC. Overall, water levels deepened through deposition of the first two units (Elatina Facies 1 and 2), shallowed during the deposition of the upper unit (Facies 3), before the post-glacial sea level rise recorded with the deposition of the Nuccaleena and Brachina Fms. (Fig. 17).

The rhythmite facies within the Elatina Fm. consists of very fine sandstone uniformly distributed throughout ~30 m of stratigraphy and across at least ~4500 km$^2$. At Warren Gorge, the previously interpreted parallel cuspate folds within the rhythmite facies (Williams 1996) have a characteristic wavelength and show birfurcating crestlines in plan view (Fig. 5j, k). In cross section, these bedforms have slightly asymmetric crestlines and show preservation of the entire crest of the bedform (Fig. 5l; Fig. 12b). At Oodnaminta in the north Flinders Ranges, these bedforms have strongly sinuous laterally migrating crestlines in cross-section, often with reversing truncations of the topsets of the bedforms. In addition, there is no evidence for soft-sediment deformation at any scale throughout these bedforms. Together, these observations are not compatible with the previous interpretation as parallel cuspate folds and slump structures, particularly as the slumps likely would migrate only in the direction of gravity and generate a variety of soft-sediment deformation at a range of spatial scales. Thus, we interpret these sedimentary structures to be stoss-depositional, reversing three-dimensional bedforms with superimposed symmetrical bedforms that orthogonally intersect the primary crestlines (Rubin and Hunter 1982). The geometry of these bedforms indicates combined flow between unidirectional and oscillatory currents. The overall eastward migration of the primary crests indicates an off-shore transport direction with ongoing wave action generating the secondary crestlines in a marine setting above fair weather wave base. Tertiary crests appear near the top of the rhythmite section that are mostly parallel to the secondary crests. The tertiary crests may indicate a change to a shallower water depth and the generation of ripples of a shorter wavelength. Thus, a relative sea level drop also is recorded within the upper rhythmites before continued shallowing that is marked by the gritty sandstone further up section. We interpret the upper rhythmites to correlate with the Facies 2–3 transition within the Elatina Fm.

The Balparana Sandstone, the current-reworked diamictite, and the tertiary combined-flow ripples in the rhythmite unit are time-synchronous facies across the ARC that all record a regression. This basin-wide relative sea level fall occurs in the upper part of Facies 2 and Facies 3 within the overall transgressive deglaciation sequence of the Elatina Fm. This regression could be caused by the retreat of local glaciers and the associated instantaneous loss of gravitational attraction that the ice sheet had on the nearby ocean. During the Pleistocene-Holocene, uniform melting across the Greenland ice sheet of a volume of ice that would have been equivalent to raising global sea level by 1 m, would have generated between ~2–10 m of local sea level fall around the Greenland coast (Mitrovica et al. 2009; Kopp et al. 2009). Although this value varies with paleogeography and the geometry of the melting ice sheet, a similar sea level fluctuation would be significant enough to generate the regression recorded in the Elatina Fm. Alternatively, the regression could be in part or solely caused by longer term ($10^4$ years) isostatic rebound associated with the shrinking ice sheet. However, if regional isostatic rebound represents a significant part of the sea level signal then the characteristic timescale for isostatic rebound, which is controlled primarily by mantle viscosity, constrains the retreat of local glaciers from the basin to at least $10^4$ years before the global deglaciation. This scenario would suggest that regional isostatic rebound occurred prior to the global glacio-eustatic sea level rise that controlled deposition of the overlying Nuccaleena Fm. cap dolostone. Together, our sedimentological observations suggest that local ice likely was present until the Elatina Facies 2–3

transition (Fig. 17). This persistence of local ice suggests that the instantaneous loss of gravitational attraction is the more parsimonious explanation for the regression within the upper Elatina Fm.

The wave component of the ripples within the rhythmite facies in the southern ARC requires open tropical seas with significant fetch that is prior to, or at least contemporaneous with local ice retreat. This timing contrasts with the model proposed for evidence of open water during peak glaciation, where local glaciers are starved of moisture and ice is sublimated away from restricted basins (Halverson et al. 2004). If the clasts within the upper diamictite in Facies 3 represent an extra-basinal source they could be derived from the melting of distant debris-laden icebergs during the global deglaciation (Fig. 17). This arrival of far-traveled icebergs to the basin would shift the onset of the global deglaciation from the basal contact of the Nuccaleena Fm. to within the upper Elatina Fm. (Raub and Evans 2008). However, a large proportion of the clasts within this diamictite in the northern region of the central Flinders Ranges are basalt and previous work attributed the source of the clasts to active diapirism. Such an intrabasinal source could represent a regional readvance that results from moisture derived from the opening oceans feeding the continental glaciers. However, there is no evidence that glaciers reached the extent of those that deposited Facies 1 given the lack of subglacial deformation and proximal deposits. Future work could test these hypotheses by determining the clast provenance and detrital zircon signature of the upper diamictite, gritty sandstone, and the Balparana Sandstone across the ARC.

## Tides During the Deglaciation

The re-interpretation of the putative soft-sediment folds as ripples weakens the iconic syn-sedimentary fold test that constrained the low-latitude position of South Australia at the time of the Elatina glaciation. While the tectonic fold test still requires that the low-latitude paleomagnetic direction is pre-Late Cambrian (Foden et al. 2006), the magnetization no longer must be syn-depositional. That said we have no reason to believe that the low-latitude direction is a result of remagnetization, and the positive reversal tests (Sohl et al. 1999) are at least consistent with syn-depositional magnetization. Tauxe and Kent (1984) showed that the detrital remnant magnetization of hematite in the modern Soan River deposits, northern Pakistan, may record an inclination (e.g. 25º) that is significantly shallower than the inclination of the *in situ* field (e.g. 50º). Similarly, laboratory experiments have shown that crystallographic orientations of hematite crystals, which are determined by the principal susceptibility axis, are dominated by depositional rather than magnetic field conditions (Lovlie and Torsvik 1984), such that the inclination of the detrital remanent magnetization held by hematite is significantly shallower than the ambient field. These results suggest that sorting by oscillatory, wave-induced currents may align platy hematite grains with the rhythmite laminations, which could account for the positive fold test (Sumner et al. 1987).

The minimal winnowing of the bedform crests, the limited migration of crestlines, and the absence of finer sand and clays in the troughs indicate that sediment was not distributed or sorted solely by wave action across the region. Williams (1989, 1991, 2000) proposed a distal ebb-tidal delta for the depositional setting where fine-grained sediment is entrained by ebb-tidal currents and transported mainly in suspension by turbid currents and jets via the main ebb channel to deeper water offshore. With increasing distance of transport, such jets transform to hyperpycnal plumes and sorted, suspended sediment settles to form normally graded laminae in distal settings. Similarly, glaciofluvial outlets at the terminus of a glacier could generate vast plumes of suspended sediment that would be delivered in diurnally and seasonally controlled pulses that, in addition to the tidal signal, might have influenced the deposition of rhythmite couplets and bundles.

At Oodnaminta Hut, rare quartz and feldspar granules at the onset of the rhythmite facies suggest overlying debris-laden icebergs. Clay drapes are restricted to these lower few metres and the very fine sand coarsens upwards throughout the section, with shorter wavelength secondary ripples only documented at the top of the section, indicating a shallowing. The primary ripples have convex-up profiles typical of oscillatory waves. These bedforms record a strong asymmetry, with ripples climbing to the northwest and a weaker asymmetry to the southeast, suggesting that the offshore current responsible for the bedforms was not constant but fluctuated in strength. The current was strongest to the northwest, and during periods when the current weakened or ceased the oscillatory flow became more dominant and the bedforms drifted to the southeast. These consistently oriented bedforms throughout the stratigraphy suggest perhaps that the waves were refracted within a protected embayment.

The bedform characteristics outlined above, particularly the vertical aggradation and small mm-scale faults on the limbs of some bedforms at Warren Gorge, are indicative of rapid sedimentation rates. However, workers for more than 35 years have argued for a tidal origin for the rhythmite facies in the southern Flinders Ranges. Although a single periodic variation in the rhythmites could suggest any number of sources, time series analysis shows a nested hierarchy of bundles that contain ~15 couplets (Williams 1989, 1991, 2000; Budnick 2012). Diurnal and seasonal fluctuations in sediment delivery by glacio-fluvial and/or katabatic wind sources could generate the individual couplet and annual periodicities. In fact, eolian delivery of sand by daily katabatic winds may explain why the couplets record a diurnal, and not the expected semi-diurnal, signal dominant in most tropical regions today. However, the cyclic nature of the couplets strongly suggests a neap-spring tidal origin that operates on the order of 14-15 days. Thus, we agree with a tidal interpretation, which can explain most of the periodicities recorded in the rhythmites.

A tidal origin places a time constraint for the deposition of the rhythmites: using the number of spring-neap bundles and assuming that it takes a month to deposit two bun-

dles, the rhythmite stratigraphy at Warren Gorge took a minimum of 33 years to accumulate. At Oodnaminta Hut, the rhythmite laminations are not as well preserved as those at Warren Gorge. However, a minimum of 19 bundles are deposited whilst the bedform migrates to the northwest, and a minimum of 9 bundles are counted as the bedform migrates to the southeast. Thus, the tidal timescale implies that the hyperpycnal current delivering the sediment was active for ~10 months, but diminished or switched off for the following ~5 months. This temporal variability in the current strength could represent a seasonally controlled subglacial or glacial-fluvial source.

The Whyalla Fm. on the adjacent Stuart Shelf could have acted as the eolian sediment source for the rhythmites. Winds reworking this eolian sand sheet may have entrained and transported the very fine sand and silt fraction offshore to supply the rhythmite facies, and the silt fraction would continue to be blown to more distal localities. Winds capable of transporting very fine sand in suspension would need to be 56 km/h and to blow most days to supply sediment for the diurnal couplets for the entire duration of rhythmite deposition (Eastwood et al. 2012). The variability in couplet thickness would be modulated by the spring-neap tidal cycle, where the stronger spring tide would deposit more sand due to enhanced current speed and tide volume, but the weaker neap tide would not be able to entrain sand, resulting in deposition of thin silt laminae. Katabatic winds at the steep terminus of coastal ice slopes are among the strongest surface winds; localities in Antarctica can experience yearly average winds in excess of ~70 km/h (Turner et al. 2009). Thus, similar winds could have supplied a diurnal and seasonal source of sand for the rhythmites. However, this scenario requires that wind blown sand would be transported and evenly distributed over an extensive area every day for ~33 years while glaciers remain in the vicinity.

## Sediment Provenance and Direction of Ice Transport

Detrital zircon data may shed light on the source of sediment for the Elatina rhythmites, as well as constrain the direction of ice transport, the extent of ice coverage, and the maximum age of the glaciation. Previous work has proposed that the Whyalla Fm. acted as a source for the Elatina Fm. across the ARC (Lemon and Gostin 1990; Williams et al. 2008). This work reported that the slumped sandstone unit at the base of the Elatina Fm. is marked by a dominance of coarse silt to fine sand and very coarse sand and granule fractions (Lemon and Gostin 1990; Williams et al. 2008). The Whyalla Fm. includes the missing medium to coarse sand fraction, and it is suggested that spatial sorting by eolian reworking generated the different grain size distributions in the Whyalla and Elatina Fms. (Lemon and Gostin 1990; Williams et al. 2008). The fine sediment would have been transported to the Elatina Fm. by wind, whereas the very coarse sand fraction would have been delivered by fluvial systems. However, if fluvial systems were draining the Stuart Shelf or adjacent uplands, it seems unlikely that only the coarse, and not the medium sand fraction, would be transported from the Whyalla Fm. Furthermore, detrital zircon data show that the provenance of the sand in the Whyalla and Elatina are different. Many zircon grains within the Elatina-equivalent Whyalla Fm. have similar ages to the Elatina Fm. within the ARC (~1.6 Ga, ~1.1 Ga and ~1.2 Ga peaks; Fig. 16). However, a pervasive ~1.7 Ga peak present throughout the Whyalla Fm. is absent from all the preglacial and Elatina Fm. stratigraphy throughout the ARC. These zircon grains likely are derived from the Yavapai-Mazatzal Province of Laurentia and/or East Antarctica that was juxtaposed to Australia for the previous 300 my (Karlstrom and Bowring 1988; Hoffman 1991; Goodge et al. 2008) and sourced locally from the Pandurra Fm. that underlies the Whyalla Fm. in many localities across the Stuart Shelf. The majority of the zircon grains responsible for the 1.7 Ga peak are less than 80 μm and would require similar windspeeds as the larger, fine sand fraction for them to be carried in suspension. Thus, it seems unlikely that the Whyalla sand sheet supplied sediment for the glacial deposits in the central region, and suggests that the source for the rhythmites must either be sub-glacially derived or from another sand sheet.

Throughout the Trezona–Elatina Fm. stratigraphy in the central ARC and the Nannipinna and Billy Springs localities to the north, the zircon age spectra record a dominant ~1.2 Ga peak (Fig. 16). Several granitoid suites were intruded into the Musgrave Block in central Australia that yield U–Pb zircon ages of ~1225–1190 Ma, associated with Grenville-age orogeny and the amalgamation of Rodinia (Maboko et al. 1991; Dalziel 1991; Hoffman 1991; Moores 1991; Camacho and Fanning 1995). Similarly, the quartz monzonite plutons and gneiss of the Albany-Fraser Province outcrop near the southern margin of the Yilgarn Block and are dated at ~1175 Ma (Pidgeon 1990) and ~1200 Ma (Black and Shaw 1992), respectively. Thus, the ~1.2 Ga peak recorded in the Flinders Ranges is consistent with an Australian intra-continental source from central and/or western Australia. Alternatively, this peak could originate from the Grenville-age Wilkes Province of East Antarctica that abutted Australia throughout the Neoproterozoic (Goodge et al. 2008).

In the northern Flinders Ranges between the Moolooloo and Lame Horse Gully localities, the dominant peaks in the detrital zircon spectra are between ~665–760 Ma (Fig. 16 [7-9]). Within the Australian continent, the Paterson Province to the east of the Pilbara Craton and the Leeuwin Complex to the southwest of the Yilgarn Craton in Western Australia are the only regions hosting such young Neoproterozoic magmatic events (Fig. 2). The Paterson Province consists of granite, such as the Mt. Crofton Granite, with ages between ~600–700 Ma (McNaughton and Goellnicht 1990; Nelson 1995). The Leeuwin Complex is dominated by granitic gneiss with ages that suggest that the protoliths of the gneiss formed over 600 million years in distinct magmatic pulses at 1200–1050 Ma, 800–650 Ma, and 580–500 Ma (Nelson 1996, 1999, 2002; Collins and Fitzsimons 2001; Wilde and Nelson 2001). Both of these source areas suggest that ice likely covered at least half of the Australian

continent. Zircons ranging from ~600–750 Ma previously have been reported in sedimentary rocks from the ARC (Compston et al. 1987), Lachlan Fold Belt (Williams et al. 1988), and New Zealand and Marie Byrd Land, Antarctica (Ireland et al. 1994), but the source regions for the sediment still remain a matter of conjecture. It has been suggested that the sediment initially was deposited in a sub-marine turbidite fan fed from the rising Delamerian-Ross Orogen of eastern Antarctica and southeastern Australia (Coney et al. 1990). Thus, another possibility is that the ~665–760 Ma zircons are derived by recycling sediment from a regional eastern Antarctic and southeastern Australian source, or if, since the sediment being recycled has ~760 Ma zircons, it too could be tapping the cratonic sources in Western Australia.

The predominance of <760 Ma young zircons at several northern Flinders localities suggests that perhaps an additional or different source supplied sediment to this region compared to the rest of the ARC. Furthermore, this area coincides with the localities that record the deepest glacial incision into the carbonate platform (Fig. 7). The modern Antarctic ice cap is drained by ice streams where regions of rapidly moving land ice are in contact with slower moving ice on either side (Alley et al. 2004). Although they account for only 10% of the volume of the ice sheet, ice streams are sizeable features, up to 50 km wide, 2000 m thick, and can reach up to 700 km long (Joughin et al. 2001). These fast flowing zones can erode up to a kilometre deep into bedrock (Young et al. 2011) and represent conveyor belts that potentially could transport sediment to the ice sheet margins. Studies have indicated that ice streams have high sediment fluxes between ~100–1000 $m^3\ yr^{-1}$ per metre of ice front, and sediment transport to continental shelves by paleo-ice streams was even greater (Alley et al. 2007). The estimated sediment flux for the Norwegian Channel paleo-ice stream is 8000 $m^3\ yr^{-1}$ per metre width of the ice stream front (Nygard et al. 2007). This sediment is derived from large interior basins. The Rutford Ice Stream in West Antarctica drains a ~45,600 $km^2$ catchment basin into the Ronne Ice Shelf (Joughin and Bamber 2005), but some Antarctic ice streams can drain basins of >100 000 $km^2$ (Dowdeswell et al. 2006). The young age of these zircon grains suggests that such a Cryogenian ice stream would have had to flow at least 2000 km across the continent from Paterson Province and/or Leeuwin Complex in Western Australia. Alternatively, these young zircon grains (<760 Ma) may represent different zircon populations transported by a more local ice stream from sources in southeastern Australia and/or eastern Antarctica.

Previous geochronological studies in the Adelaide Rift Complex have placed constraints on the maximum age of the Elatina glaciation. Ireland et al. (1998) noted several young detrital zircons at ca. 650 Ma from the correlative Marino Arkose Member in the Hallett Cove area south of Adelaide. In particular, a detrital zircon U–Pb age of 657 ± 17 Ma was obtained for a single grain that may place an upper limit on the depositional age of the Marino Arkose (Ireland et al. 1998; Preiss 2000). Our data corroborate these findings: the youngest zircon grains between ca. 650–665 Ma are found within the Marino Arkose at Halletts Cove (Fig. 16), the Elatina Fm. at Elatina Creek and Walter's Well (Fig. 16 [3,7]), and in the correlative Whyalla Fm. on the Stuart Shelf (n=7; Fig. 16 [13,14]).

## CONCLUSIONS

The basin scale architecture and wide range of sedimentary facies of the pre- and syn- late Cryogenian glacial sedimentary rocks of the ARC establish important constraints on the dynamics of the Elatina glaciation in South Australia, providing insight into several contentious aspects of the snowball Earth hypothesis. The Yaltipena Fm. tidal flat sediments interfingered with and prograded over the pre-glacial carbonate platform, which heralded the onset of the glaciation. This influx of sediment and possible associated sea level fall suggests that ice originated from land, and thereby challenges a corollary of the snowball Earth model that suggests the first ice in the tropics would arrive by the advance of sea glaciers (Hoffman et al. 2002). Measured stratigraphic sections and carbon isotopes were used to quantify ~130 m of glacial erosion across the carbonate platform and at least 500 m of erosion is inferred based upon the correlation of carbonate clasts within the diamictite to the underlying regional chemostratigraphy. The $\delta^{13}C$ measurements of carbonate clasts within the glacial diamictites give insight to the relative timing of $\delta^{13}C$ acquisition. The wide variability of the clasts shows that they record the full isotopic range from –9‰ to +10‰ present in the carbonate platform $\delta^{13}C$ profile. This isotope conglomerate test supports the conclusion that the Trezona $\delta^{13}C$ anomaly was recorded long before burial diagenesis could have occurred (Rose et al. 2012).

Evidence for sub-glacial erosion of the carbonate platform by ice streams and ice-front instability within an overall deglacial sequence remains compatible with snowball Earth models (Donnadieu et al. 2003; Halverson et al. 2004). Our evidence suggests that the local deglaciation and instantaneous loss of gravitational attraction of the ice sheet on the nearby ocean caused a relative sea level fall, which may be comparable to Greenland during Pleistocene deglaciations. Current and wave-generated combined-flow ripples across the ARC attest to open seas with significant fetch during the initial retreat of local glaciers. The current and wave-generated combined-flow ripples also figure prominently into determining the low-latitude of the Elatina glaciation. We re-interpret the folds used in the syn-sedimentary paleomagnetic fold test, as stoss-depositional transverse ripples with superimposed oscillatory wave ripples. Although these observations weaken the existing paleomagnetic constraint because the low paleolatitude is now only required to be pre-Late Cambrian, there is no evidence to suggest that the low-latitude direction is a result of remagnetization, and the positive reversal tests are at least consistent with syn-depositional magnetization (Sohl et al. 1999).

Detrital zircon data provide new constraints on the provenance of the glacial sediment. The distribution of zircon ages indicate that at least some glacial sediment derived from the

cratons of Western Australia. Additionally, zircon data from the late Cryogenian periglacial Whyalla Fm., which long has been held as the stratigraphic equivalent and potential source for the Elatina Fm., are sufficiently different from the Elatina Fm. to infer that the Whyalla Fm. does not provide a significant source of sediment to the Elatina Fm.

Environmental and climatic conditions are challenging to interpret from the spatially heterogeneous glacial sedimentary rocks, especially when studied in isolation. However, our work within the Elatina Fm. demonstrates that an approach that integrates basin-scale analysis with detailed sedimentology and chemostratigraphy, when set in the context of the pre- and post-glacial sediments, can provide new insights into the dynamics of extensive glaciations of the Cryogenian. New studies pairing the sedimentology, geochemical and stratigraphic methodologies applied to the Elatina Fm. in South Australia to the pre-, syn- and post-glacial deposits on other continents will be required to make progress in understanding Cryogenian glacial sediments.

## ACKNOWLEDGEMENTS

Field, stable isotope and geochronology work was supported by NSF grant EAR-0842946 and a Sloan Foundation Fellowship awarded to Maloof. Jon Husson provided numerous constructive comments on drafts that greatly improved the paper. Paul Myrow provided stimulating discussion in the field and Mauricio Perillo gave thoughtful comments concerning bedforms within the Elatina Fm. Fiona Best, Blake Dyer, Brehnin Keller, Laura Poppick, Justin Strauss, Nick Swanson-Hysell, Erica Wallstrom and Nora Xu provided enthusiastic assistance in the field. Darren Crawford and Arthur Coulthard gave invaluable help accessing the Flinders and Gammon Ranges National Parks. We are very grateful to the landowners and pastoralists for land access. Ayami Aoyama, Claire Calmet, Galen Gorski, Will Jacobsen, Jacquie Nesbit, Laura Poppick, Justin Strauss, and Nora Xu helped with sample preparation. Some stable isotope measurements were performed at the University of Michigan by Lora Wingate and Kacey Lohmann and at Princeton University by Laura Poppick. Some major element analyses for the CIA samples were run at Michigan State University by Tom Vogel, and carbonate content of these samples was determined at Northwestern University by Petra Sheaffova and Brad Sageman. We are thankful to Gerald Poirier and Nan Yao for help with the XRD analyses at Princeton Institute for the Science and Technology of Materials. Andrew Kylander-Clark and Gareth Seward are thanked for assistance with U–Pb geochronologic analyses at UCSB.

## REFERENCES

Abbot, D.S., Voigt, A., and Koll, D., 2011, The Jormungand global climate state and implications for Neoproterozoic glaciations: Journal of Geophysical Research, v. 116, D18103, http://dx.doi.org/10.1029/2011JD015927.

Allen, P.A., and Etienne, J.L., 2008, Sedimentary challenge to Snowball Earth: Nature Geoscience, v. 1, p. 817–825, http://dx.doi.org/10.1038/ngeo355.

Alley, R.B., Anandakrishnan, S., Dupont, T.K., and Parizek, B.R., 2004, Ice streams —fast, and faster?: Comptes Rendus Physique, v. 5, p. 723–734, http://dx.doi.org/10.1016/j.crhy.2004.08.002.

Alley, R.B., Anandakrishnan, S., Dupont, T.K., Parizek, B.R., and Pollard, D., 2007, Effect of sedimentation on ice-sheet grounding-line stability: Science, v. 315, p. 1838–1841, http://dx.doi.org/10.1126/science.1138396.

Arnaud, E. and Eyles, C.H., 2006, Neoproterozoic environmental change recorded in the Port Askaig Formation, Scotland: Climatic *vs* tectonic controls: Sedimentary Geology, v. 183, p. 99–124.

Bahlburg, H. and Dobrzinski, N., 2011, A review of the Chemical Index of Alteration (CIA) and its application to the study of Neoproterozoic glacial deposits and climate transitions, *in* Arnaud, E., Halverson, G.P., and Shields–Zhou, G., *eds.*, The Geological Record of Neoproterozoic Glaciations: Geological Society London, Memoirs, v. 36, p. 81–92, http://dx.doi.org/ 10.1144/M36.6.

Binks, P.J., 1968, Orroroo South Australia 1:250 000 geological series map. Sheet SI/54-1, Bureau of Mineral Resources, Australia.

Black, L.P., and Shaw, R.D., 1992, U–Pb zircon chronology of prograde Proterozoic events in the Central and Southern Provinces of the Arunta Block, central Australia: Australian Journal of Earth Sciences, v. 39, p. 153–171, http://dx.doi.org/10.1080/08120099208728012.

Bowring, S.A., Grotzinger, J.P., Condon, D.J., Ramezani, J., Newall, M.J., and Allen, P.A., 2007, Geochronologic constraints on the chronostratigraphic framework of the Neoproterozoic Huqf Supergroup, Sultanate of Oman: American Journal of Science, v. 307, p. 1097–1145, http://dx.doi.org/10.2475/10.2007.01.

Brenchley-Gaal, A.J., 1985, The influence of faulting on late Proterozoic sedimentation and Delamerian tectonic development within the Nuccaleena area, Central Flinders Ranges, South Australia: Unpublished B.Sc. (Honours) thesis, University of Adelaide, Adelaide.

Budnick, A.S., 2012, Origins of the Elatina Rhythmites and the history of the Earth–Moon orbit: Junior Paper, Princeton University, Princeton, NJ.

Camacho, A., and Fanning, C.M., 1995, Some isotopic constraints on the evolution of the granulite and upper amphibolite facies terranes in the eastern Musgrave Block, central Australia: Precambrian Research, v. 71, p. 155–181, http://dx.doi.org/10.1016/0301-9268(94)00060-5.

Chen, C., 2012, Insights on Earth's deepest $\delta^{13}C$ excursion from paleocanyon structures at Saint Ronan, Beltana Station, South Australia: Junior Paper, Princeton University, Princeton, NJ.

Christie-Blick, N., Sohl, L.E., and Kennedy, M., 1999, Considering a Neoproterozoic Snowball Earth: Science, v. 284, p. 1087, http://dx.doi.org/10.1126/science.284.5417.1087a.

Coats, R., 1965, Diapirism in the Adelaide Geosyncline: Australian Petroleum Exploration Association Journal, v. 1965, p. 98–102.

Coats, R.P., 1981, Late Proterozoic (Adelaidean) tillites of the Adelaide Geosyncline, *in* Hambrey, M.J., and Harland, W.B., *eds.*, Earth's Pre-Pleistocene Glacial Record, Cambridge University Press, Cambridge, p. 537–548.

Coats, R.P., and Blisset, A.H., 1971, Regional and economic geology of the Mount Painter Province: Geological Survey of South Australia Bulletin, no. 43, p. 66–88.

Coats, R., Callen, R., Williams, A., and Thompson, B., 1973, Copley 1:250 000 Geological Map Sheet: Technical

report, Geological Survey of South Australia, Department of Mines Adelaide.

Colin, C., Kissel, C., Blamart, D., and Turpin, L., 1998, Magnetic properties of sediments in the Bay of Bengal and the Andaman Sea: impact of rapid North Atlantic Ocean climatic events on the strength of the Indian monsoon: Earth and Planetary Science Letters, v. 160, p. 623–635, http://dx.doi.org/10.1016/S0012-821X(98)00116-2.

Collins, A., and Fitzsimons, I., 2001, Structural, isotopic and geochemical constraints on the evolution of the Leeuwin Complex, SW Australia (abstract), *in* Sircombe, K., and Li, Z., *eds.*, From Basins to Mountains: Rodinia at the turn of the century: Geological Society of Australia Abstract Series 65, p. 16–19.

Compston, W., Crawford, A., and Bofinger, V., 1966, A radiometric estimate of the duration of sedimentation in the Adelaide Geosyncline, South Australia: Journal of the Geological Society of Australia, v. 13, p. 229–276, http://dx.doi.org/10.1080/00167616608728611.

Compston, W., Williams, I.S., Jenkins, R.J.F., Gostin, V.A., and Haines, P.W., 1987, Zircon age evidence for the Late Precambrian Acraman ejecta blanket: Australian Journal of Earth Sciences, v. 34, p. 435–445, http://dx.doi.org/10.1080/08120098708729424.

Condon, D.J., Prave, A.R., and Benn, D.I., 2002, Neoproterozoic glacial-rainout intervals: Observations and implications: Geology, v. 30, p. 35–38, http://dx.doi.org/10.1130/0091-7613(2002)030<0035:NGRIOA>2.0.CO;2.

Condon, D., Zhu, Maoyan, Bowring, S., Wang, Wei, Yang, Aihua, and Jin, Yugan, 2005, U–Pb ages from the Neoproterozoic Doushantuo Formation, China: Science, v. 308, p. 95–98, http://dx.doi.org/10.1126/science.1107765.

Coney, P.J., Edwards, A., Hine, R., Morrison, F., and Windrim, D., 1990, The regional tectonics of the Tasman orogenic system, eastern Australia: Journal of Structural Geology, v. 12, p. 519–543, http://dx.doi.org/10.1016/0191-8141(90)90071-6.

Corcoran, P.L., and Mueller, W.U., 2002, The effects of weathering, sorting and source composition in Archaean high-relief basins: examples from the Slave Province, Northwest Territories, Canada, *in* Altermann, W., and Corcoran, P., *eds.*, Precambrian Sedimentary Environments: A Modern Approach to Ancient Depositional Systems: Special Publication 33 of the International Association of Sedimentologists, p. 183–211.

Cottle, J.M, Horstwood, M.S.A., and Parrish, R.R., 2009a, A new approach to single shot laser ablation analysis and its application to in situ Pb/U geochronology: Journal of Analytical Atomic Spectrometry, v. 24, p. 1355–1363, http://dx.doi.org/10.1039/b821899d.

Cottle, J.M., Jessup, M.J., Newell, D.L., Horstwood, M.S.A., Noble, S.R., Parrish, R.R., Waters, D.J., and Searle, M.P., 2009b, Geochronology of granulitized eclogite from the Ama Drime Massif: Implications for the tectonic evolution of the South Tibetan Himalaya: Tectonics, v. 28, p. TC1002, http://dx.doi.org/10.1029/2008TC002256.

Cottle, J.M., Searle, M.P., Horstwood, M.S.A., and Waters, D.J., 2009c, Timing of midcrustal metamorphism, melting and deformation in the Mount Everest region of southern Tibet revealed by U(–Th)–Pb geochronology: The Journal of Geology, v. 117, p. 643–664, http://dx.doi.org/10.1086/605994.

Cox, R., Lowe, D.R., and Cullers, R.L., 1995, The influence of sediment recycling and basement composition on evolution of mudrock chemistry in the southwestern United States: Geochimica et Cosmochimicha Acta, v. 59, p. 2919–2940, http://dx.doi.org/10.1016/0016-7037(95)00185-9.

Dalgarno, C.R. and Johnson, J.E., 1964, Glacials of the Marinoan Series, central Flinders Ranges: Geological Survey of South Australia Quarterly Geology Notes, v. 11, p. 3–4.

Dalgarno, C.R. and Johnson, J.E., 1968, Diapiric structures and late Precambrian–early Cambrian sedimentation in the Flinders Ranges, South Australia: American Association of Petroleum Geologists Special Volumes, Memoir v. 8, p. 301–314.

Dalziel, I.W.D., 1991, Pacific margins of Laurentia and East Antarctica–Australia as a conjugate rift pair: Evidence and implications for an Eocambrian supercontinent: Geology, v. 19, p. 598–601, http://dx.doi.org/10.1130/0091-7613(1991)019<0598:PMOLAE>2.3.CO;2.

DeCelles, P.G., Quade, J., Kapp, P., Fan, M., Dettman, D.L., and Ding, L., 2007, High and dry in central Tibetan during the Late Oligocene: Earth and Planetary Science Letters, v. 253, p. 389–401, http://dx.doi.org/10.1016/j.epsl.2006.11.001.

Deynoux, M., 1985, Terrestrial or waterlain glacial diamictites? Three case studies from the late Proterozoic and late Ordovician glacial drifts in West Africa: Palaeogeography, Palaeoclimatology, Palaeoecology, v. 51, p. 97–141, http://dx.doi.org/10.1016/0031-0182(85)90082-3.

Deynoux, M. and Trompette, R., 1976, Late Precambrian mixtites: Glacial and/or nonglacial? Dealing especially with the mixtites of West Africa (Discussion): American Journal of Science, v. 276, p. 1302–1315, http://dx.doi.org/10.2475/ajs.276.10.1302.

Dobrzinski, N., Bahlburg, H., Strauss, H., and Zhang, Qirui, 2004, Geochemical climate proxies applied to the Neoproterozoic glacial succession on the Yangtze Platform, South China, *in* Jenkins, G.S., McMenamin, M.A.S., McKay, C.P., and Sohl, L., *eds.*, The Extreme Proterozoic: Geology, Geochemistry, and Climate: American Geophysical Union, Geophysical Monograph Series v. 146, p. 13–32.

Donnadieu, Y., Fluteau, F., Ramstein, G., Ritz, C., and Besse, J., 2003, Is there a conflict between the Neoproterozoic glacial deposits and the snowball Earth interpretation: an improved understanding with numerical modeling: Earth and Planetary Science Letters, v. 208, p. 101–112, http://dx.doi.org/10.1016/S0012-821X(02)01152-4.

Dowdeswell, J.A., Ottesen, D., and Rise, L., 2006, Flow switching and large-scale deposition by ice streams draining former ice sheets: Geology, v. 34, p. 313–316, http://dx.doi.org/10.1130/G22253.1.

Drexel, J., and Preiss, W.V., *eds.*, 1995, The geology of South Australia, Volume 2, The Phanerozoic: Geological Survey of South Australia Bulletin, v. 54, 347 p.

Dyson, I., 1992, Stratigraphic nomenclature and sequence stratigraphy of the lower Wilpena Group, Adelaide Geosyncline: the Sandison Subgroup: Geological Survey of South Australia Quarterly Geology Notes, v. 122, p. 2–13.

Eastwood, E.N., Kocurek, G., Mohrig, D., and Swanson, T., 2012, Methodology for reconstructing wind direction, wind speed and duration of wind events from aeolian cross-strata: Journal of Geophysical Research, v. 117, F03035, http://dx.doi.org/

10.1029/2012JF002368.
Elburg, M.A., Bons, P.D., Dougherty-Page, J., Janka, C.E., Neumann, N., and Schaefer, B., 2001, Age and metasomatic alteration of the Mt Neill Granite at Nooldoonooldoona Waterhole, Mt Painter Inlier, South Australia: Australian Journal of Earth Sciences, v. 48, p. 721–730, http:dx.doi.org/10.1046/j.1440-0952.2001.485890.x.
Embleton, B.J.J., and Williams, G.E., 1986, Low palaeolatitude of deposition for late Precambrian periglacial varvites in South Australia: implications for palaeoclimatology: Earth and Planetary Science Letters, v. 79, p. 419–430, http://dx.doi.org/10.1016/0012-821X(86)90197-4.
Evans, D.A.D., 2000, Stratigraphic, geochronological, and paleomagnetic constraints upon the Neoproterozoic climatic paradox: American Journal of Science, v. 300, p. 347–433, http://dx.doi.org/10.2475/ajs.300.5.347.
Evans, D.A.D. and Raub, T.D., 2011, Neoproterozoic glacial palaeolatitudes: a global update, *inI* Arnaud, E., Halverson, G.P., and Sheilds-Zhou, G., *eds.*, The Geological Record of Neoproterozoic Glaciations: The Geological Society, London, Memoirs, v. 36, p. 93–112, http:dx.doi.org/10.1144/M36.7.
Eyles, C.H., Eyles, N., and Grey, K., 2007, Palaeoclimate implications from deep drilling of Neoproterozoic strata in the Officer Basin and Adelaide Rift Complex of Australia; a marine record of wet-based glaciers: Palaeogeography, Palaeoclimatology, Palaeoecology, v. 248, p. 291–312, http://dx.doi.org/10.1016/j.palaeo.2006.12.008.
Eyles, N., 1993, Earth's glacial record and its tectonic setting: Earth–Science Reviews, v. 35, p. 1–248, http://dx.doi.org/10.1016/0012-8252(93)90002-O.
Eyles, N., and Januszczak, N., 2004, 'Zipper-rift': a tectonic model for Neoproterozoic glaciations during the breakup of Rodinia after 750 Ma: Earth–Science Reviews, v. 65, p. 1–73, http://dx.doi.org/10.1016/S0012-8252(03)00080-1.
Fairchild, I.J., 1993, Balmy shores and icy wastes: The paradox of carbonates associated with glacial deposits in Neoproterozoic times, *in* Wright, V.P., Sedimentology Review, v. 1: Blackwell Publishing Ltd, Oxford, UK, p. 1–16, http://dx.doi.org/10.1002/9781444304534.ch1.
Fanning, C., Ludwig, K., Forbes, B., and Preiss, W., 1986, Single and multiple grain U–Pb zircon analyses for the Early Adelaidean Rook Tuff, Willouran Ranges, South Australia (abstract): Geological Society of Australia, Abstract Series AB 15, p. 71–72.
Fanning, M.C., 2006, Constraints on the timing of the Sturtian glaciation from southern Australia; IE for the true Sturtian (abstract): Geological Society of America Abstracts with Programs, v. 38, p. 115.
Fedo, C.M., Nesbitt, H.W., and Young, G.M., 1995, Unraveling the effects of potassium metasomatism in sedimentary rocks and paleosols, with implications for paleoweathering conditions and provenance: Geology, v. 23, p. 921–924, http://dx.doi.org/10.1130/0091-7613(1995)023<0921:UTEOPM>2.3.CO;2.
Fedo, C.M., Eriksson, K.A., and Krogstad, E.J., 1996, Geochemistry of shales from the Archean (~3.0 Ga) Buhwa Greenstone Belt, Zimbabwe: Implications for provenance and source-area weathering: Geochimica et Cosmochimicha Acta, v. 60, p. 1751–1763, http://dx.doi.org/10.1016/0016-7037(96)00058-0.
Fedo, C.M., Young, G.M., Nesbitt, H.W., and Hanchar, J.M., 1997a, Potassic and sodic metasomatism in the Southern Province of the Canadian Shield: Evidence from the Paleoproterozoic Serpent Formation, Huronian Supergroup, Canada: Precambrian Research, v. 84, p. 17–36, http://dx.doi.org/10.1016/S0301-9268(96)00058-7.
Fedo, C.M., Young, G.M., and Nesbitt, H.W., 1997b, Paleoclimatic control on the composition of the Paleoproterozoic Serpent Formation, Huronian Supergroup, Canada: a greenhouse to icehouse transition: Precambrian Research, v. 86, p. 201–223, http://dx.doi.org/10.1016/S0301-9268(97)00049-1.
Fike, D.A., Grotzinger, J.P., Pratt, L.M., and Summons, R.E., 2006, Oxidation of the Ediacaran Ocean: Nature, v. 444, p. 744–747, http://dx.doi.org/10.1038/nature05345.
Foden, J., Elburg, M.A., Dougherty-Page, J., and Burtt, A., 2006, The timing and duration of the Delamerian Orogeny: Correlation with the Ross Orogen and implications for Gondwana assembly: The Journal of Geology, v. 114, p. 189–210, http://dx.doi.org/10.1086/499570.
Forbes, B. and Preiss, W., 1987, Stratigraphy of the Wilpena Group, *in* Preiss, W.V., *ed.*, The Adelaide Geosyncline: Late Proterozoic stratigraphy, sedimentation, palaeontology and tectonics: Geological Survey of South Australia Bulletin, v. 53, p. 211–248.
Fralick, P.W. and Kronberg, B.I., 1997, Geochemical discrimination of clastic sedimentary rock sources: Sedimentary Geology, v. 113, p. 111–124, http://dx.doi.org/10.1016/S0037-0738(97)00049-3.
Fromhold, T.A., and Wallace, M.W., 2011, Nature and significance of the Neoproterozoic Sturtian– Marinoan Boundary, Northern Adelaide Geosyncline, South Australia: Australian Journal of Earth Sciences, v. 58, p. 599–613, http://dx.doi.org/10.1080/08120099.2011.579624.
Gerdes, A. and Zeh, A., 2006, Combined U–Pb and Hf isotope LA–(MC–) ICP–MS analyses of detrital zircons: Comparison with SHRIMP and new constraints for the provenance and age of an Armorican metasediment in Central Germany: Earth and Planetary Science Letters, v. 249, p. 47–61, http://dx.doi.org/10.1016/j.epsl.2006.06.039.
Giddings, J.A., and Wallace, M.W., 2009, Facies-dependent $\delta^{13}C$ variation from a Cryogenian platform margin, South Australia: Evidence for stratified Neoproterozoic oceans?: Palaeogeography, Palaeoclimatology, Palaeoecology, v. 271, p. 196–214, http://dx.doi.org/10.1016/j.palaeo.2008.10.011.
Giddings, J.A., Wallace, M.W., and Woon, E.M.S., 2009, Interglacial carbonates of the Cryogenian Umberatana Group, northern Flinders Ranges, South Australia: Australian Journal of Earth Sciences, v. 56, p. 907–925, http://dx.doi.org/10.1080/08120090903005378.
Goodge, J.W., Vervoort, J.D., Fanning, C.M., Brecke, D.M., Farmer, G.L., Williams, I.S., Myrow, P.M., and DePaola, D.J., 2008, A Positive Test of East Antarctica–Laurentia juxtaposition within the Rodinia Supercontinent: Science, v. 321, p. 235–240, http://dx.doi.org/10.1126/science.1159189.
Grantham, J.H., and Velbel, M.A., 1988, The influence of climate and topography on rock-fragment abundance in modern fluvial sands of the southern Blue Ridge Mountains, North Carolina: Journal of Sedimentary Research, v. 58, p. 219–227, http://dx.doi.org/10.1306/212F8D5F-2B24-11D7-8648000102C1865D.
Grotzinger, J.P., Watters, W.A., and Knoll, A.H., 2000, Calcified metazoans in thrombolite-stromatolite reefs of the terminal Proterozoic Nama Group, Namibia: Paleobiology, v. 26, p.

334–359, http://dx.doi.org/10.1666/0094-8373(2000)026<0334:CMITSR>2.0.CO;2.

Gubbins, D., 1999, The distinction between geomagnetic excursions and reversals: Geophysical Journal International, v. 137, p. F1–F4, http://dx.doi.org/10.1046/j.1365-246x.1999.00810.x.

Halverson, G.P., Hoffman, P.F., Schrag, D.P., and Kaufman, A.J., 2002, A major perturbation of the carbon cycle before the Ghaub glaciation (Neoproterozoic) in Namibia: Prelude to snowball Earth?: Geochemistry, Geophysics, Geosystems, v. 3(6), p. 1–24, http://dx.doi.org/10.1029/2001GC000244.

Halverson, G.P., Maloof, A.C., and Hoffman, P.F., 2004, The Marinoan glaciation (Neoproterozoic) in northeast Svalbard: Basin Research, v. 16, p. 297–324, http://dx.doi.org/10.1111/j.1365-2117.2004.00234.x.

Halverson, G.P., Hoffman, P.F., Schrag, D.P., Maloof, A.C., and Rice, A.H.N., 2005, Toward a Neoproterozoic composite carbon-isotope record: Geological Society of America Bulletin, v. 117, p. 1181–1207, http://dx.doi.org/10.1130/B25630.1.

Hambrey, M.J., and Harland, W.B., 1981, Earth's Pre-Pleistocene Glacial Record: Cambridge University Press, Cambridge, 1024 p.

Higgins, J.A., and Schrag, D.P., 2003, Aftermath of a snowball Earth: Geochemistry, Geophysics, Geosystems, v. 4, p. 1028, http:dx.doi.org/10.1029/2002GC000403.

Hoffman, P.F., 1991, Did the breakout of Laurentia turn Gondwanaland inside–out?: Science, v. 252, p. 1409–1412, http://dx.doi.org/10.1126/science.252.5011.1409.

Hoffman, P.F., 2005, On Cryogenian (Neoproterozoic) ice-sheet dynamics and the limitations of the glacial sedimentary record: 28th DeBeers Alex. Du Toit Memorial Lecture, 2004, South African Journal of Geology, v. 108, p. 557–577, http://dx.doi.org/10.2113/108.4.557.

Hoffman, P.F., 2011, Strange bedfellows: glacial diamictite and cap carbonate from the Marinoan (635 Ma) glaciation in Nambia: Sedimentology, v. 58, p. 57–119, http://dx.doi.org/10.1111/j.1365-3091.2010.01206.x.

Hoffman, P.F., and Schrag, D.P., 2002, The snowball Earth hypothesis: testing the limits of global change: Terra Nova, v. 14, p. 129–155, http://dx.doi.org/10.1046/j.1365-3121.2002.00408.x.

Hoffman, P.F., Kaufman, A.J., Halverson, G.P., and Schrag, D.P., 1998, A Neoproterozoic Snowball Earth: Science, v. 281, p. 1342–1346, http://dx.doi.org/10.1126/science.281.5381.1342.

Hoffman, P.F., Halverson, G.P., and Grotzinger, J.P., 2002, Are Proterozoic cap carbonates and isotopic excursions a record of gas hydrate destabilization following Earth's coldest intervals? (Comment): Geology, v. 30, p. 286–287, http://dx.doi.org/10.1130/0091-7613(2002)030<0286:APCCAI>2.0.CO;2.

Hoffman, P.F., Halverson, G.P., Domack, E.W., Husson, J.M., Higgins, J.A., and Schrag, D.P., 2007, Are basal Ediacaran (635 Ma) post-glacial "cap dolostones" diachronous?: Earth and Planetary Science Letters, v. 258, p. 114–131, http://dx.doi.org/10.1016/j.epsl.2007.03.032.

Hoffmann, K.-H., Condon, D.J., Bowring, S.A., and Crowley, J.L., 2004, A U–Pb zircon date from the Neoproterozoic Ghaub Formation, Namibia: Constraints on Marinoan glaciation: Geology, v. 32, p. 817–820, http://dx.doi.org/10.1130/G20519.1.

Holland, D.M., Thomas, R.H., de Young, B., Ribergaard, M.H., and Lyberth, B., 2008, Acceleration of Jakobshavn Isbræ triggered by warm subsurface ocean waters: Nature Geoscience, v. 1, p. 659–664, http://dx.doi.org/10.1038/ngeo316.

Husson, J.M., Maloof, A.C., and Schoene, B., 2012, A syn-depositional age for Earth's deepest $\delta^{13}C$ excursion required by isotope conglomerate tests: Terra Nova, v. 24, p. 318–325, http://dx.doi.org/10.1111/j.1365-3121.2012.01067.x.

Ireland, T.R., Bradshaw, J.D., Muir, R., Weaver, S., and Adams, C., 1994, Zircon age distributions in granites, greywackes, and gneisses from the southwest Pacific Gondwana region (abstract): 8th International Conference on Geochronology, Cosmochronology and Isotope Geology, p. 151.

Ireland, T.R., Flöttmann, T., Fanning, C.M., Gibson, G.M., and Preiss, W.V., 1998, Development of the early Paleozoic Pacific margin of Gondwana from detrital-zircon ages across the Delamerian orogen: Geology, v. 26, p. 243–246, http://dx.doi.org/10.1130/0091-7613(1998)026<0243:DOTEPP>2.3.CO;2.

Jablonski, H., 1975, Late Precambrian geology of the Warren–Buckaringa Gorge area, Flinders Ranges, South Australia: Unpublished B.Sc. (Honours) thesis, University of Adelaide, Adelaide.

Jackson, S.E., Pearson, N.J., Griffin, W.L., and Belousova, E.A., 2004, The application of laser ablation- inductively coupled plasma-mass spectrometry to in situ U–Pb zircon geochronology: Chemical Geology, v. 211, p. 47–69, http://dx.doi.org/10.1016/j.chemgeo.2004.06.017.

James, N.P., Narbonne, G.M., and Kyser, T.K., 2001, Late Neoproterozoic cap carbonates: Mackenzie Mountains, northwestern Canada: precipitation and global glaciation meltdown: Canadian Journal of Earth Sciences, v. 38, p. 1229–1262, http://dx.doi.org/10.1139/e01-046.

Jenkins, R.J.F., 1990, The Adelaide Fold Belt: Tectonic reappraisal, *in* Jago, J.B., and Moore, P.S., *eds.*, The Evolution of a Late Precambrian–Early Palaeozoic Rift Complex: the Adelaide Geosyncline: Geological Society of Australia Special Publication, v. 16, p. 396–420.

Johnsson, M.J., 1993, The system controlling the composition of clastic sediments, *in* Johnsson, M.J., and Basu, A., *eds.*, Processes Controlling the Composition of Clastic Sediments, Geological Society America, Special Papers, v. 284, p. 1–20, http://dx.doi.org/10.1130/SPE284-p1.

Joughin, I. and Bamber, J.L., 2005, Thickening of the ice stream catchments feeding the Filchner–Ronne Ice Shelf, Antarctica: Geophysical Research Letters, v. 32, p. L17503, http://dx.doi.org/10.1029/2005GL023844.

Joughin, I., Fahnestock, M.F., MacAyeal, D., Bamber, J.L., and Gogineni, P., 2001, Observation and analysis of ice flow in the largest Greenland ice stream: Journal of Geophysical Research, v. 106, p. 34021–34034, http://dx.doi.org/10.1029/2001JD900087.

Karlstrom, K.E., and Bowring, S.A., 1988, Early Proterozoic assembly of tectonostratigraphic terranes in southwestern North America: The Journal of Geology, v. 96, p. 561–576, http://dx.doi.org/10.1086/629252.

Kendall, B., Creaser, R.A., and Selby, D., 2006, Re–Os geochronology of postglacial black shales in Australia: Constraints on the timing of "Sturtian" glaciation: Geology, v. 34, p. 729–732, http://dx.doi.org/10.1130/G22775.1.

Kennedy, M.J., 1996, Stratigraphy, sedimentology, and isotopic geochemistry of Australian Neoproterozoic postglacial cap dolostones; Deglaciation, $\delta^{13}C$ excursions, and carbonate precipitation: Journal of Sedimentary Research,

v. 66, p. 1050–1064, http://dx.doi.org/10.2110/jsr.66.1050.
Kennedy, M.J., Runnegar, B., Prave, A.R., Hoffmann, K.-H., and Arthur, M.A., 1998, Two or four Neoproterozoic glaciations?: Geology, v. 26, p. 1059–1063, http://dx.doi.org/10.1130/0091-7613(1998)026<1059:TOFNG>2.3.CO;2.
Kennedy, M.J., Christie-Blick, N., and Sohl, L.E., 2001, Are Proterozoic cap carbonates and isotopic excursions a record of gas hydrate destabilization following Earth's coldest intervals?: Geology, v. 29, p. 443–446, http://dx.doi.org/10.1130/0091-7613(2001)029<0443:APCCAI>2.0.CO;2.
Kilner, B., Mac Niocaill, C., and Brasier, M., 2005, Low-latitude glaciation in the Neoproterozoic of Oman: Geology, v. 33, p. 413–416, http://dx.doi.org/10.1130/G21227.1.
Kirschvink, J.L., 1992, Late Proterozoic low-latitude global glaciation: The snowball Earth, *in* Schopf, J.W., and Klein, C., *eds.*, The Proterozoic Biosphere: a multidisciplinary study: Cambridge University Press, p. 51–52.
Knoll, A., Walter, M., Narbonne, G., and Christie-Blick, N., 2006, The Ediacaran Period: a new addition to the geologic time scale: Lethaia, v. 39, p. 13–30, http://dx.doi.org/10.1080/00241160500409223.
Kopp, R.E., Simons, F.J., Mitrovica, J.X., Maloof, A.C., and Oppenheimer, M., 2009, Probabilistic assessment of sea level during the last interglacial stage: Nature, v. 462, p. 863–868, http://dx.doi.org/10.1038/nature08686.
Krissek, L.A., and Kyle, P.R., 1998, Geochemical indicators of weathering and Cenozoic palaeoclimates in sediments from CRP-1 and CIROS-1, McMurdo Sound, Antarctica: Terra Antartica, v. 5, p. 673–680.
Lamb, M.P., Fischer, W.W., Raub, T.D., Perron, J.T., and Myrow, P.M., 2012, Origin of giant wave ripples in snowball Earth cap carbonate: Geology, v. 40, p. 827–830, http://dx.doi.org/10.1130/G33093.1.
Leather, J., Allen, P.A., Brasier, M.D., and Cozzi, A., 2002, Neoproterozoic snowball Earth under scrutiny: Evidence from the Fiq glaciation of Oman: Geology, v. 30, p. 891–894, http://dx.doi.org/10.1130/0091-7613(2002)030<0891:NSEUSE>2.0.CO;2.
Leeson, B., 1970, Geology of the Beltana 1:63 360 map area: Technical report, Geological Survey of South Australia.
Le Heron, D.P., 2012, The Cryogenian record of glaciation and deglaciation in South Australia: Sedimentary Geology, v. 243–244, p. 57–69, http://dx.doi.org/10.1016/j.sedgeo.2011.09.013.
Le Heron, D.P., Cox, G., Trundley, A., and Collins, A.S., 2011a, Two Cryogenian glacial successions compared: Aspects of the Sturt and Elatina sediment records of South Australia: Precambrian Research, v. 186, p. 147–168, http://dx.doi.org/10.1016/j.precamres.2011.01.014.
Le Heron, D.P., Cox, G., Trundley, A., and Collins, A., 2011b, Sea ice-free conditions during the Sturtian glaciation (early Cryogenian), South Australia: Geology, v. 39, p. 31–34, http://dx.doi.org/10.1130/G31547.1.
Lemon, N., 1985, Physical modeling of sedimentation adjacent to diapirs and comparison with late Precambrian Oratunga breccia body in central Flinders Ranges, South Australia: American Association of Petroleum Geologists Bulletin, v. 69, p. 1327–1338.
Lemon, N.M., 2000, A Neoproterozoic fringing stromatolite reef complex, Flinders Ranges, South Australia: Precambrian Research, v. 100, p. 109–120, http://dx.doi.org/10.1016/S0301-9268(99)00071-6.
Lemon, N., and Gostin, V., 1990, Glacigenic sediments of the late Proterozoic Elatina Forma- tion and equivalents, Adelaide Geosyncline, South Australia, *in* Jago, J.B., and Moore, P.S., *eds.*, The Evolution of a Late Precambrian–Early Palaeozoic Rift Complex: the Adelaide Geosyncline: Geological Society of Australia Special Publication Geological Society of Australia Special Publication, v. 16, p. 149–164.
Lemon, N.M., and Reid, P.W., 1998, The Yaltipena Formation of the Central Flinders Ranges: MESA Journal, v. 8, p. 37–39.
Løvlie, R., and Torsvik, T., 1984, Magnetic remanence and fabric properties of laboratory-deposited hematite-bearing red sandstone: Geophysical Research Letters, v. 11, p. 221–224, http://dx.doi.org/10.1029/GL011i003p00221.
Maboko, M.A.H., Williams, I.S., and Compston, W., 1991, Zircon U–Pb chronometry of the pressure and temperature history of granulites in the Musgrave Ranges, central Australia: The Journal of Geology, v. 99, p. 675–697, http://dx.doi.org/10.1086/629532.
Macdonald, F.A., Schmitz, M.D., Crowley, J.L., Roots, C.F., Jones, D.S., Maloof, A.C., Strauss, J.V., Cohen, P.A., Johnston, D.T., and Schrag, D.P., 2010, Calibrating the Cryogenian: Science, v. 327, p. 1241–1243, http://dx.doi.org/10.1126/science.1183325.
Malmon, D.V., Dunne, T., and Reneau, S.L., 2003, Stochastic theory of particle trajectories through alluvial valley floors: The Journal of Geology, v. 111, p. 525–542, http://dx.doi.org/10.1086/376764.
Maloof, A.C., Rose, C.V., Beach, R., Samuels, B.M., Calmet, C.C., Erwin, D.H., Poirier, G.R., Yao, Nan, and Simons, F.J., 2010, Possible animal-body fossils in pre-Marinoan limestones from South Australia: Nature Geoscience, v. 3, p. 653–659, http://dx.doi.org/10.1038/ngeo934.
Mawson, D., 1949, A third occurrence of glaciation evidenced in the Adelaide System: Transactions of the Royal Society of South Australia, v. 73, p. 117–121.
McLennan, S.M., Hemming, S., McDaniel, D.K., and Hanson, G.N., 1993, Geochemical approaches to sedimentation, provenance and tectonics, *in* Johnsson, M.J., and Basu, A., *eds.*, Processes Controlling the Composition of Clastic Sediments: Geological Society of America Special Papers, v. 284, p. 21–40, http://dx.doi.org/10.1130/SPE284-p21.
McNaughton, N.J., and Goellnicht, N.M., 1990, The age and radiothermal properties of the Mount Crofton Granite, Telfer area, Western Australia: Australian Journal of Earth Sciences, v. 37, p. 103–106, http://dx.doi.org/10.1080/08120099008727909.
Miller, R.K., 1975, The late Precambrian geology of the Wyacca Bluff–Buckaringa Gorge area, Flinders Ranges, South Australia: Unpublished B.Sc. (Honours) thesis, University of Adelaide, Adelaide.
Mitrovica, J.X., Gomez, N., and Clark, P.U., 2009, The sea-level fingerprint of West Antarctic collapse: Science, v. 323, p. 753, http://dx.doi.org/10.1126/science.1166510.
Moores, E.M., 1991, Southwest US–East Antarctic (SWEAT) connection: A hypothesis: Geology, v. 19, p. 425–428, http://dx.doi.org/10.1130/0091-7613(1991)019<0425:SUSEAS>2.3.CO;2.
Myrow, P.M., 1992, Pot and gutter casts from the Chapel Island Formation, Southeast Newfoundland: Journal of Sedimentary Research, v. 62, p. 992–1007,

http://dx.doi.org/10.2110/jsr.62.992.
Nelson, D.R., 1995, Compilation of SHRIMP U–Pb zircon geochronology data, 1994: Geological Survey of Western Australia Geological Survey, Record 1995/3, 244 p.
Nelson, D.R., 1996, Compilation of SHRIMP U–Pb zircon geochronology data, 1995: Geological Survey of Western Australia, Record 1996/ 5, 168 p.
Nelson, D.R., 1999, Compilation of geochronology data, 1998: Geological Survey of Western Australia, Record 1999/2, 222 p.
Nelson, D., 2002, Compilation of Geochronological Data, 2001: Geological Survey of Western Australia, v. 2.
Nesbitt, H.W., and Young, G.M., 1982, Early Proterozoic climates and plate motions inferred from major element chemistry of lutites: Nature, v. 299, p. 715–717, http://dx.doi.org/10.1038/299715a0.
Nesbitt, H.W., and Young, G.M., 1984, Prediction of some weathering trends of plutonic and volcanic rocks based on thermodynamic and kinetic considerations: Geochimica et Cosmochimicha Acta, v. 48, 1523–1534, http://dx.doi.org/10.1016/0016-7037(84)90408-3.
Nesbitt, H.W., and Young, G.M., 1989, Formation and diagenesis of weathering profiles: The Journal of Geology, v. 97, p. 129–147, http://dx.doi.org/10.1086/629290.
Nesbitt, H.W., and Young, G.M., 1996, Petrogenesis of sediments in the absence of chemical weathering: effects of abrasion and sorting on bulk composition and mineralogy: Sedimentology, v. 43, p. 341–358, http://dx.doi.org/10.1046/j.1365-3091.1996.d01-12.x.
Noyes, R.W., Weiss, N.O., and Vaughan, A.H., 1984, The relation between stellar rotation rate and activity cycle periods: Astrophysics Journal, v. 287, p. 769–773, http://dx.doi.org/10.1086/162735.
Nygård, A., Sejrup, H.P., Haflidason, H., Lekens, W.A.H., Clark, C.D., and Bigg, G.R., 2007, Extreme sediment and ice discharge from marine-based ice streams: New evidence from the North Sea: Geology, v. 35, p. 395–398, http://dx.doi.org/10.1130/G23364A.1.
Panahi, A. and Young, G.M., 1997, A geochemical investigation into the provenance of the Neoproterozoic Port Askaig Tillite, Dalradian Supergoup, western Scotland: Precambrian Research, v. 85, p. 81–96, http://dx.doi.org/10.1016/S0301-9268(97)00033-8.
Paton, J., Woodhead, J.D., Hellstrom, J.C., Hergt, J.M., Greig, A., and Maas, R., 2010, Improved laser ablation U–Pb zircon geochronology through robust downhole fractionation correction: Geochemistry, Geophysics, Geosystems, v. 11, Q0AA06, http://dx.doi.org/10.1029/2009GC002618.
Pell, S.D., Williams, I.S., and Chivas, A.R., 1997, The use of protolith zircon-age fingerprints in determining the protosource areas for some Australian dune sands: Sedimentary Geology, v. 109, p. 233–260, http://dx.doi.org/10.1016/S0037-0738(96)00061-9.
Pidgeon, R.T., 1990, Timing of plutonism in the Proterozoic Albany Mobile Belt, southwestern Australia: Precambrian Research, v. 47, p. 157–167, http://dx.doi.org/10.1016/0301-9268(90)90036-P.
Plummer, P.S., 1978, Note on the palaeoenvironmental significance of the Nuccaleena formation (upper Precambrian), central Flinders Ranges, South Australia: Journal of the Geological Society of Australia, v. 25, p. 395–402, http://dx.doi.org/10.1080/00167617808729049.
Preiss, W.V., 1987, Stratigraphic nomenclature and classification: *in* Preiss, W.V., *ed.*, The Adelaide Geosyncline: Late Proterozoic stratigraphy, sedimentation, palaeontology and tectonics: Geological Survey of South Australia, v. 53.
Preiss, W.V., 2000, The Adelaide Geosyncline of South Australia and its significance in Neoproterozoic continental reconstruction: Precambrian Research, v. 100, p. 21–63, http://dx.doi.org/10.1016/S0301-9268(99)00068-6.
Preiss, W.V., and Forbes, B.G., 1981, Stratigraphy, correlation and sedimentary history of Adelaidean (late Proterozoic) basins in Australia: Precambrian Research, v. 15, p. 255–304, http://dx.doi.org/10.1016/0301-9268(81)90054-1.
Preiss, W. and Robertson, R., 2002, South Australian mineral explorers guide: Technical report, Department of Primary Industries and Regions (PIRSA), Government of South Australia.
Preiss, W., Dyson, I., Reid, P., and Cowley, W., 1998, Revision of lithostratigraphic classification of the Umberatana Group: MESA Journal, v. 9, p. 36–42.Raub, T.D., and Evans, D.A., 2006, Magnetic reversals in basal Ediacaran cap carbonates: A critical review (abstract): Eos, TransactionsAmerican Geophysical Union, v. 87, p. GP41B–02.
Raub, T. and Evans, D., 2008, Paleolatitudes of Neoproterozoic snowball glacial deposits: Biases and synthesis: The 33rd International Geological Congress, Oslo.
Rieu, R., Allen, P.A., Cozzi, A., Kosler, J., and Bussy, F., 2007a, A composite stratigraphy for the Neoproterozoic Huqf Supergroup of Oman: integrating new litho-, chemo- and chronostratigraphic data of the Mirbat area, southern Oman: Journal of the Geological Society, v. 164, p. 997–1009, http://dx.doi.org/10.1144/0016-76492006-114.
Rieu, R., Allen, P.A., Plötze, M., and Pettke, T., 2007b, Climatic cycles during a Neoproterozoic "snowball" glacial epoch: Geology, v. 35, p. 299 – 302, http://dx.doi.org/10.1130/G23400A.1.
Rieu, R., Allen, P.A., Plotze, M., and Pettke, T., 2007c, Compositional and mineralogical variations in a Neoproterozoic glacially influenced succession, Mirbat area, south Oman: Implications for paleoweathering conditions: Precambrian Research, v. 154, p. 248–265, http://dx.doi.org/10.1016/j.precamres.2007.01.003.
Rose, C.V., and Maloof, A.C., 2010, Testing models for post-glacial 'cap dolostone' deposition: Nuccaleena Formation, South Australia: Earth and Planetary Science Letters, v. 296, p. 165–180, http://dx.doi.org/10.1016/j.epsl.2010.03.031.
Rose, C.V., Swanson-Hysell, N.L., Husson, J.M., Poppick, L.N., Cottle, J.M., Schoene, B., and Maloof, A.C., 2012, Constraints on the origin and relative timing of the Trezona $\delta^{13}C$ anomaly below the end-Cryogenian glaciation: Earth and Planetary Science Letters, v. 319–320, p. 241–250, http://dx.doi.org/10.1016/j.epsl.2011.12.027.
Rothman, D.H., Hayes, J.M., and Summons, R.E., 2003, Dynamics of the Neoproterozoic carbon cycle: Proceedings of the National Academy of Sciences, v. 100, p. 8124–8129, http://dx.doi.org/10.1073/pnas.0832439100.
Rubin, D.M., and Hunter, R., 1982, Bedform climbing in theory and nature: Sedimentology, v. 29, p. 121–138, http://dx.doi.org/10.1111/j.1365-3091.1982.tb01714.x.
Scheffler, K., Hoernes, S., and Schwark, L., 2003, Global changes during Carboniferous–Permian glaciation of Gondwana: Linking polar and equato-

rial climate evolution by geochemical proxies: Geology, v. 31, p. 605–608, http://dx.doi.org/10.1130/0091-7613(2003)031<0605:GCDC-GO>2.0.CO;2.

Schermerhorn, L.J.G., 1974, Later Precambrian mixites: Glacial and/or non-glacial?: American Journal of Science, v. 274, p. 673–824, http://dx.doi.org/10.2475/ajs.274.7.673.

Schmidt, P.W., and Williams, G.E., 1995, The Neoproterozoic climatic paradox: Equatorial palaeolatitude for Marinoan glaciation near sea level in South Australia: Earth and Planetary Science Letters, v. 134, p. 107–124, http://dx.doi.org/10.1016/0012-821X(95)00106-M.

Schmidt, P.W., Williams, G.E., and McWilliams, M.O., 2009, Palaeomagnetism and magnetic anisotropy of late Neoproterozoic strata, South Australia: Implications for the palaeolatitude of late Cryogenian glaciation, cap carbonate and the Ediacaran System: Precambrian Research, v. 174, p. 35–52, http://dx.doi.org/10.1016/j.precamres.2009.06.002.

Sheldon, N.D., Retallack, G.T., and Tanaka, S., 2002, Geochemical Climofunctions from North American Soils and Application to Paleosols across the Eocene–Oligocene Boundary in Oregon: The Journal of Geology, v. 110, p. 687–696, http://dx.doi.org/10.1086/342865.

Shields, G.A., 2005, Neoproterozoic cap carbonates: a critical appraisal of existing models and the *plumeworld* hypothesis: Terra Nova, v. 17, p. 299–310, http://dx.doi.org/10.1111/j.1365-3121.2005.00638.x.

Sohl, L.E., Christie–Blick, N., and Kent, D.V., 1999, Paleomagnetic polarity reversals in Marinoan (ca. 600 Ma) glacial deposits of Australia: Implications for the duration of low-latitude glaciation in Neoproterozoic time: Geological Society of America Bulletin, v. 111, p. 1120–1139, http://dx.doi.org/10.1130/0016-7606(1999)111<1120:PPRIMC>2.3.CO;2.

Spencer, A.M., 1971, Late Pre-cambrian glaciation in Scotland: Geological Society, London, Memoirs, v. 6, p. 5–100, http://dx.doi.org/10.1144/GSL.MEM.1971.006.01.02.

Stacey, J.S., and Kramers, J.D., 1975, Approximation of terrestrial lead isotope evolution by a two-stage model: Earth and Planetary Science Letters, v. 26, p. 207–221, http://dx.doi.org/10.1016/0012-821X(75)90088-6.

Sumner, D.Y., Kirschvink, J.L., and Runnegar, B.N., 1987, Soft-sediment paleomagnetic field tests of late Precambrian glaciogenic sediments (abstract): EOS Transactions of the American Geophysical Union, v. 68, p. 1251.

Swanson-Hysell, N.L., Rose, C.V., Calmet, C.C., Halverson, G.P., Hurtgen, M.T., and Maloof, A.C., 2010, Cryogenian glaciation and the onset of carbon–isotope decoupling: Science, v. 328, p. 608– 611, http://dx.doi.org/10.1126/science.1184508.

Swart, P.K., and Kennedy, M.J., 2012, Does the global stratigraphic reproducibility of $\delta^{13}C$ in Neoproterozoic carbonates require a marine origin? A Pliocene–Pleistocene comparison: Geology, v. 40, p. 87–90, http://dx.doi.org/10.1130/G32538.1.

Tauxe, L., and Kent, D.V., 1984, Properties of a detrital remanence carried by hematite from study of modern river deposits and laboratory redeposition experiments: Geophysical Journal of the Royal Astronomical Society, v. 76, p. 543–561, http://dx.doi.org/10.1111/j.1365-246X.1984.tb01909.x.

Teale, G., 1993, Mount Painter and Mount Babbage Inliers, *in* Drexel, J., Preiss, W., and Parker, A., *eds.*, The Geology of South Australia I. The Precambrian: Geological Survey South Australia Bulletin, v. 54, p. 93–100.

Thomson, B., Coats, R., Mirams, R., Forbes, B., Dalgarno, C., and Johnson, J., 1964, Precambrian rock groups in the Adelaide Geosyncline: new subdivision.: Quarterly Journal of the Geological Survey of South Australia, v. 9, p. 1–19.

Trindade, R.I.F., Font, E., D'Agrella-Filho, M.S., Nogueira, A.C.R., and Riccomini, C., 2003, Low-latitude and multiple geomagnetic reversals in the Neoproterozoic Puga cap carbonate, Amazon craton: Terra Nova, v. 15, p. 441–446, http://dx.doi.org/10.1046/j.1365-3121.2003.00510.x.

Turner, J., Chenoli, S.N., abu Samah, A., Marshall, G., Phillips, T., and Orr, A., 2009, Strong wind events in the Antarctic: Journal of Geophysical Research, v. 114, D18103, http://dx.doi.org/10.1029/2008JD011642.

Walter, M.R., and Bauld, J., 1983, The association of sulphate evaporites, stromatolitic carbonates and glacial sediments: Examples from the Proterozoic of Australia and the Cainozoic of Antarctica: Precambrian Research, v. 21, p. 129–148, http://dx.doi.org/10.1016/0301-9268(83)90008-6.

Webb, B., 1960, Diapiric structures in the Flinders Ranges, South Australia: Australian Journal of Science, v. 22, p. 390–391.

Wiedenbeck, M., Alle, P., Corfu, F., Griffin, W., Meier, M., Oberli, F., Von Quadt, A., Roddick, J., and Spiegel, W., 1995, Three natural zircon standards for U–Th–Pb, Lu–Hf, trace element and REE analyses: Geostandards Newsletter, v. 19, p. 1–23, http://dx.doi.org/10.1111/j.1751-908X.1995.tb00147.x.

Wilde, S. and Nelson, D., 2001, Geology of the western Yilgarn Craton and Leeuwin Complex, Western Australia—a field guide: Geological Survey of Western Australia Record 2001, v. 15.

Williams, G.E., 1977, Late Precambrian dolomites, Vendian glaciation, and synchroneity of Vendian glaciations: A discussion: The Journal of Geology, v. 85, p. 250–251, http://dx.doi.org/10.1086/628291.

Williams, G.E., 1979, Sedimentology, stable-isotope geochemistry and palaeoenvironment of dolostones capping late Precambrian glacial sequences in Australia: Journal of the Geological Society of Australia, v. 26, p. 377–386, http://dx.doi.org/10.1080/00167617908729104.

Williams, G.E., 1981, Sunspot Periods in the late Precambrian glacial climate and solar-planetary relations: Nature, v. 291, p. 624–628, http://dx.doi.org/10.1038/291624a0.

Williams, G.E., 1985, Solar affinity of sedimentary cycles in the Late Precambrian Elatina Formation: Australian Journal of Physics, v. 38, p. 1027–1044, http://dx.doi.org/10.1071/PH851027.

Williams, G.E., 1986, Precambrian permafrost horizons as indicators of palaeoclimate: Precambrian Research, v. 32, p. 233–242, http://dx.doi.org/10.1016/0301-9268(86)90008-2.

Williams, G.E., 1988, Cyclicity in the late Precambrian Elatina Formation, South Australia: Solar or Tidal Signature?: Climate Change, v. 13, p. 117–128, http://dx.doi.org/10.1007/BF00140565.

Williams, G.E., 1989, Late Precambrian tidal rhythmites in South Australia and the history of the Earth's rotation: Journal of the Geological Society, v. 146, p. 97–111, http://dx.doi.org/10.1144/gsjgs.146.1.0097.

Williams, G.E., 1991, Upper Proterozoic tidal rhythmites South Australia: sedimentary features, deposition, and implications for the Earths paleorotation, *in* Smith, D.G., Reinson, G.E., Zaitlin, B.A., and Rahmani, R.A., *eds.*, Clastic Tidal Sedimentology: Canadian Society of Petroleum Geologists,

Memoir, v. 16, p. 161–178.
Williams, G.E., 1994, The enigmatic Late Proterozoic glacial climate: an Australian perspective, *in* Deynoux, M., Miller, J.M.G., Domack, E.W., Eyles, N., Fairchild, I., and Young, G.M., *eds.*, Earth's Glacial Record: Cambridge University Press, p. 146–164, http://dx.doi.org/10.1017/CBO9780511628900.012.
Williams, G.E., 1996, Soft-sediment deformation structures from the Marinoan glacial succession, Adelaide foldbelt: implications for the palaeoaltitude of late Neoproterozoic glaciation: Sedimentary Geology, v. 106, p. 165–175, http://dx.doi.org/10.1016/S0037-0738(96)00062-0.
Williams, G.E., 1997, Precambrian length of day and the validity of tidal rhythmite paleotidal values: Geophysical Research Letters, v. 24, p. 421–424, http://dx.doi.org/10.1029/97GL00234.
Williams, G.E., 1998, Late Neoproterozoic periglacial aeolian sand sheet, Stuart Shelf, South Australia: Australian Journal of Earth Sciences, v. 45, p. 733–741, http://dx.doi.org/10.1080/08120099808728429.
Williams, G.E., 2000, Geological constraints on the Precambrian history of Earth's rotation and the Moon's orbit: Reviews of Geophysics, v. 38, p. 37–59, http://dx.doi.org/10.1029/1999RG900016.
Williams, G.E., and Sonett, C.P., 1985, Solar signature in sedimentary cycles from the late Precambrian Elatina Formation, Australia: Nature, v. 318, p. 523–527, http://dx.doi.org/10.1038/318523a0.
Williams, G.E., and Tonkin, D.G., 1985, Periglacial structures and palaeoclimatic significance of a late Precambrian block field in the Cattle Grid copper mine, Mount Gunson, South Australia: Australian Journal of Earth Sciences, v. 32, p. 287–300, http:dx.doi.org/10.1080/08120098508729331.
Williams, G.E., Gostin, V.A., McKirdy, D.M., and Preiss, W.V., 2008, The Elatina glaciation, late Cryogenian (Marinoan Epoch), South Australia: Sedimentary facies and palaeoenvironments: Precambrian Research, v. 163, p. 307–331, http://dx.doi.org/10.1016/j.precamres.2007.12.001.
Williams, I., Chen, Y., Chappell, B., and Compston, W., 1988, Dating the sources of Bega batholith granites by ion microprobe (abstract): 9th Australian Geological Convention, p. 424.
Willis, I.L., Brown, R.E., Stroud, W.J., and Stevens, B.P.J., 1983, The Early Proterozoic Willyama supergroup: Stratigraphic subdivision and interpretation of high to low-grade metamorphic rocks in the Broken Hill Block, New South Wales: Journal of the Geological Society of Australia, v. 30, p. 195–224, http://dx.doi.org/10.1080/00167618308729249.
Wingate, M.T.D., Campbell, I.H., Compston, W. and Gibson, G.M., 1998, Ion microprobe U–Pb ages for Neoproterozoic basaltic magmatism in south-central Australia and implications for the breakup of Rodinia: Precambrian Research, v. 87, p. 135–159, http://dx.doi.org/10.1016/S0301-9268(97)00072-7.
Young, D.A., Wright, A.P., Roberts, J.L., Warner, R.C., Young, N.W., Greenbaum, J.S., Schroeder, D.M., Holt, J.W., Sugden, D.E., Blankenship, D.D., van Ommen, T.D., and Siegert, M.J., 2011, A dynamic early East Antarctic Ice Sheet suggested by ice-covered fjord landscapes: Nature, v. 474, p. 72–75, http://dx.doi.org/10.1038/nature10114.
Young, G.M., 2002, Stratigraphic and tectonic settings of Proterozoic glaciogenic rocks and banded iron-formations: relevance to the snowball Earth debate: Journal of African Earth Sciences, v. 35, p. 451–466, http://dx.doi.org/10.1016/S0899-5362(02)00158-6.
Zahnle, K.J., and Walker, J.C.G., 1987, Climatic oscillations during the Precambrian era: Climatic Change, v. 10, p. 269–284, http://dx.doi.org/10.1007/BF00143906.

**Received January 2013**
**Accepted as revised August 2013**

For access to Rose et al. supplementary material and large fold-out figures 6 through 11, please visit the GAC's open source GC Data Repository at: http://www.gac.ca/wp/?page_id=306.